Constructor University Bremen

School of Natural Sciences

# Non-Markovian Mesoscopic Dynamics of DC Electromagnetized Acqueous Electrolytic Solutions

---

Bachelor Thesis

submitted by
**Noah Horne**

Supervisor:
Prof. Dr. Ulrich Kleinekathöfer

Bachelor of Science in Physics & Data Science
May 14, 2026

# Acknowledgements

I would like to express my sincere gratitude to my supervisor, Prof. Dr. Ulrich Kleinekathöfer, for his guidance, support, and encouragement throughout the development of this undergraduate thesis. His insight and expertise provided the foundation upon which this work was built.

I am especially thankful to Tristan Mauck for his continual assistance, countless discussions, and unwavering willingness to help at every stage of this project. His mentorship and dedication had an immeasurable impact on both this work and my growth as a physicist.

I am deeply grateful to both for their time, patience, and support throughout this journey.

# Abstract

This thesis develops a unified theoretical and computational framework for the nonequilibrium transport of electromagnetized electrolytic fluids across microscopic, mesoscopic, and macroscopic regimes. Through foundations in stochastic microscopic ion dynamics subject to Lorentz forcing, thermal fluctuations, and solvent-mediated interactions, this work systematically derives kinetic and hydrodynamic transport descriptions which resolve both transient and asymptotic electrolyte behavior under DC fields. A perturbative analysis of the memoryless Vlasov–Fokker–Planck equation is first performed to establish the baseline Markovian response of an $N$-species electrolyte, yielding analytic first- and second-order conductivity tensors together with explicit transient distributional solutions. While Markovian formulations of electromagnetohydrodynamics successfully predict nonlinear Hall-type bulk transport proportional to $\vec{E} \times \vec{B}$, it is shown to violate momentum conservation and Galilean invariance through its assumption of instantaneous solvent equilibration.

To resolve these inconsistencies, the theory is generalized through the Mori-Zwanzig projection formalism, yielding a non-Markovian Generalized Langevin Equation with hydrodynamic memory effects derived directly from microscopic phase-space dynamics. Through Klimontovich coarse-graining and ensemble averaging, the microscopic stochastic equations are elevated to a mesoscopic kinetic framework incorporating temporally nonlocal solvent relaxation and self-consistent hydrodynamic coupling. The resulting integro-differential transport equations unify the transient relaxation dynamics with asymptotic steady-state electrolyte motion, providing a bridge between stochastic microscopic dynamics, kinetic theory, and macroscopic fluid transport.

Analytical investigation of the resulting Volterra transport system is performed using Laplace transform methods, Green-Kubo theory, and meromorphic pole-structure analysis to characterize relaxation timescales, transient current evolution, and long-time asymptotic behavior. The theoretical predictions are then compared against momentum-conserving nonequilibrium molecular dynamics simulations performed in OpenMM under externally applied electromagnetic fields. Numerical results demonstrate both the predicted asymptotic drift behavior and the existence of non-Markovian transient relaxation dynamics. Finally, a differential-evolution-based reconstruction methodology is introduced to extract effective electrolyte memory kernels directly from simulated velocity autocorrelation data, enabling quantitative comparison between analytical theory and computational observation of transients.

# Contents


**1 Perturbative Solution of the Memoryless Vlasov-Fokker-Planck Equation 2**
- 1.1 Introduction, Motivation and Scope . . . 2
- 1.2 The Memoryless Vlasov-Fokker-Planck PDE . . . 3
  - 1.2.1 Distributional Solutions of First and Second Order . . . 6
  - 1.2.2 Fundamental Limitations of the Markovian Model . . . 10

**2 The Mori-Zwanzig Formalism and Generalized Langevin Equation 12**
- 2.1 Derivation of Microscopic Equations of Motion . . . 12
  - 2.1.1 Subdiffusive Nonequilibrium Motivation . . . 12
  - 2.1.2 The Bogoliubov Product . . . 12
  - 2.1.3 Dyson Decomposition of the Liouville Equation . . . 14
  - 2.1.4 Physical Instantiation of the Generalized Langevin Dynamics . . 15
- 2.2 Mesocopic Klimontovich Coarse-Graining of Microscopic Dynamics . . . 16
  - 2.2.1 Fine-Grained Klimontovich Distribution . . . 16
  - 2.2.2 Coarse-Graining to the Mesoscopic Picture via Ensemble Averaging 17
- 2.3 Macroscopic Ion Transport and Navier-Stokes Coupling . . . 20
  - 2.3.1 Bulk Flow Assumption Imposition . . . 20
  - 2.3.2 Spatially Homogeneous Integro-Differential Bulk Dynamics . . . 22
  - 2.3.3 Macroscopic Navier Stokes Solvent Drag Coupling . . . 23

**3 Analytic Analysis 24**
- 3.1 Asymptotics of the Volterra System . . . 24
  - 3.1.1 Laplace Transform of the Integro-Differential System . . . 24
- 3.2 Green-Kubo Formulation and Transient Dynamics of Non-Markovian Ionic Transport . . . 26
  - 3.2.1 Linearization of the Non-Markovian Kinetic Equation and the Conductivity Tensor . . . 26
  - 3.2.2 Markovian Conductivity Tensor . . . 29
  - 3.2.3 Transient Correlation Decay Dynamics from Pole Structure . . . 30
  - 3.2.4 Analytic Determination of Current Transients and Relaxation Timescales . . . 32
  - 3.2.5 Discussion of Markovian Transients and Analytic Summary . . . 33

**4 Computational Momentum-Conserving Molecular Dynamics 35**
- 4.1 OpenMM and Momentum Conserving MHD . . . 35
- 4.2 Asymptotic Analysis . . . 38
  - 4.2.1 Timescale Limitations in Magnetohydrodynamic Simulations . . 38
  - 4.2.2 Commentary on Required OpenMM Simulation Parameters . . . 39
  - 4.2.3 Demonstration of Predicted Drift: 2D Parameter Sweep . . . 42
  - 4.2.4 Commentary on Asymptotic Computational Results . . . 45

4.3 Transient Relaxation Analysis & Electrolyte Memory Kernel Extraction 45
4.3.1 Proposed Transient Kernel Reconstruction Methodology: Differential Evolution Optimization . . . 47
4.3.2 Velocity Autocorrelation Formulation . . . 47
4.3.3 Parameterized Memory Kernel Reconstruction . . . 49
4.3.4 Numerical Solution of the Coupled Volterra System . . . 50
4.3.5 Global Optimization of the Kernel Parameters . . . 51
4.3.6 Demonstration of Memory Kernel Reconstruction: Differential Evolution Optimization Computational Results . . . 52
4.3.7 Reconstruction of Transient Dynamics from the Differential Evolution Optimized Memory Kernel . . . 53

**5 Conclusion** **57**
5.1 Discussion of Computational Results: Asymptotic and Transient . . . 57
5.1.1 Asymptotic Computational Results . . . 57
5.1.2 Transient Computational Results . . . 58

**Appendix** **60**
A Time-Reversal Antisymmetry and Entropy Production of the Ornstein-Uhlenbeck Operator . . . 60
B (Action of the OU Semigroup) . . . 62
C Dyson Decomposition . . . 63
D Commentary on the Thermodynamic Consistencies of the Derived Boltzmann Equation . . . 63
E Derivation of the Asymptotic Drift Velocities . . . 69
F Commentary: Acceleration Root-Finding via the Bisection Method . . . 70
G Plot of Bisection Convergence . . . 71
H Bisection Search Steady-State Velocity Finding Algorithm & Helper Functions Pseudocode . . . 72
I DPD Thermostat Pseudocode . . . 73
J Boris Integration Step Pseudocode . . . 74

# 1 Perturbative Solution of the Memoryless Vlasov-Fokker-Planck Equation

## 1.1 Introduction, Motivation and Scope

The transport properties of charged particles in an electrolyte subject to external electromagnetic fields constitute a foundational problem in kinetic theory. When treated through the microscopic perspective adopted by Onsager, particles undergo continuous, reversible interaction with their surrounding counterparts [1]. At macroscopic levels, field-theoretic methods can be applied to explicitly determine phase space observable evolution. This investigation aims to address the subtlety of shifting between these dynamical regimes, and provides an analytic and computational commentary on the nonlinear transport of electromagnetized electrolytes. For such electromagnetized mesoscopic systems, further care must be adopted in treating the magnetic field—due to its time-reversal antisymmetry—which introduces inherent dynamical complexity and challenges the traditional Onsager reciprocal relations [2].

In the computational study of such electrolytic systems, various methodologies are employed for the numerical treatment of systems on varying spatial and temporal scales. On microscopic and nanoscopic regimes, magnetic non-equilibrium molecular dynamics (MD) provides a natural framework, wherein individual particle trajectories are obtained through the numerical integration of coupled equations of motion derived from inter- and intramolecular interaction potentials within a discretized, classical Newtonian setting. For larger, macroscopic regimes, where observables such as local macroscopic streaming velocities or pressure gradients are desired, alternative approaches are adopted in the variational solution of the field-coupled Navier Stokes equations, and related transport/continuity equations. Particularly, discrete variational solution methods for partial differential equations (PDEs) such as the Finite Element Method (FEM)—incorporated directly into various Python modules such as FEniCS—offer a flexible and robust framework for such problems. For the purposes of this investigation, methods in nonequilibrium electromagnetic molecular dynamics are adopted on the basis of their tunability, capacity for individual ion trajectory analysis, and applicability to bulk transient behavior through ensemble methods. Figure 1.1 details the precise nanoscopic model to be examined computationally with purpose to verify the performed analytical work of this thesis—such computational results detailed in Chapter 4.

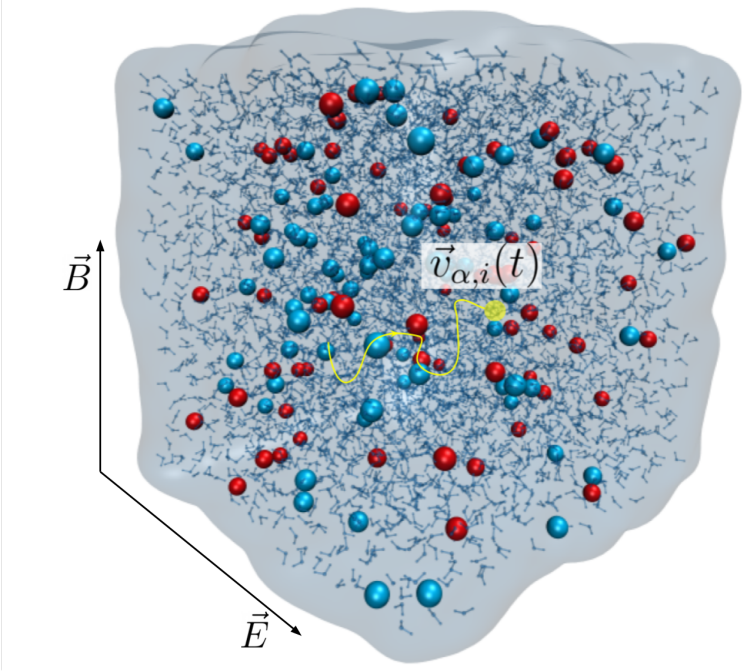


**Figure 1.1:** Electromagnetic Molecular Dynamics Setup: (red) $K^+$ ions, (blue) $Cl^-$ ions, (solvent) $H_2O$. A single ion trajectory is sketched in yellow.

A standard—albeit naive—approach to the analytic modelling of ion-solvent systems is to adopt assumptions of instantaneous and time-uncorrelated interaction between particles, resulting in a Markovian description of ion dynamics. As a foundational step, one considers the memoryless Langevin formulation of ionic motion, in which the complex many-body influence of the surrounding solvent is reduced to a linear friction term, with Gaussian white noise satisfying the fluctuation-dissipation relation. Under this approximation, the evolution of the single-particle-phase-space distribution function is governed by the Vlasov-Fokker-Planck equation, which provides a kinetic description incorporating both deterministic electromagnetic Lorentz forcing $q(\vec{E} + \vec{v} \times \vec{B})$ and stochastic thermalization [3]. In this chapter, the Markovian kinetic framework is adopted as a controlled baseline. By constructing a perturbative expansion of the distribution function in powers of the applied electric field, the first- and second-order corrections to the ionic distribution and the associated current density are explicitly calculated.

## 1.2 The Memoryless Vlasov-Fokker-Planck PDE

One may approach an electrolytic system as a collection of charged particle species embedded in a drag imposing, thermally diffusive, static fluid. It can be assumed concomitantly that the solvent (water) serves as a thermal bath of fixed temperature $T$, providing friction and velocity diffusion to each ion species individually. Each ion species is assigned a relaxation time of $\tau = \gamma_\alpha^{-1}$, where $\alpha \in \{+, -\}$ is the ion species index for cations and anions respectively. Under such imposed conditions, one may investigate the macroscopic effects of an externally-imposed DC electric and magnetic

field—$\vec{E}$ and $\vec{B}$ respectively—on the bulk electrolyte. The associated inertial Langevin equations of motion for an individual ion with position $\vec{r}$ and velocity $\vec{v}$ at time $t$ with a Lorentz forcing term is given as:

$$\frac{d\vec{r}_\alpha}{dt} = \vec{v}_\alpha, \tag{1.1}$$

$$m_\alpha \frac{d\vec{v}_\alpha}{dt} = \underbrace{q_\alpha \left(\vec{E}(\vec{r}_\alpha) + \vec{v}_\alpha \times \vec{B}(\vec{r}_\alpha)\right)}_{\text{Lorentz Force}} - \underbrace{m_\alpha \gamma_\alpha \vec{v}_\alpha}_{\text{Stokes Drag}} + \underbrace{\sqrt{2m_\alpha \gamma_\alpha k_B T}\vec{\zeta}(t)}_{\text{Ion-Solvent Collisions}}, \tag{1.2}$$

where $m_\alpha$ and $q_\alpha$ denote the mass and charge of ion species $\alpha$ respectively, and $\vec{\eta}(t)$ is a noise term which describes the stochastic ion-solvent interaction [4]. Under memoryless, solvent-equilibrium assumptions, one defines $\vec{\eta}(t)$ as Gaussian white noise such that $\langle \eta_i(t) \rangle = 0$, and $\langle \eta_i(t)\eta_j(t') \rangle = \delta_{ij}\delta(t-t')$. Note that this does not assume nonequilibrium behavior of the background solvent, nor acknowledges the effect of ion flow on the solvent itself. From an applications perspective, this static-solvent behavior would be most closely modelled by a near-edge solution in an ionic channel, where edge friction and the no-slip condition dominates forward shear friction, leading to a locally static solvent behavior [5]. Solutions to the latter mid-channel problem involve the consideration of subdiffusive behavior and the introduction of a relative velocity memory-dependent functional, which will be considered in the non-equilibrium solvent case in chapter 2.

To perform the transition from microscopic dynamics to a phase-space distributional picture, one defines the associated ion phase-space probability density $f_\alpha(\vec{r}_\alpha, \vec{v}_\alpha, t)$, where $n_\alpha f_\alpha(t) d^3x d^3v$ denotes the expected number of ions of species $\alpha$ adherent to a particular phase-space region with species-wise number density $n_\alpha$.

It is clear that 1.2 defines a stochastic differential equation (SDE) of the form

$$\frac{dX}{dt} = A(X) + B\zeta(t), \tag{1.3}$$

where $X = (\vec{r}, \vec{v})$. The associated Fokker-Planck PDE for SDE's of this type is

$$\partial_t f_\alpha = -\nabla_X \cdot (A f_\alpha) + \frac{1}{2} \sum_{i,j} \frac{\partial^2}{\partial X_i \partial X_j} \left( (BB^T)_{ij} f_\alpha \right). \tag{1.4}$$

The vector function quantities from 1.2 which relate to 1.4 are given by

$$A = \begin{pmatrix} \vec{v}_\alpha \\ \frac{q_\alpha}{m_\alpha}(\vec{E} + \vec{v}_\alpha \times \vec{B}) - \gamma_\alpha \vec{v}_\alpha \end{pmatrix}, \quad B = \sqrt{\frac{2\gamma_\alpha k_B T}{m_\alpha}} I_{3\times 3}, \quad \nabla_X = \begin{pmatrix} \nabla_{\vec{r}_\alpha} \\ \nabla_{\vec{v}_\alpha} \end{pmatrix}, \tag{1.5}$$

which yields through substitution and simplification the Vlasov-Fokker-Planck equation [4, 6–8]. Note that the stochastic solvent noise only acts in velocity space, so the corresponding double sum can be reduced to a sum over only velocity coordinates. The equation then reduces, e.g:

$$\partial_t f_\alpha = -\begin{pmatrix} \nabla_{\vec{r}_\alpha} \\ \nabla_{\vec{v}_\alpha} \end{pmatrix} \cdot \begin{pmatrix} \vec{v}_\alpha \\ \frac{q_\alpha}{m_\alpha}(\vec{E} + \vec{v}_\alpha \times \vec{B}) - \gamma_\alpha \vec{v}_\alpha \end{pmatrix} f_\alpha + \frac{1}{2} \sum_{i,j} \frac{\partial^2}{\partial X_i \partial X_j} \left[ \frac{2\gamma_\alpha k_B T}{m_\alpha} \delta_{ij} f_\alpha \right]$$

$$\partial_t f_\alpha + \vec{v}_\alpha \cdot \nabla_{\vec{r}_\alpha} f_\alpha + \frac{q_\alpha}{m_\alpha}(\vec{E} + \vec{v}_\alpha \times \vec{B}) \cdot \nabla_{\vec{v}_\alpha} f_\alpha = \gamma_\alpha \nabla_{\vec{v}_\alpha} \cdot (\vec{v}_\alpha f_\alpha + \frac{k_B T}{m_\alpha} \nabla_{\vec{v}_\alpha} f_\alpha) \tag{1.6}$$

Equation 1.6 describes the precise phase-space distributional dynamics of electrolyte ion probability densities. Through the application of the Fokker-Planck framework on stochastic differential equations, one promotes the single ion trajectory to a full distributional picture via implicit dynamical ensemble averaging (See Figure 1.2).

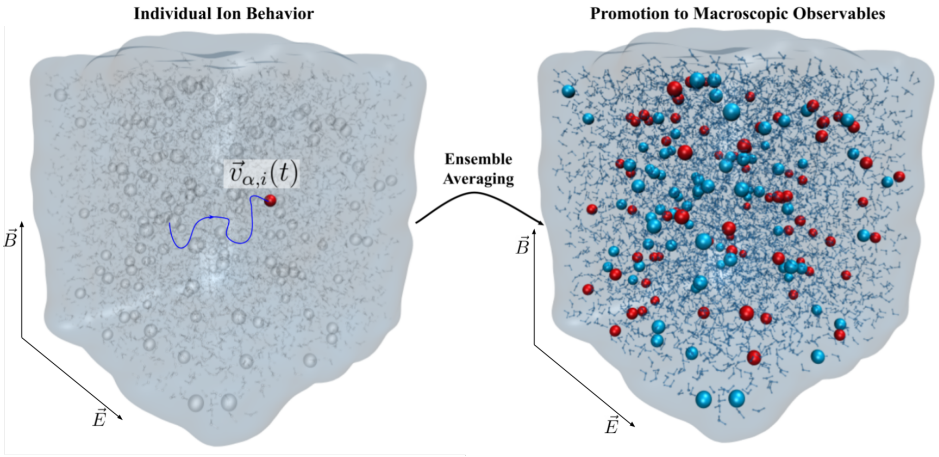


**Figure 1.2:** Visualization of ensemble averaging from ion trajectories to distributional PDE-induced dynamics. The left diagram demonstrates the picture described by the Langevin equation, the right by Fokker-Planck.

One may also note that the left hand side of this equation is exactly equivalent to the collisionless Vlasov equation for magnetized plasmas [9]. The right hand side of the equation serves as the collision operator, and is commonly known as an Ornstein-Uhlenbeck (OU) operator $\mathcal{L}_\alpha f_\alpha = \gamma_\alpha \nabla_{\vec{v}_\alpha} \cdot (\vec{v}_\alpha f_\alpha + \frac{k_B T}{m_\alpha} \nabla_{\vec{v}_\alpha} f_\alpha)$, implementing thermal diffusion and Stokes drag macro-deterministically [10]. It is important to acknowledge that the OU operator is non-Hamiltonian, entropy producing, and demonstrably not time-reversal invariant. From a thermostat implementation point of view, the OU operator can be thought of as the differential operator instantiation of the Langevin thermostat on the solvent, as momentum conservation is ignored. A precise proof of entropy production and lack of time-reversal invariance of the OU operator is detailed in Appendix A.

As the investigation only concerns itself with bulk velocity flows, one may additionally impose spatial homogeneity $\nabla_{\vec{r}_\alpha} f_\alpha = 0$ as an assumption to remove the spatial derivative term from 1.6—assuming the absence of boundary shear flows and edge effects. Doing so yields an equation which describes velocity phase space dynamics of the ion distribution over time with respect to the externally incident fields:

$$\partial_t f_\alpha + \frac{q_\alpha}{m_\alpha}(\vec{E} + \vec{v}_\alpha \times \vec{B}) \cdot \nabla_{\vec{v}_\alpha} f_\alpha = \gamma_\alpha \nabla_{\vec{v}_\alpha} \cdot \left( \vec{v}_\alpha f_\alpha + \frac{k_B T}{m_\alpha} \nabla_{\vec{v}_\alpha} f_\alpha \right). \tag{1.7}$$

To better infer the qualitative dynamical properties of the electrolyte through equation 1.7, one may perturbatively expand the velocity phase-space distribution function under the small DC field approximation $E \mapsto \varepsilon E$, $B \mapsto \varepsilon B$, where $\varepsilon \ll 1$ serves as a bookkeeping parameter for orders of expansion. Assuming that a Maxwellian of the

velocity distribution exists—which we will denote $f_\alpha^{(0)}$—and that the response is analytic in field strengths, the distribution function $f_\alpha$ can be written as

$$f_\alpha(\vec{v}_\alpha, t) = f_\alpha^{(0)} + \varepsilon f_\alpha^{(1)} + \varepsilon^2 f_\alpha^{(2)} + \mathcal{O}(\varepsilon^3). \tag{1.8}$$

Substituting 1.8 into 1.7 and collecting terms for zeroth, first, second, and higher order responses in $\varepsilon$, one may construct specific PDEs which describe dynamical behavior at each order. To begin we calculate the zeroth order distribution, and ensure that the model is consistent with the Maxwell-Boltzmann distribution before proceeding to higher orders. Substituting the expansion 1.8 into 1.7, recalling as well to include the small field approximation,

$$\begin{aligned}\partial_t[f_\alpha^{(0)} + \varepsilon f_\alpha^{(1)} + \cdots] + \varepsilon\frac{q_\alpha}{m_\alpha}(\vec{E} + \vec{v}_\alpha \times \vec{B}) \cdot \nabla_{\vec{v}_\alpha}[f_\alpha^{(0)} + \varepsilon f_\alpha^{(1)} + \cdots] \\ = \gamma_\alpha \nabla_{\vec{v}_\alpha} \cdot \left(\vec{v}_\alpha[f_\alpha^{(0)} + \varepsilon f_\alpha^{(1)} + \cdots] + \frac{k_B T}{m_\alpha}\nabla_{\vec{v}_\alpha}\right),\end{aligned} \tag{1.9}$$

and collecting all order zero terms, one may notice that the equilibrium distribution dynamics are independent of the electric and magnetic fields. Operating under equilibrium assumptions, one may impose the additional simplification of setting $\partial_t f_\alpha^{(0)} = 0$. Doing so, our equilibrium PDE to solve becomes the stationary Fokker-Planck equation for an Ornstein-Uhlenbeck process in velocity space,

$$\nabla_{\vec{v}_\alpha} \cdot (\vec{v}_\alpha f_\alpha^{(0)} + \frac{k_B T}{m_\alpha}\nabla_{\vec{v}_\alpha} f_\alpha^{(0)}) = 0. \tag{1.10}$$

Defining the velocity space probability current $\vec{J}_\alpha(\vec{v}_\alpha) = \vec{v}_\alpha f_\alpha^{(0)} + \frac{k_B T}{m_\alpha}\nabla_{\vec{v}_\alpha} f_\alpha^{(0)}$, equation 1.10 is equivalent to a continuity equation in velocity space, e.g.

$$\nabla_{\vec{v}_\alpha} \cdot \vec{J}_\alpha(\vec{v}_\alpha) = 0 \tag{1.11}$$

At equilibrium, there is no net probablility flux at infinity, so $\vec{J}_\alpha^{(0)}(\vec{v}_\alpha) = 0$. Integrating 1.11 and solving for the zeroth order distribution $f_\alpha^{(0)}$, one achieves the Maxwell-Boltzmann velocity distribution, completely independent of $\gamma_\alpha$ .

$$f_\alpha^{(0)}(\vec{v}_\alpha) = n_\alpha \left(\frac{m_\alpha}{2\pi k_B T}\right)^{\frac{3}{2}} \exp\left(\frac{-m_\alpha}{2k_B T} \cdot |\vec{v}_\alpha|^2\right) \tag{1.12}$$

This demonstrates the consistency of the Vlasov-Fokker-Planck PDE with the known behavior of an equilibrated thermodynamic system in an NVT ensemble [11].

### 1.2.1 Distributional Solutions of First and Second Order

Proceeding similarly as the Maxwellian was derived, one finds the corresponding first and second order PDEs governing the first and second order distributional responses, respectively. For first order in $\varepsilon$, where $\mathcal{L}_\alpha$ is the Ornstein-Uhlenbeck collision operator for ion species $\alpha$, equation 1.7 groups to

$$\partial_t f_\alpha^{(1)} = \mathcal{L}_\alpha f_\alpha^{(1)} + \frac{q_\alpha}{k_B T}(\vec{E} \cdot \vec{v}_\alpha) f_\alpha^{(0)} \tag{1.13}$$

for first order, and

$$\partial_t f_\alpha^{(2)} = \mathcal{L}_\alpha f_\alpha^{(2)} - \frac{q_\alpha}{m_\alpha}(\vec{E} + \vec{v}_\alpha \times \vec{B}) \cdot \nabla_{\vec{v}_\alpha} f_\alpha^{(1)} \tag{1.14}$$

for second order. By applying Duhamel's principle to solve the initial-value problem, the first and second order transient solutions can be obtained [6].

**Theorem 1.2.1** (Duhamel's Principle) *Consider a linear inhomogeneous evolution equation for a time dependent function on a domain $D \subseteq \mathbb{R}^n$, $f_\alpha^{(1)} : D \times (0, \infty) \to \mathbb{R}$ in the form*

$$\partial_t f_\alpha^{(1)} - \mathcal{L}_\alpha f_\alpha^{(1)} = g(\vec{v}_\alpha, t), \tag{1.15}$$

$$f_\alpha^{(1)}|_{\partial D} = 0, \tag{1.16}$$

$$f_\alpha^{(1)}(\vec{v}_\alpha, 0) = 0, \vec{v}_\alpha \in D \tag{1.17}$$

*where $\mathcal{L}_\alpha$ is some linear differential operator. Then, the solution to this problem is exactly*

$$f_\alpha^{(1)}(\vec{v}_\alpha, t) = \int_0^t e^{(t-s)\mathcal{L}_\alpha} g(\vec{v}_\alpha, s) ds, \tag{1.18}$$

*where $e^{t\mathcal{L}_\alpha}$ is the semigroup induced by the operator $\mathcal{L}_\alpha$.*

For first order, the perturbed solution is given by Duhamel's principle explicitly:

$$\begin{aligned} f_\alpha^{(1)}(\vec{v}_\alpha, t) &= \int_0^t e^{(t-s)\mathcal{L}_\alpha} \left[ \frac{q_\alpha}{k_B T} (\vec{E} \cdot \vec{v}_\alpha) f_\alpha^{(0)} \right] ds \\ &= \frac{q_\alpha}{k_B T} \int_0^t e^{(t-s)\mathcal{L}_\alpha} (\vec{E} \cdot \vec{v}_\alpha) f_\alpha^{(0)} ds. \end{aligned} \tag{1.19}$$

It can be demonstrably proven (see Appendix B) that the action of the Ornstein-Uhlenbeck (OU) semigroup $e^{t\mathcal{L}_\alpha}$ on the velocity-scaled equilibrium Maxwellian $(\vec{E} \cdot \vec{v}_\alpha) f_\alpha^{(0)}(\vec{v}_\alpha)$ is precisely:

$$e^{t\mathcal{L}_\alpha} (\vec{E} \cdot \vec{v}) f_\alpha^{(0)}(\vec{v}_\alpha) = e^{-\gamma_\alpha t} (\vec{E} \cdot \vec{v}_\alpha) f_\alpha^{(0)}(\vec{v}_\alpha). \tag{1.20}$$

Substituting 1.20 into the perturbed solution 1.19 and integrating, the first order transient distributional response of the ionic phase space for switched on electric and magnetic fields is given by:

$$f_\alpha^{(1)} = \frac{q_\alpha}{\gamma_\alpha k_B T} [1 - e^{-\gamma_\alpha t}] (\vec{E} \cdot \vec{v}_\alpha) f_\alpha^{(0)} \tag{1.21}$$

It may be interesting to acknowledge the lack of magnetic field dependence on first-order transient system response. The full system exponentially decays towards an electric feld dependent steady-state. As time approaches infinity ($t \to +\infty$), the first-order distribution approaches:

$$f_{\alpha,\infty}^{(1)}(\vec{v}_\alpha) = \frac{q_\alpha}{\gamma_\alpha k_B T} (\vec{E} \cdot \vec{v}_\alpha) f_\alpha^{(0)}. \tag{1.22}$$

Examining the steady state current behavior $\vec{J}_\infty^{(1)}$, it is possible recover an explicit first order conductivity tensor $\sigma^{(1)}$, e.g.

$$\vec{J}_\infty = \sum_\alpha q_\alpha \left[ \frac{q_\alpha}{\gamma_\alpha k_B T} \int_{\mathbb{R}^3} \vec{v}_\alpha (\vec{E} \cdot \vec{v}_\alpha) f_\alpha^{(0)}(\vec{v}_\alpha) d^3 v_\alpha \right] = \sum_\alpha \frac{n_\alpha q_\alpha^2}{\gamma_\alpha m_\alpha} \vec{E}. \tag{1.23}$$

Using Ohm's law, $\vec{J} = \sigma^{(1)} \vec{E}$, the components of the conductivity tensor $\sigma_{ij}^{(1)}$ can be directly read off as a diagonal matrix, immediately recognizable as the DC Drude conductivity [12]:

$$\sigma_{ij}^{(1)} = \sum_\alpha \frac{n_\alpha q_\alpha^2}{\gamma_\alpha m_\alpha} \delta_{ij} \tag{1.24}$$

At the first-order, only linear Ohmic drift is observed—cations flow with the electric field, anions flow against the electric field, and so the charge currents $\vec{J}_{\alpha,\infty}$ constructively superpose in the asymptotic picture. However, under the assumptions of a symmetric, electroneutral electrolyte, where we have equal masses $m_\alpha$, relaxation times $\gamma_\alpha$, and opposite charges $q_- = -q_+ = q$, the first order bulk velocity of the fluid remains zero. To describe nonlinear transport in the memoryless solvent equilibrium picture, higher order responses must be considered.

At the second order, one substitutes the derived first order distributional solution into the second order PDE 1.14 in recursive fashion to arrive at a PDE without first order terms. Applying previously derived actions of the gradient on the Maxwellian $f_\alpha^{(0)}$, the time-dependent gradient can be computed, and equation 1.14 reduces to:

$$\partial_t f_\alpha^2 = \mathcal{L}_\alpha f_\alpha^{(2)} - \frac{q_\alpha^2}{m_\alpha \gamma_\alpha k_B T}(1 - e^{-\gamma_\alpha t}) [\underbrace{|\vec{E}|^2 - \frac{m_\alpha}{k_B T}(\vec{E} \cdot \vec{v}_\alpha)^2}_{\propto |\vec{E}|^2} + \underbrace{(\vec{v}_\alpha \times \vec{B}) \cdot \vec{E}}_{\propto (\vec{E} \times \vec{B})}] f_\alpha^{(0)}. \tag{1.25}$$

Notice the presence of two source terms in 1.25. The first term is proportional to the square of the electric field, and the other is proportional to the cross of electric and magnetic fields. Since the Ornstein-Uhlenbeck operator is a linear differential operator, one may decompose the second order PDE into two distinct parts: $f_\alpha^{(2)} = f_{\alpha,|\vec{E}|^2}^{(2)} + f_{\alpha,\vec{E}\times\vec{B}}^{(2)}$, and solve the equations

$$\partial_t f_{\alpha,|\vec{E}|^2}^{(2)} = \mathcal{L}_\alpha f_{\alpha,|\vec{E}|^2} - \frac{q_\alpha^2}{m_\alpha \gamma_\alpha k_B T} \left[ |\vec{E}|^2 - \frac{m_\alpha}{k_B T}(\vec{E} \cdot \vec{v}_\alpha)^2 + (\vec{v}_\alpha \times \vec{B}) \cdot \vec{E} \right] f_\alpha^{(0)}, \tag{1.26}$$

$$\partial_t f_{\alpha,\vec{E}\times\vec{B}}^{(2)} = \mathcal{L}_\alpha f_{\alpha,\vec{E}\times\vec{B}}^{(2)} - \frac{q_\alpha^2}{m_\alpha \gamma_\alpha k_B T} (\vec{v}_\alpha \times \vec{B}) \cdot \vec{E} f_\alpha^{(0)}, \tag{1.27}$$

independently. Similar to the derivation before, both equations can be solved using Duhamel's principle. For the $|\vec{E}|^2$ equation, the transient solution is calculated to be:

$$\begin{aligned} f_{\alpha,|\vec{E}|^2}^{(2)} = & \frac{-2q_\alpha^2 |\vec{E}|^2}{\gamma_\alpha m_\alpha k_B T} \left( t - \frac{1 - e^{-\gamma_\alpha t}}{\gamma_\alpha} \right) f_\alpha^{(0)} + \\ & \frac{q_\alpha^2}{\gamma_\alpha (k_B T)^2} \left( \frac{1 - e^{-2\gamma_\alpha t}}{2\gamma_\alpha} - \frac{e^{-\gamma_\alpha t} - e^{-2\gamma_\alpha t}}{\gamma_\alpha} \right) (\vec{E} \cdot \vec{v}_\alpha)^2 f_\alpha^{(0)} + \\ & \frac{q_\alpha^2}{\gamma_\alpha m_\alpha k_B T} |\vec{E}|^2 \left( \frac{1 - e^{-2\gamma_\alpha t}}{2\gamma_\alpha} - \frac{e^{-\gamma_\alpha t} - e^{-2\gamma_\alpha t}}{\gamma_\alpha} \right) f_\alpha^{(0)} \end{aligned} \tag{1.28}$$

Taking the limit one observes growth in the velocity distribution linear in time.

$$f^{(2)}_{\alpha,|\vec{E}|^2} \sim \frac{-2q_\alpha^2|\vec{E}|^2}{\gamma_\alpha m_\alpha k_B T} t f^{(0)}_\alpha \tag{1.29}$$

Such growth is consistent with macroscopic electrodynamics, as the kinetic energy density $\Delta E_k(t)$ is predicted to increase exactly linearly with the square of the electric field, e.g. the cummulative volumetric work is exactly consistent with Joule heating of the electrolytic system [12, 13]:

$$\Delta E_k(t) = \int \frac{1}{2} m|\vec{v}_\alpha|^2 f^{(2)}_{\alpha,|\vec{E}|^2}(\vec{v}_\alpha, t) d^3 v_\alpha \propto \frac{q_\alpha|\vec{E}|^2}{m_\alpha \gamma_\alpha} t, \tag{1.30}$$

and so one achieves the result exactly,

$$E_k(t) \sim \sigma|\vec{E}|^2 t. \tag{1.31}$$

The second-order distribution contains a secular $|\vec{E}|^2$ contribution which grows linearly in time, reflecting the continuous Joule heating under DC driving. This growth signals the abscence of an energy sink in the kinetic model and does not affect the transport observables, which remain bounded. However, it does demonstrate that the momentum of the system is not locally preserved, and the energy introduced transfers directly to heat, rather than nonequilibrium motion of the system. Physically, this is not entirely consistent with the macroscopic picture—the solvent remaining stationary locally challenges momentum conservation, manifesting itself as heating of the system.

To finish the perturbative solvent equilibrium investigation, one applies Duhamel's principle to equation 1.27 in the same recursive fashion. Doing so, integrating, and applying associated eigenfunction identities of the OU operator, the final transient solution for the second-order velocity distribution can be described as

$$\begin{aligned} f^{(2)}_{\alpha,\vec{E}\times\vec{B}} =& \frac{q_\alpha^2}{m_\alpha \gamma_\alpha^2 k_B T}(\vec{E}\times\vec{B})\cdot\vec{v}_\alpha f^{(0)}_\alpha(\vec{v}_\alpha) - \\ & \frac{q_\alpha^2}{m_\alpha \gamma_\alpha^2 k_B T}\left[e^{-\gamma_\alpha t} + \gamma_\alpha t e^{-\gamma_\alpha t}\right](\vec{E}\times\vec{B})\cdot\vec{v}_\alpha f^{(0)}_\alpha(\vec{v}_\alpha), \end{aligned} \tag{1.32}$$

where in the long time limit, all exponential decaying transient artifacts vanish, yielding

$$f^{(2)}_{\alpha,\vec{E}\times\vec{B},\infty} = \frac{q_\alpha^2}{m_\alpha \gamma_\alpha^2 k_B T}(\vec{E}\times\vec{B})\cdot\vec{v}_\alpha f^{(0)}_\alpha(\vec{v}_\alpha). \tag{1.33}$$

In similar fashion to the derivation of the first order conducitvity tensor, one may construct a second order conductivity tensor $\sigma^{(2)}$ describing ionic Hall drift. Component-wise the steady-state current is given as

$$J^{(2)}_{i,\infty} = \sum_\alpha q_\alpha \int_{\mathbb{R}^3} v_{\alpha,i} f^{(2)}_{\alpha,\vec{E}\times\vec{B},\infty}(\vec{v}_\alpha) d^3 v_\alpha = \left(\sum_\alpha \frac{n_\alpha q_\alpha^3}{m_\alpha^2 \gamma_\alpha^2}\right)\varepsilon_{ijk} E_j B_k, \tag{1.34}$$

so the second-order conductivity tensor is given as:

$$\sigma^{(2)}_{ijk} = \left(\sum_\alpha \frac{n_\alpha q_\alpha^3}{m_\alpha^2 \gamma_\alpha^2}\right)\varepsilon_{ijk}, \tag{1.35}$$

where $\varepsilon_{ijk}$ is the Levi-Civita tensor. Note that in contrast to the first-order conductivity $\sigma_{ij}^{(1)}$, the second-order tensor is charge antisymmetric, implying a net zero charge current for a symmetric electrolyte, and a constructively superposing, charge symmetric bulk-transport velocity:

$$\vec{v}_\infty^{(2)} = \frac{1}{\rho}\sum_\alpha \frac{n_\alpha q_\alpha^2}{m_\alpha \gamma_\alpha^2}(\vec{E}\times\vec{B}) = \frac{nq^2}{\rho}\left(\frac{1}{m_+\gamma_+^2}+\frac{1}{m_-\gamma_-^2}\right)(\vec{E}\times\vec{B}), \tag{1.36}$$

where $n$ is the symmetric charge carrier number density, $\rho$ is the charge carrier mass density, $q$ is the symmetric charge, and $m_+, m_-, \gamma_+, \gamma_-$ are the charge dependent masses and drag coefficients, respectively. Note that albeit quite small, given the square of the charge in the numerator, and the large drag factors in the denominator, a non-zero bulk velocity of the ions in the stationary equilibrated solvent is observed in the Hall transport direction, indicative of nonlinear transport in an electromagnetized electrolyte.

### 1.2.2 Fundamental Limitations of the Markovian Model

While the Markovian result demonstrably proves the existence of nonlinear transport in electromagnetized electrolytic systems, it remains fundamentally flawed in its equilibrium assumptions on the solvent. In a real fluid, momentum conservation dictates that the solvent cannot act as an infinite, inert momentum sink. As the second-order bulk transport velocity $\vec{v}_\infty^{(2)}$ is charge-symmetric, both cations and anions drift in the exact same $\vec{E}\times\vec{B}$ direction. Consequently, the momentum continuously transferred from the migrating ions to the solvent via the frictional drag forces does not cancel out as in the first order solution. Instead, it constructively superposes, exerting a net, macroscopic volumetric body force on the background fluid—which currently lies under equilibrium assumptions.

The assumption of a stationary solvent ($\vec{u}=0$) implicitly breaks Galilean invariance by ignoring this reciprocal momentum exchange, and imposing Joule heating instead. In a real electrolyte, the ionic drift will inevitably drag the surrounding solvent along with it, inducing a bulk nonequilibrium hydrodynamic flow. Under the current assumptions, introducing a Galilean boost causes the drag to increase unphysically (See Figure 1.3). To properly resolve nonlinear transport and capture true steady-state dynamics, the kinetic description of the electrolytic system must be explicitly coupled to the hydrodynamics of the surrounding fluid.

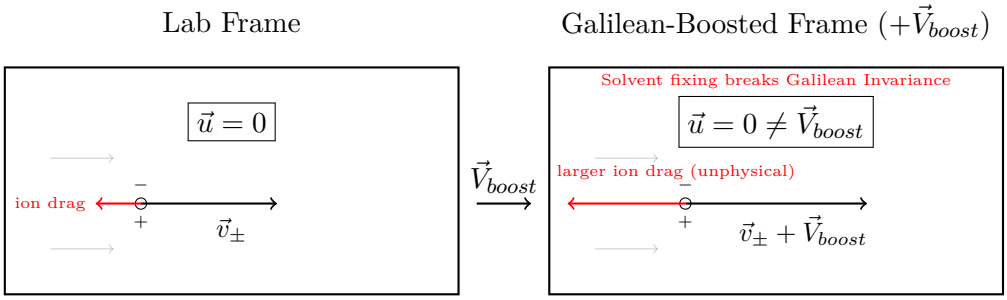


**Figure 1.3:** Galilean-Invariance Breaking Consequence of Solvent Equilibrium

Correspondingly, the phenomenological drag term in the underlying Langevin equation—and consequently the OU collision operator within the Vlasov-Fokker-Planck framework—must be reformulated to depend on the relative species-wise phase-space velocity $\vec{v}_\alpha - \vec{u}(\vec{r},t)$, where $\vec{u}(\vec{r},t)$ is the local macroscopic velocity of the solvent. Introducing the velocity dynamics by such means reinforces galilean invariance, e.g.

$$\vec{v}_\alpha - \vec{u}(\vec{r},t) \xrightarrow[\text{Galilean Boost } \vec{V}]{} (\vec{v}_\alpha + \vec{V}) - (\vec{u}(\vec{r},t) + \vec{V}) = \vec{v}_\alpha - \vec{u}(\vec{r},t) \tag{1.37}$$

This descriptional modification necessitates a self-consistent electromagnetohydrodynamic treatment where the phase-space distributions of the ionic species evolve in tandem with the bulk-flow Navier-Stokes equations. In this coupled regime, the Navier-Stokes equations are actively driven by a momentum source term corresponding to the collective Lorentz body force density $\vec{J} \times \vec{B} + \rho\vec{E}$. Only by abandoning the stationary background assumption and accounting for this continuous kinetic-hydrodynamic feedback can one accurately derive the long-time asymptotic velocity of the electromagnetized electrolyte.

Furthermore, the assumption of instantaneous momentum dissipation inherently limits the temporal fidelity of the model. In standard hydrodynamic and kinetic formulations, fluidic drag is treated as a strictly Markovian process, where the frictional force exerted on an ion depends solely on its current relative velocity. However, on the intermediate timescales characteristic of rapid field-driven transients or dense, structured ionic interactions, the background solvent demonstrably does not equilibrate instantaneously. Various sources indicate that the true relaxation behavior of a fluid decays via a power law $\propto t^{-3/2}$ (under the Basset-Bousinesq framework), or even exponential kernels under visco-elastic assumptions [14]. The finite response time of the surrounding solvation shell necessitates the introduction of a hydrodynamic memory kernel—a temporally non-local operator that weights the historical phase-space trajectory of the fluid and the moving ion [15]. Formally, we replace linear (memoryless) drag $\gamma_\alpha\delta(t)$ with some generalized, relaxation-time dependent analog $K_\alpha(t)$. Physically, this memory kernel encodes the viscoelastic retardation, structural relaxation, and acoustic transit times within the solvent: e.g. the drag force at any given moment can be treated as a convolution of past velocities and the kernel.

To faithfully capture the transient transport phenomena and the precise time-evolution observed in nonequilibrium molecular dynamics, the model must be generalized. The standard instantaneous Langevin picture must be extended into a proposed Generalized Langevin Equation (GLE) framework, replacing the scalar drag coefficients within the Ornstein-Uhlenbeck operator with a non-Markovian relaxation model that explicitly accounts for this delayed hydrodynamic feedback. Similar approaches to fluidic description have been adopted in recent works [16], however the description of electromagnetic fluid dynamics through such a framework remains sparse. The bulk theoretical work of this thesis relates directly to the strict resolution of these aforementioned effects, building upon the theory introduced by Hajime Mori and Robert Zwanzig [17–19], ultimately arriving to a physically coherent asymptotic nonequilibrium picture for bulk electromagnetized ion-solvent flows under a generalized memory kernel description.

# 2 The Mori-Zwanzig Formalism and Generalized Langevin Equation

## 2.1 Derivation of Microscopic Equations of Motion

### 2.1.1 Subdiffusive Nonequilibrium Motivation

While the previous model was developed from a solvent-equilibrium perspective, the assumption of a static background more faithfully adheres to the behavior exhibited by a non-momentum conserving thermostat. To better model the precise behavior and momentum conservation, a non-equlibrium solvent picture must be adopted, alongside strict non-markovian ion-solvent coupling to extend generality to subdiffusive solvent behavior. Earlier one worked under the assumption of a static solvent background, consistent only with near edge solvent flow conditions, or very heavy solvent behavior, where ions collide with an immovable stochastic solvent. The electrolyte was treated as a velocity phase space distribution governed by a Vlasov-Fokker-Planck equation where collisions were introduced via an Ornstein-Uhlenbeck operator, as detailed in equation 1.7. Now, the theory no longer assumes Stoke's drag, instead, drag introduced by a memory kernel, allowing to take non-instantaneous velocity autocorrelations and assume bulk motion of the solvent.

### 2.1.2 The Bogoliubov Product

The evolution of an observable $A(\Gamma)$ under some Hamiltonian $\mathcal{H}$ in phase space $\Gamma = dp_i \wedge dr_i \subseteq \mathbb{R}^{6N}$ is understood in the classical sense via the Liouville equation:

$$\frac{dA}{dt} = \{A, H\} = i\mathcal{L}A, \tag{2.1}$$

where $\mathcal{L}$ is the liouvillian operator, and $\{\cdot,\cdot\}$ is the usual Poisson bracket on the symplectic $6N$ dimensional phase space manifold $\Gamma$. Formally, the solution to this equation can be written in terms of a pseudo-differential operator of the liouvillian:

$$A(t) = e^{i\mathcal{L}t}A(0) \tag{2.2}$$

In the limit of infinite dilution (consistent with a low molarity electrolyte), the mean inter-ionic distance vastly exceeds the Bjerrum length of the fluid [20]. Under these assumptions, the Coulombic interactions between ions—already attenuated by the dielectric screening of the surrounding solvent molecules—become negligible compared to the thermal energy of the system ($\propto k_B T$). Consequently, one may assume ion-ion correlations to be near zero, allowing the system to be simply modeled as a collection

of $N-1$ neutral solvent particles (water) and a single tagged ion with an associated phase-space microstate $(\vec{r},\vec{p}) \in \Gamma$. Operating within this independent-particle regime is mathematically highly advantageous, and permits the rigorous derivation of the generalized ion-solvent drag dynamics without the confounding cross-correlations of collective ionic relaxation or electrophoretic retardation effects.

To isolate the dynamics of the tagged ion from the complex many-body Van der Waal interactions of the surrounding solvent, it is convenient to define a projection operator $\mathcal{P}_A$ on phase space. This explicitly decomposes the total Liouvillian evolution of the system into a resolved subspace spanned by the slow variables of the tagged ion, and an orthogonal subspace containing the fast and fluctuating degrees of freedom of the solvent bath. Formally, this involves the introduction of a natural inner product on the symplectic manifold. For a kinetic, thermodynamic system, the Bogoliubov inner product for two observables $X$ and $Y$ is a natural imposition, and it is precisely the thermal correlation function of the observables in NVT equilibrium [21]. Formally, the Bogoliubov product $(\cdot,\cdot)$ defines orthogonality such that two thermodynamically independent observables would be considered orthogonal.

$$(X,Y) = \langle X \otimes Y^T \rangle_{eq} = \frac{1}{\mathcal{Z}} \int d\Gamma e^{-\beta H(\Gamma)} (X \otimes Y) \tag{2.3}$$

where $\mathcal{Z} = \int d\Gamma e^{-\beta H(\Gamma)}$ is the canonical partition function, and $\beta = 1/(k_B T)$ is the corresponding inverse temperature. This idea is originally credited to Nikolay Bogoliubov, who laid the foundational physics of such kinetic theory by establishing the means to integrate out fast degrees of freedom and yield kinetic equations, and formally defining the mathematical inner product used to prove thermodynamic orthogonality [22]. One now may equip the $6N$ dimensional phase space $\Gamma$ with the Bogoliubov inner product, and define the canonical projection operator for an observable $A$ as $\mathcal{P}_A$. Let $X$ be some phase-space observable, then,

$$\mathcal{P}_A X = (X,A)(A,A)^{-1} A, \tag{2.4}$$

and let,

$$\mathcal{Q}_A = 1 - \mathcal{P}_A \tag{2.5}$$

be the complementary operator for ease in defining orthogonal subspaces—for the ion and solvent respectively. Note that these two operators satisfy the identity:

$$\mathcal{P}_A + \mathcal{Q}_A = \mathbf{1}, \tag{2.6}$$

where $\mathbf{1}$ is the identity operator. Now, one takes the Liouville equation 2.1, and splits the Liouvillian operator into equilibrium transport and external transport: $\mathcal{L} = \mathcal{L}_0 + \mathcal{L}_{ext}$. Here $\mathcal{L}_0$ is treated to govern internal forces and velocity preserving fields. Contrarily $\mathcal{L}_{ext}$ is defined for perturbative forces, such as the electric force $q_\alpha \vec{E}$, e.g. $i\mathcal{L}_{ext}\vec{p} = q_\alpha \vec{E}$, where $q_\alpha$ is the charge of the ion of species $\alpha$. Together, the Liouville equation of the tagged ion momentum—the primary subject of investigation—becomes

$$\frac{d\vec{p}}{dt} = i\mathcal{L}\vec{p}(t) = i\mathcal{L}_0\vec{p}(t) + i\mathcal{L}_{ext}\vec{p}(t) = i\mathcal{L}_0\vec{p}(t) + q\vec{E} \tag{2.7}$$

To avoid notational encumberment, the internal evolution of the momentum is treated independently, as the only external force is the electric force $q\vec{E}$. After sufficient work

in decomposition has been performed, the external driving force will be reintroduced. Treating the internal evolution now, the Liouville equation becomes

$$\frac{d\vec{p}}{dt} = i\mathcal{L}_0\vec{p}(t) = e^{i\mathcal{L}_0 t} i\mathcal{L}_0\vec{p}(0) \tag{2.8}$$

### 2.1.3 Dyson Decomposition of the Liouville Equation

Using the projector operator identity 2.6, one may decompose the evolution of the ion momentum $\vec{p}$ into orthogonal subspaces corresponding to field forces on the ion, $\mathcal{P}_{\vec{p}}$, and solvent forces, $\mathcal{Q}_{\vec{p}}$, on each phase subspace respectively.

$$\frac{d\vec{p}}{dt} = e^{i\mathcal{L}_0 t}(\mathcal{P}_{\vec{p}} + \mathcal{Q}_{\vec{p}}) i\mathcal{L}_0\vec{p}(0) = e^{i\mathcal{L}_0 t}(i\mathcal{L}_0\vec{p}, \vec{p})(\vec{p}, \vec{p})^{-1}\vec{p}(0) + e^{i\mathcal{L}_0 t}\mathcal{Q}_{\vec{p}} i\mathcal{L}_0\vec{p}(0) \tag{2.9}$$

Simplifying the notation by defining a frequency matrix $i\mathbf{\Omega} := (i\mathcal{L}_0\vec{p}, \vec{p})(\vec{p}, \vec{p})^{-1}$, and performing the Dyson decomposition (see C):

$$e^{i\mathcal{L}_0 t} = e^{i\mathcal{Q}_{\vec{p}}\mathcal{L}_0 t} + \int_0^t e^{i\mathcal{L}_0(t-\tau)}\mathcal{P}_{\vec{p}} i\mathcal{L}_0 e^{i\mathcal{Q}_{\vec{p}}\mathcal{L}_0\tau} d\tau \tag{2.10}$$

on the internal evolution operator $e^{i\mathcal{L}_0 t}$ into orthogonal dynamical subspaces, the internal Liouville equation 2.9 is written as

$$\frac{d\vec{p}}{dt} = i\mathbf{\Omega}\vec{p}(t) + \mathcal{Q}_{\vec{p}} i\mathcal{L}_0\vec{p}(t) + \left[\int_0^t e^{i\mathcal{L}_0(t-\tau)}\mathcal{P}_{\vec{p}} i\mathcal{L}_0 e^{i\mathcal{Q}_{\vec{p}} i\mathcal{L}_0\tau} d\tau\right] \mathcal{Q}_{\vec{p}} i\mathcal{L}_0\vec{p}(0). \tag{2.11}$$

Equation 2.11 is now decomposed into three terms. The first term describes the instantaneous, reversible, and non-dissipative interactions within the ion-solvent system. The frequency matrix determines the precise mechanism as to how the momentum enters the forcing term. The second term appears as a projection of the force on the ion into the solvent subspace, which considers all constituent forcing on the tagged ion imposed by the external solvent. By the Central Limit Theorem—since the net change in ion momentum is the sum of many ion-solvent collisions—one may assume the stochastic forcing to be a zero mean colored gaussian random process [23]:

$$\vec{\zeta}(t) =: \mathcal{Q}_{\vec{p}} i\mathcal{L}_0\vec{p}(t). \tag{2.12}$$

As the integral term also contains such a stochastic component $\vec{\zeta}(0) = e^{i\mathcal{L}_0\tau}\mathcal{Q}_{\vec{p}} i\mathcal{L}_0\vec{p}(0) = \mathcal{Q}_{\vec{p}} i\mathcal{L}_0\vec{p}(\tau)$, one may simplify this to gaussian noise as well.

$$\frac{d\vec{p}}{dt} = i\mathbf{\Omega}\vec{p}(t) + \vec{\zeta}(t) + \int_0^t (\vec{\zeta}(t), \vec{\zeta}(0))(\vec{p}(0), \vec{p}(0))^{-1}\vec{p}(t-\tau) d\tau \tag{2.13}$$

With the projection operator simplified and solvent noise definition applied, the integrand in 2.13 consists of a convolution between the scaled solvent noise autocorrelation and the tagged ion momentum. Defining the noise autocorrelation normalized by the Bogoliubov norm of the initial momentum as the memory kernel $\mathbf{K}(t) = (\vec{\zeta}(t), \vec{\zeta}(0))(\vec{p}(0), \vec{p}(0))^{-1}$, the standard Generalized Langevin Equation (GLE) with frequency matrix $i\Omega$, memory kernel $\mathbf{K}(t)$, and gaussian colored noise $\vec{\zeta}(t)$ is achieved.

$$\frac{d\vec{p}}{dt} = i\mathbf{\Omega}\vec{p}(t) + \vec{\zeta}(t) + \int_0^t \mathbf{K}(t)\vec{p}(t-\tau) d\tau \tag{2.14}$$

### 2.1.4 Physical Instantiation of the Generalized Langevin Dynamics

To determine the explicit frequency matrix $i\mathbf{\Omega}$ for the electrolyte exposed to external electromagnetic fields, the formal definition of the frequency matrix must be evaluated using the Bogoliubov inner product (defined in section 2.1.2). Specifically,

$$i\mathbf{\Omega} = (i\mathcal{L}_0\vec{p}, \vec{p})(\vec{p}, \vec{p})^{-1} = \langle i\mathcal{L}_0\vec{p} \otimes \vec{p}^T\rangle_{\text{eq}}\langle\vec{p} \otimes \vec{p}^T\rangle_{\text{eq}}^{-1}. \tag{2.15}$$

Within the Mori-Zwanzig projection formalism, the action of the unperturbed Liouvillian on the momentum, $i\mathcal{L}_0\vec{p} = \frac{d\vec{p}}{dt}$, represents the total internal microscopic force acting on the tagged ion [18, 19]. This force can be decomposed into the conservative interactions with the surrounding solvent molecules, $\vec{F}_{\text{sol}}$, and the Lorentz force exerted by the static external magnetic field $\vec{B}$. For an ion of species $\alpha$ with charge $q_\alpha$ and mass $m_\alpha$, the frequency matrix becomes

$$i\mathbf{\Omega} = \left[\langle\vec{F}_{\text{sol}} \otimes \vec{p}^T\rangle_{\text{eq}} + \frac{q_\alpha}{m_\alpha}\langle(\vec{p} \times \vec{B}) \otimes \vec{p}^T\rangle_{\text{eq}}\right]\langle\vec{p} \otimes \vec{p}^T\rangle_{\text{eq}}^{-1}. \tag{2.16}$$

In thermal equilibrium, the expectation value of the microscopic solvent forces vanishes ($\langle\vec{F}_{\text{sol}} \otimes \vec{p}^T\rangle_{\text{eq}} = \mathbf{0}$) due to parity constraints; the conservative solvent forces depend solely on spatial coordinates (which are even under time reversal), while momentum is odd. Consequenty, only contributions from the magnetic Lorentz force remain. To factor the cross product out of the canonical expectation value, it is convenient introduce the antisymmetric tensor $\mathbf{M}$, defined such that $\mathbf{M}\vec{p} = \vec{p} \times \vec{B}$:

$$\mathbf{M} = \begin{pmatrix} 0 & B_z & -B_y \\ -B_z & 0 & B_x \\ B_y & -B_x & 0 \end{pmatrix} \quad \Longleftrightarrow \quad \mathbf{M}\vec{p} = \vec{p} \times \vec{B}. \tag{2.17}$$

Substituting this tensor representation into the frequency matrix allows $\mathbf{M}$ to be factored out. Since the equilibrium momentum correlation matrix is strictly diagonal according to the equipartition theorem—yielding $\langle\vec{p} \otimes \vec{p}^T\rangle_{\text{eq}} = m_\alpha k_B T\mathbf{I}$, where $\mathbf{I}$ is the identity matrix—the correlation matrices perfectly cancel:

$$i\mathbf{\Omega} = \frac{q_\alpha}{m_\alpha}\mathbf{M}\langle\vec{p} \otimes \vec{p}^T\rangle_{\text{eq}}\langle\vec{p} \otimes \vec{p}^T\rangle_{\text{eq}}^{-1} = \frac{q_\alpha}{m_\alpha}\mathbf{M}, \tag{2.18}$$

and the frequency matrix enters the Generalized Langevin Equation (GLE) purely as the scaled magnetic rotation operator representing the Lorentz force.

Similarly, the structure and action of the memory kernel $\mathbf{K}(t)$ on the momentum can be simplified. According to the second fluctuation-dissipation theorem, the memory matrix is defined by the normalized auto-correlation of the orthogonal fluctuating solvent forces $\vec{\zeta}(t)$ [24]. Under the assumption of an isotropic fluid, the fluctuating forces are uncorrelated across distinct spatial dimensions. The memory kernel is therefore diagonal and directly proportional to the momentum covariance. Explicitly,

$$\mathbf{K}(t) = \langle\vec{\zeta}(t) \otimes \vec{\zeta}(0)\rangle_{\text{eq}}\langle\vec{p}(0) \otimes \vec{p}(0)\rangle_{\text{eq}}^{-1} = \left(m_\alpha k_B T K(t)\mathbf{I}\right)\left(\frac{1}{m_\alpha k_B T}\mathbf{I}\right) = K(t)\mathbf{I}. \tag{2.19}$$

This allows the tensorial memory matrix $\mathbf{K}(t)$ to be replaced by a single scalar memory function $K(t)$ corresponding to its diagonal entries.

To complete the physical description of the driven system, the external electric field $\vec{E}$ must be reintroduced. As the electric field acts as an external driving force that explicitly breaks thermodynamic equilibrium, it is absent from the unperturbed equilibrium Liouvillian $\mathcal{L}_0$ and must be added deterministically to the equations of motion.

Furthermore, the standard GLE implicitly assumes a stationary background fluid. To ensure Galilean invariance and properly couple the kinetic dynamics to the macroscopic fluid hydrodynamics, the phenomenological drag must depend on the relative phase-space velocity. The tagged ion velocity $\vec{v}(\tau)$ is therefore shifted to $\vec{v}(\tau)-\vec{u}(\tau)$, where $\vec{u}(\tau)$ represents the local macroscopic bulk velocity of the solvent. Dividing the momentum evolution equation by the mass $m_\alpha$ yields the final driven, Galilean-invariant GLE for the electromagnetized tagged ion:

$$\frac{d\vec{v}}{dt} = \frac{q_\alpha}{m_\alpha}\left(\vec{E} + \vec{v} \times \vec{B}\right) - \int_0^t K_\alpha(t-\tau)[\vec{v}(\tau) - \vec{u}(\tau)]d\tau + \frac{1}{m_\alpha}\vec{\zeta}(t) \tag{2.20}$$

From a completely microscopic perspective of a single tagged ion, one could view equation 2.20 as a complete stochastic description of the dynamical behavior of a single tagged ion. To transition to a mesoscopic distributional picture, it is now necessary to perform a Vlasov mean field approximation and coarse graining of the equations of motion to a full electrolytic system of many electromagnetized ions.

## 2.2 Mesocopic Klimontovich Coarse-Graining of Microscopic Dynamics

### 2.2.1 Fine-Grained Klimontovich Distribution

Having now established the Generalized Langevin Equation (GLE) for the single tagged ion, the analysis is extended to a macroscopic system comprising of $N$ identical ions of generalized species $\alpha$. To describe the exact microstate configuration of this $N$-particle system, one must define an empirical, fine-grained phase-space density $N_\alpha$, often called the Klimontovich density after Yuri L'vovich Klimontovich's groundbreaking work on the theory of microscopic fluctiations [25, 26]. This distribution is constructed as a superposition of Dirac delta ($\delta$) functions, formulaically representing the sharply localized ion trajectories in the now $6N$-dimensional phase space:

$$N_\alpha(\vec{r}_\alpha, \vec{v}_\alpha, t) = \sum_{i=1}^{N} \delta(\vec{r}_\alpha - \vec{r}_{i,\alpha}(t))\delta(\vec{v}_\alpha - \vec{v}_{i,\alpha}(t)). \tag{2.21}$$

In the assumed canonical (NVT) ensemble over which the Bogoliubov product is defined, the total particle number $N$ is conserved throughout temporal evolution. Resultantly, the discrete Klimontovich phase-space density must strictly obey a continuity equation: In the context of plasma physics and kinetic theory, this exact microscopic conservation law is known as the Klimontovich equation [27].

$$\frac{\partial N_\alpha}{\partial t} + \vec{v}_\alpha \cdot \nabla_{\vec{r}_\alpha} N_\alpha + \nabla_{\vec{v}_\alpha} \cdot (\dot{\vec{v}}_\alpha N_\alpha) = 0. \tag{2.22}$$

To impose the previously derived stochastic dynamics of each ion, the explicit acceleration term $\dot{\vec{v}}_\alpha$ is replaced according to the derived GLE 2.20. Substituting this dynamic constraint into Equation 2.22 explicitly couples the microscopic particle conservation to the underlying non-Markovian, nonequilibrium stochastic dynamics, yielding an exact stochastic partial differential equation (SPDE) for the fine-grained density $N_\alpha$:

$$\frac{\partial N_\alpha}{\partial t} + \vec{v}_\alpha \cdot \nabla_{\vec{r}_\alpha} N_\alpha + \nabla_{\vec{v}_\alpha} \cdot \left[ \left( \frac{q_\alpha}{m_\alpha}(\vec{E} + \vec{v}_\alpha \times \vec{B}) - \int_0^t K_\alpha(t-\tau)[\vec{v}_\alpha(\tau) - \vec{u}(\tau)]d\tau + \frac{1}{m_\alpha}\vec{\zeta}(t) \right) N_\alpha \right] = 0. \tag{2.23}$$

### 2.2.2 Coarse-Graining to the Mesoscopic Picture via Ensemble Averaging

As the fine-grained density $N_\alpha$ is highly singular and fundamentally stochastic, it is mathematically incompatible with the mean field solvent description of the Navier-Stokes equations, and is thereby intractable for the direct macroscopic hydrodynamic coupling which is to be performed. Consequently, a transition to the mesoscopic regime is required via a mean-field approximation of the fine-grained density. By taking the thermodynamic ensemble average over the stochastic realizations of the noise and initial conditions, one may define the smooth, continuous phase space distribution function $f_\alpha$:

$$f_\alpha(\vec{r}_\alpha, \vec{v}_\alpha, t) := \langle N_\alpha(\vec{r}_\alpha, \vec{v}_\alpha, t) \rangle_{\text{eq}}. \tag{2.24}$$

Applying this ensemble average to the Klimontovich-GLE equation 2.23—and operating under the previously established infinite dilution limit where bare ion-ion Coulombic interactions are fully screened—results in the following averaged kinetic density equation:

$$\begin{aligned} &\frac{\partial f_\alpha}{\partial t} + \langle \vec{v}_\alpha \cdot \nabla_{\vec{r}_\alpha} N_\alpha \rangle_{\text{eq}} + \frac{q_\alpha}{m_\alpha} \langle \nabla_{\vec{v}_\alpha} \cdot (\vec{E} + \vec{v}_\alpha \times \vec{B}) N_\alpha \rangle_{\text{eq}} \\ &= \langle \nabla_{\vec{v}_\alpha} \cdot \int_0^t K_\alpha(t-\tau)[\vec{v}_\alpha(\tau) - \vec{u}(\tau)] N_\alpha d\tau \rangle_{\text{eq}} - \frac{1}{m_\alpha} \nabla_{\vec{v}_\alpha} \cdot \langle \vec{\zeta}(t) N_\alpha(t) \rangle_{\text{eq}}. \end{aligned} \tag{2.25}$$

To accurately evaluate the remaining equilibrium expectations in equation 2.25, it is crucial to establish a strict notational distinction: $\vec{v}_\alpha$ denotes the independent Eulerian phase-space coordinate, whereas $\vec{v}_\alpha(t)$ (or $\vec{v}_\alpha(\tau)$) represents the Lagrangian stochastic trajectory of the particle. Since the Eulerian phase-space coordinates $\vec{r}_\alpha$ and $\vec{v}_\alpha$ are deterministic, the spatial and velocity gradient operators commute with the ensemble average. Consequently, the drift term simplifies directly:

$$\langle \vec{v}_\alpha \cdot \nabla_{\vec{r}_\alpha} N_\alpha \rangle_{\text{eq}} = \vec{v}_\alpha \cdot \nabla_{\vec{r}_\alpha} f_\alpha. \tag{2.26}$$

Similarly, the external DC electric and magnetic fields, $\vec{E}$ and $\vec{B}$, are treated as macroscopic, deterministic constants. Furthermore, since the divergence of the magnetic Lorentz force with respect to the velocity coordinate vanishes identically ($\nabla_{\vec{v}_\alpha} \cdot (\vec{v}_\alpha \times \vec{B}) = 0$), the force operator can be pulled through the derivative and the ensemble expectation value:

$$\frac{q_\alpha}{m_\alpha} \langle \nabla_{\vec{v}_\alpha} \cdot (\vec{E} + \vec{v}_\alpha \times \vec{B}) N_\alpha \rangle_{\text{eq}} = \frac{q_\alpha}{m_\alpha} \left( \vec{E} + \vec{v}_\alpha \times \vec{B} \right) \cdot \nabla_{\vec{v}_\alpha} f_\alpha. \tag{2.27}$$

The evaluation of the memory kernel expectation requires more care. As the GLE describes non-Markovian, subdiffusive dynamics, the current microstate of the fluid depends inherently on its past trajectory. Consequently, the stochastic particle velocity $\vec{v}_\alpha(\tau)$ and the fine-grained distribution $N_\alpha(t)$ at future time $t$ cannot be assumed statistically independent. To formalize this delayed hydrodynamic feedback, it is necessary to introduce a two-time phase-space correlation function, defined as $\vec{F}_\alpha^{(2)}(\vec{r}_\alpha, \vec{v}_\alpha, t; \tau) := \langle \vec{v}_\alpha(\tau) N_\alpha(t) \rangle_{\text{eq}}$. Applying this definition, alongside the deterministic nature of the macroscopic solvent velocity $\vec{u}(\tau)$, the integral memory kernel operator expands as follows:

$$
\begin{aligned}
&\langle \nabla_{\vec{v}_\alpha} \cdot \int_0^t K_\alpha(t-\tau)[\vec{v}_\alpha(\tau) - \vec{u}(\tau)] N_\alpha d\tau \rangle_{\text{eq}} \\
&= \nabla_{\vec{v}_\alpha} \cdot \int_0^t K_\alpha(t-\tau) \langle [\vec{v}_\alpha(\tau) - \vec{u}(\tau)] N_\alpha \rangle_{\text{eq}} d\tau \\
&= \nabla_{\vec{v}_\alpha} \cdot \int_0^t K_\alpha(t-\tau) \left[ \langle \vec{v}_\alpha(\tau) N_\alpha \rangle_{\text{eq}} - \vec{u}(\tau) \langle N_\alpha \rangle_{\text{eq}} \right] d\tau \qquad (2.28) \\
&= \nabla_{\vec{v}_\alpha} \cdot \int_0^t K_\alpha(t-\tau) \left[ \vec{F}_\alpha^{(2)}(\vec{r}_\alpha, \vec{v}_\alpha, t; \tau) - \vec{u}(\tau) f_\alpha \right] d\tau. \qquad (2.29)
\end{aligned}
$$

Last to be considered is the noise-distribution correlation on the right side of the equality: $-\frac{1}{m_\alpha} \nabla_{\vec{v}_\alpha} \cdot \langle \vec{\zeta}(t) N_\alpha(t) \rangle_{\text{eq}}$. Since the empirical fine-grained density $N_\alpha(t)$ is a functional that implicitly contains the entire integrated history of the random gaussian colored noise forces up to time $t$, standard statistical factorization is impossible. However, operating under the assumption that the colored noise $\vec{\zeta}(t)$ is a Gaussian random process, this term can be systematically decomposed using the Furutsu-Novikov theorem [28, 29].

**Theorem 2.2.1** (Furustu-Novikov) *Given a colored Gaussian vector field $\vec{\zeta}(t)$ and a functional $N_\alpha(t)$, the correlation between the Gaussian noise term and the functional is given by*

$$
\langle \vec{\zeta}(t) N_\alpha(t) \rangle = \int_0^t \langle \vec{\zeta}(t) \otimes \vec{\zeta}(\tau) \rangle \cdot \left\langle \frac{\delta N_\alpha}{\delta \vec{\zeta}(\tau)} \right\rangle d\tau, \qquad (2.30)
$$

*where $\frac{\delta N_\alpha}{\delta \vec{\zeta}(\tau)}$ denotes the variational derivative of the function with respect to $\vec{\zeta}$.*

To apply this theorem, the functional derivative of the Klimontovich density with respect to the noise history must be explicitly computed. Applying the chain rule to the spatial and velocity dependencies of $N_\alpha$ yields:

$$
\delta N_\alpha = -\nabla_{\vec{r}_\alpha} N_\alpha \cdot \delta \vec{r}_\alpha(t) - \nabla_{\vec{v}_\alpha} N_\alpha \cdot \delta \vec{v}_\alpha(t). \qquad (2.31)
$$

Dividing by the noise variation isolates the functional derivatives:

$$
\frac{\delta N_\alpha}{\delta \vec{\zeta}(\tau)} = -\nabla_{\vec{r}_\alpha} N_\alpha \frac{\delta \vec{r}_\alpha(t)}{\delta \vec{\zeta}(\tau)} - \nabla_{\vec{v}_\alpha} N_\alpha \frac{\delta \vec{v}_\alpha(t)}{\delta \vec{\zeta}(\tau)}. \qquad (2.32)
$$

It is mathematically convenient to define response tensors that capture the deterministic sensitivity of the particle trajectory to historical stochastic noise fluctuations. Formally, these can be thought of as Green's functions under evolution governed by the SPDE 2.25:

$$
\mathbf{G}(t, \tau) := \frac{\delta \vec{v}_\alpha(t)}{\delta \vec{\zeta}(\tau)}, \qquad \mathbf{H}(t, \tau) := \frac{\delta \vec{r}_\alpha(t)}{\delta \vec{\zeta}(\tau)}. \qquad (2.33)
$$

Note that the exact kinematic relation $\dot{\vec{r}}_\alpha = \vec{v}_\alpha$ rigorously couples position and velocity, so the spatial response tensor $\mathbf{H}(t,\tau)$ is fundamentally defined as the time-integral of the velocity response tensor $\mathbf{G}(t,\tau)$, e.g:

$$\mathbf{H}(t,\tau) = \int_\tau^t \mathbf{G}(s,\tau)\, ds. \tag{2.34}$$

Taking the ensemble average of the functional derivative and applying the definition of the macroscopic distribution from 2.24 simplifies the expression to:

$$\left\langle \frac{\delta N_\alpha}{\delta \vec{\zeta}(\tau)} \right\rangle = -\nabla_{\vec{r}_\alpha} f_\alpha \cdot \mathbf{H}(t,\tau) - \nabla_{\vec{v}_\alpha} f_\alpha \cdot \mathbf{G}(t,\tau). \tag{2.35}$$

Substituting this variation back into the Furutsu-Novikov integral yields the full noise-distribution correlation:

$$\langle \vec{\zeta}(t) N_\alpha(t) \rangle = -\int_0^t \langle \vec{\zeta}(t) \otimes \vec{\zeta}(\tau) \rangle \cdot \left[ \mathbf{H}(t,\tau) \cdot \nabla_{\vec{r}_\alpha} f_\alpha + \mathbf{G}(t,\tau) \cdot \nabla_{\vec{v}_\alpha} f_\alpha \right] d\tau. \tag{2.36}$$

By invoking the second fluctuation-dissipation theorem again, which explicitly equates the noise covariance to the physical memory kernel via $\langle \vec{\zeta}(t) \otimes \vec{\zeta}(\tau) \rangle = m_\alpha k_B T K_\alpha(|t-\tau|)\mathbf{1}$, the explicit form of the correlation is obtained without noise as:

$$\langle \vec{\zeta}(t) N_\alpha(t) \rangle = -m_\alpha k_B T \int_0^t K_\alpha(t-\tau) \left[ \mathbf{H}(t,\tau) \cdot \nabla_{\vec{r}_\alpha} f_\alpha + \mathbf{G}(t,\tau) \cdot \nabla_{\vec{v}_\alpha} f_\alpha \right] d\tau. \tag{2.37}$$

Reintroducing the mass scalar and the velocity divergence operator yields the final resolved form of the stochastic forcing term:

$$\frac{-1}{m_\alpha} \nabla_{\vec{v}_\alpha} \cdot \langle \vec{\zeta}(t) N_\alpha(t) \rangle = k_B T \nabla_{\vec{v}_\alpha} \cdot \int_0^t K_\alpha(t-\tau) \left[ \mathbf{H}(t,\tau) \cdot \nabla_{\vec{r}_\alpha} f_\alpha + \mathbf{G}(t,\tau) \cdot \nabla_{\vec{v}_\alpha} f_\alpha \right] d\tau. \tag{2.38}$$

Inserting this resolved correlation operator and the prior deterministic expectations back into the averaged continuity equation yields the final, closed non-Markovian kinetic equation. This partial integro-differential equation completely governs the coarse-grained phase-space evolution of the electromagnetized ionic species $\alpha$, and no longer explicitly contains a term stochastic in $t$:

$$\begin{aligned} &\frac{\partial f_\alpha}{\partial t} + \vec{v}_\alpha \cdot \nabla_{\vec{r}_\alpha} f_\alpha + \frac{q_\alpha}{m_\alpha} (\vec{E} + \vec{v}_\alpha \times \vec{B}) \cdot \nabla_{\vec{v}_\alpha} f_\alpha \\ &= \nabla_{\vec{v}_\alpha} \cdot \int_0^t K_\alpha(t-\tau) [\vec{F}_\alpha^{(2)}(\vec{r}_\alpha, \vec{v}_\alpha, t; \tau) - \vec{u}(\tau) f_\alpha]\, d\tau \\ &+ k_B T \nabla_{\vec{v}_\alpha} \cdot \int_0^t K_\alpha(t-\tau) \left[ \mathbf{H}(t,\tau) \cdot \nabla_{\vec{r}_\alpha} f_\alpha + \mathbf{G}(t,\tau) \cdot \nabla_{\vec{v}_\alpha} f_\alpha \right] d\tau. \end{aligned} \tag{2.39}$$

Note that equation 2.39 is a precise instance of a Boltzmann equation for the ion densities, which describes the precise subdiffusive evolution in velocity and position space. The left hand side of the equation consists explicitly of the usual streaming terms and temporal variation consistent with the Lorentz force, and the right hand side is a precise collision operator specific to the electrolytic system. As a mathematical framework, this equation can be treated immediately, however it is instructive and

physically relevant to ensure that this this formulation does not violate the second law of thermodynamics. To do so, one must prove that the local entropy production remains non-negative. By taking the appropriate moments of the collision operator, and applying the Boltzmann H-theorem for the relative entropy of the coarse grained distribution,

$$H_{rel}(t) = \int f_\alpha(\vec{v}, t) \ln\left(\frac{f_\alpha(\vec{v}, t)}{f_{\alpha,eq}(\vec{v})}\right) d\vec{v}, \tag{2.40}$$

where $f_{\alpha,eq}$ is the equilibrium distribution—demonstrated to be the usual Maxwellian under 2.39—thermodynamic consistency is explicitly demonstrated through a thorough, rigorous derivation (See D).

## 2.3 Macroscopic Ion Transport and Navier-Stokes Coupling

### 2.3.1 Bulk Flow Assumption Imposition

To determine the asymptotic macroscopic behavior of the ion and solvent velocities, it is necessary to transition from the mesoscopic kinetic description to a macroscopic hydrodynamic framework. This is achieved by taking the first velocity moment of the derived kinetic equation (Eq. 2.39). The macroscopic number density $n_\alpha$ and the mean bulk velocity $\vec{V}_\alpha$ of ion species $\alpha$ are formally defined as the zeroth and first velocity moments of the distribution function, respectively:

$$\begin{aligned} n_\alpha(\vec{r}_\alpha, t) &= \int f_\alpha(\vec{r}_\alpha, \vec{v}_\alpha, t) d^3 v_\alpha, \\ \vec{V}_\alpha(\vec{r}_\alpha, t) &= \frac{1}{n_\alpha} \int \vec{v}_\alpha f_\alpha(\vec{r}_\alpha, \vec{v}_\alpha, t) d^3 v_\alpha. \end{aligned} \tag{2.41}$$

Multiplying the full kinetic equation by the microscopic momentum $m_\alpha \vec{v}_\alpha$ and integrating over all velocity space yields the general macroscopic momentum balance equation:

$$\int m_\alpha \vec{v}_\alpha \left(\frac{\partial f_\alpha}{\partial t} + \vec{v}_\alpha \cdot \nabla_{\vec{r}_\alpha} f_\alpha + \frac{q_\alpha}{m_\alpha}(\vec{E} + \vec{v}_\alpha \times \vec{B}) \cdot \nabla_{\vec{v}_\alpha} f_\alpha\right) d^3 v_\alpha = \int m_\alpha \vec{v}_\alpha \, \mathcal{R}_\alpha \, d^3 v_\alpha, \tag{2.42}$$

where $\mathcal{R}_\alpha$ denotes the right-hand side of Eq. 2.39 containing the memory and noise correlation operators. Each term in this integro-differential equation must be evaluated independently. Beginning with the temporal derivative, the integration over velocity space commutes with the partial time derivative, directly yielding the rate of change of the macroscopic momentum density:

$$\int m_\alpha \vec{v}_\alpha \frac{\partial f_\alpha}{\partial t} d^3 v_\alpha = \frac{\partial}{\partial t} \int m_\alpha \vec{v}_\alpha f_\alpha d^3 v_\alpha = \frac{\partial}{\partial t}(m_\alpha n_\alpha \vec{V}_\alpha). \tag{2.43}$$

The advective streaming term is resolved by decomposing the microscopic velocity into the macroscopic bulk flow and a fluctuating thermal component. Defining the

kinetic pressure tensor as $\mathbf{P}_\alpha = m_\alpha \int (\vec{v}_\alpha - \vec{V}_\alpha) \otimes (\vec{v}_\alpha - \vec{V}_\alpha) f_\alpha d^3 v_\alpha$, the spatial divergence evaluates exactly to the sum of the convective momentum transport and the pressure gradient:

$$\int m_\alpha \vec{v}_\alpha (\vec{v}_\alpha \cdot \nabla_{\vec{r}_\alpha} f_\alpha) d^3 v_\alpha = \nabla_{\vec{r}_\alpha} \cdot (m_\alpha n_\alpha \vec{V}_\alpha \otimes \vec{V}_\alpha + \mathbf{P}_\alpha). \tag{2.44}$$

Evaluation of the Lorentz force term requires integration by parts over velocity space. Under the physical assumption that the distribution function rapidly vanishes at infinite velocities ($f_\alpha \to 0$ as $|\vec{v}_\alpha| \to \infty$), the boundary surface terms evaluate to zero. Because the velocity divergence of the magnetic rotation operator is zero ($\nabla_{\vec{v}_\alpha} \cdot (\vec{v}_\alpha \times \vec{B}) = 0$), the integral simplifies precisely to the macroscopic volumetric force density:

$$\int q_\alpha \vec{v}_\alpha (\vec{E} + \vec{v}_\alpha \times \vec{B}) \cdot \nabla_{\vec{v}_\alpha} f_\alpha \, d^3 v_\alpha = -q_\alpha n_\alpha \left( \vec{E} + \vec{V}_\alpha \times \vec{B} \right). \tag{2.45}$$

Evaluating the first moment of the non-Markovian memory integral requires isolating the macroscopic variables from the velocity divergence. It is mathematically convenient to define a shorthand vector functional representing the integral contents: $\vec{X}_\alpha := \int_0^t K_\alpha(t-\tau) \left[ \vec{F}_\alpha^{(2)}(\vec{r}_\alpha, \vec{v}_\alpha, t; \tau) - \vec{u}(\tau) f_\alpha \right] d\tau$. Applying the standard vector identity $\nabla_{\vec{v}_\alpha} \cdot (\vec{v}_\alpha \otimes \vec{X}_\alpha) = \vec{v}_\alpha (\nabla_{\vec{v}_\alpha} \cdot \vec{X}_\alpha) + \vec{X}_\alpha$ and integrating over velocity space yields:

$$\int \nabla_{\vec{v}_\alpha} \cdot (\vec{v}_\alpha \otimes \vec{X}_\alpha) d^3 v_\alpha = \int \vec{v}_\alpha (\nabla_{\vec{v}_\alpha} \cdot \vec{X}_\alpha) d^3 v_\alpha + \int \vec{X}_\alpha d^3 v_\alpha. \tag{2.46}$$

By applying the divergence theorem, the left-hand side converts to a surface integral over the velocity-space boundary at infinity. Under the assumption that the correlations decay rapidly at large velocities ($\vec{X}_\alpha \to 0$ as $|\vec{v}_\alpha| \to \infty$), this boundary integral vanishes, imposing the strict mathematical relation:

$$\int \vec{v}_\alpha (\nabla_{\vec{v}_\alpha} \cdot \vec{X}_\alpha) d^3 v_\alpha = -\int \vec{X}_\alpha d^3 v_\alpha. \tag{2.47}$$

Applying this identity to the explicit memory kernel term shifts the integration onto the internal functional components:

$$\begin{aligned} m_\alpha \int \vec{v}_\alpha \left( \nabla_{\vec{v}_\alpha} \cdot \int_0^t K_\alpha(t-\tau) \left[ \vec{F}_\alpha^{(2)}(\vec{r}_\alpha, \vec{v}_\alpha, t; \tau) - \vec{u}(\tau) f_\alpha \right] d\tau \right) d^3 v_\alpha = -\int \vec{X}_\alpha d^3 v_\alpha \\ = -m_\alpha \int_0^t K_\alpha(t-\tau) \left[ \int \vec{F}_\alpha^{(2)} d^3 v_\alpha - \vec{u}(\tau) \int f_\alpha d^3 v_\alpha \right] d\tau. \end{aligned} \tag{2.48}$$

By the definition of the Klimontovich density, integrating over velocity space yields the microscopic spatial density: $\int N_\alpha(\vec{r}_\alpha, \vec{v}_\alpha, t) d^3 v_\alpha = n_\alpha(\vec{r}_\alpha, t)$. Consequently, the integrated two-time phase-space correlation reduces to a macroscopic density-velocity correlation, defined as $M_\alpha^{(2)}(\vec{r}_\alpha, t; \tau) := \langle \vec{v}_\alpha(\tau) n_\alpha(\vec{r}_\alpha, t) \rangle$. Treating $\vec{v}_\alpha(\tau)$ explicitly as a stochastic Lagrangian trajectory rather than an Eulerian coordinate, the memory term simplifies to:

$$-m_\alpha \int_0^t K_\alpha(t-\tau) M_\alpha^{(2)}(\vec{r}_\alpha, t; \tau) d\tau + m_\alpha n_\alpha \int_0^t K_\alpha(t-\tau) \vec{u}(\tau) d\tau. \tag{2.49}$$

The final term to evaluate is the distribution-noise correlation derived via the Furutsu-Novikov theorem. Applying the same divergence identity established above, the velocity moment of the noise correlation simplifies to:

$$\begin{aligned}&-k_B T m_\alpha \int \vec{v}_\alpha \left( \nabla_{\vec{v}_\alpha} \cdot \int_0^t K_\alpha(t-\tau) \mathbf{G}(t,\tau) \cdot \nabla_{\vec{v}_\alpha} f_\alpha \, d\tau \right) d^3 v_\alpha \\ =&k_B T m_\alpha \int_0^t K_\alpha(t-\tau) \left( \int \mathbf{G}(t,\tau) \cdot \nabla_{\vec{v}_\alpha} f_\alpha \, d^3 v_\alpha \right) d\tau. \end{aligned} \tag{2.50}$$

It can be shown rigorously that the inner velocity-space integral vanishes. Applying integration by parts to this inner term yields:

$$\int \mathbf{G}(t,\tau) \cdot \nabla_{\vec{v}_\alpha} f_\alpha \, d^3 v_\alpha = \int \nabla_{\vec{v}_\alpha} \cdot (f_\alpha \mathbf{G}) \, d^3 v_\alpha - \int f_\alpha (\nabla_{\vec{v}_\alpha} \cdot \mathbf{G}) \, d^3 v_\alpha. \tag{2.51}$$

By the divergence theorem, the first term vanishes due to the asymptotic decay of $f_\alpha$ at infinity. The second term vanishes because the response tensor $\mathbf{G}(t,\tau)$ does not depend explicitly on the velocity coordinate $\vec{v}_\alpha$. Within the framework of the Generalized Langevin Equation, $\mathbf{G}$ represents the deterministic functional response of the particle trajectory to the colored Gaussian noise. Since the underlying stochastic dynamics are linear with respect to the noise forces, the functional derivative produces a coordinate-independent response matrix, rendering $\nabla_{\vec{v}_\alpha} \cdot \mathbf{G} = 0$. Assembling all evaluated moments yields the general macroscopic momentum transport equation for an electromagnetically driven, non-Markovian electrolyte, completely independent of any spatial homogeneity assumptions:

$$\begin{aligned}&\frac{\partial}{\partial t}(m_\alpha n_\alpha \vec{V}_\alpha) + \nabla_{\vec{r}_\alpha} \cdot (m_\alpha n_\alpha \vec{V}_\alpha \otimes \vec{V}_\alpha + \mathbf{P}_\alpha) - q_\alpha n_\alpha (\vec{E} + \vec{V}_\alpha \times \vec{B}) \\ =& -m_\alpha \int_0^t K_\alpha(t-\tau) M_\alpha^{(2)}(\vec{r}_\alpha, t; \tau) d\tau + m_\alpha n_\alpha \int_0^t K_\alpha(t-\tau) \vec{u}(\tau) d\tau. \end{aligned} \tag{2.52}$$

### 2.3.2 Spatially Homogeneous Integro-Differential Bulk Dynamics

To explicitly isolate the transient and asymptotic dynamics of the bulk ionic flow, one may invoke the assumption of spatial homogeneity. Under isothermal (NVT) conditions in an infinite or periodic bulk fluid, spatial gradients vanish. This guarantees that the density profile is flat ($\nabla_{\vec{r}_\alpha} n_\alpha = 0$), implying $n_\alpha(\vec{r}_\alpha, t) = n_\alpha \in \mathbb{R}$. Consequently, the divergences of both the convective momentum flux and the pressure tensor are exactly zero: $\nabla_{\vec{r}_\alpha} \cdot (m_\alpha n_\alpha \vec{V}_\alpha \otimes \vec{V}_\alpha + \mathbf{P}_\alpha) = 0$. Furthermore, the spatial uniformity of the number density allows it to be factored out of the macroscopic two-time correlation function:

$$M_\alpha^{(2)}(\vec{r}_\alpha, t; \tau) = \langle \vec{v}_\alpha(\tau) n_\alpha \rangle = n_\alpha \langle \vec{v}_\alpha(\tau) \rangle = n_\alpha \vec{V}_\alpha(\tau). \tag{2.53}$$

Applying these uniform bulk-flow constraints to Eq. 2.52 and dividing out the constant mass and density parameters reduces the system to a fundamental linear integro-differential equation governing the macroscopic bulk velocity of the ionic species:

$$\boxed{\frac{d\vec{V}_\alpha}{dt} = \frac{q_\alpha}{m_\alpha} \left( \vec{E} + \vec{V}_\alpha \times \vec{B} \right) - \int_0^t K_\alpha(t-\tau) \left[ \vec{V}_\alpha(\tau) - \vec{u}(\tau) \right] d\tau.} \tag{2.54}$$

### 2.3.3 Macroscopic Navier Stokes Solvent Drag Coupling

Note that in equation 2.54 the bulk solvent velocity, $\vec{u}(t)$, is directly referenced. To properly describe the coupled dynamics, one must introduce another PDE to describe such solvent dynamics, namely, the Navier-Stokes equation [5, 30]. As this derivation operates under bulk flow and mean-field assumptions, one may drop many of the extra terms, and assume that the velocity landscape of the solvent has no curvature. Doing so, the Navier Stokes equation for the solvent in the mean field picture simplifies to a manifestation of a density-picture Newton's second law:

$$\rho_{sol}\frac{d\vec{u}}{dt} = \vec{F}_{ext}, \tag{2.55}$$

where $\rho_{sol}$ is the mass density of the solvent, and $\vec{F}_{ext}$ is the external forcing on the solvent. In the case of our ion-solvent electrolyte system, this external force would be exactly the drag of the ions on the solvent, introduced through the memory kernel and relative velocity in 2.54. Note that in the coarse grained picture, water molecules are exactly electroneutral and do not interact via a magnetic moment, so no magnetic nor electric Lorentz contributions to the external force arise in the solvent mean field picture. Replacing $\vec{F}_{ext}$ with the drag term summed for each ion species $\alpha$, the two equations reduce to a first order system of integro-differential equations of the velocity. Explicitly, the dynamics of the arbitrary species, spatially homogeneous, electrolytic system are given by:

$$\frac{d\vec{V}_\alpha}{dt} = \frac{q_\alpha}{m_\alpha}\left(\vec{E} + \vec{V}_\alpha \times \vec{B}\right) - \int_0^t K_\alpha(t-\tau)\left[\vec{V}_\alpha(\tau) - \vec{u}(\tau)\right]d\tau \tag{2.56}$$

$$\rho_{sol}\frac{d\vec{u}}{dt} = \sum_\alpha m_\alpha n_\alpha \int_0^t K_\alpha(t-\tau)\left[\vec{V}_\alpha(\tau) - \vec{u}(\tau)\right]d\tau \tag{2.57}$$

Solving this system of coupled, linear Volterra integro-differential equations of the convolution type yields the precise bulk flow behavior of an electromagnetized electrolytic fluid. While it was managed to obtain an analytic description of transient behavior, the process is incredibly cumbersome. One such method of solution requires an explicit treatment of the Laplace transformed system of nine equations, algebraic inversion of the system via Schur complementation, and explicit inverse Laplace transformation for the analytic result. While such a derivation is analytically tractable, meaningful results are memory kernel and initial-condition dependent, and such transient behavior decays on very short timescales. Therefore, an asymptotic analysis of this system is much more informative, and demonstrates emergent observable properties of the macroscopic electrolytic fluid dynamics. For analytical tractability, a simplified two-species acqueous ionic system is considered, however all methodology employed in Chapter 3 is applicable for more general systems.

# 3 Analytic Analysis

## 3.1 Asymptotics of the Volterra System

### 3.1.1 Laplace Transform of the Integro-Differential System

Consider a binary symmetric electrolyte characterized by equivalent ionic masses $m_+ = m_- = m$, symmetric number densities $n_+ = n_- = n$, identical non-Markovian friction memory kernels $K_+(t) = K_-(t) = K(t)$, and strictly opposite charges $q_\pm = \pm q$. The system is subjected to orthogonal external fields, specifically a transverse electric field $\vec{E} = E_x\hat{x}$ and a longitudinal magnetic field $\vec{B} = B_z\hat{z}$. Assuming the fluid is initially at rest, such that $\vec{V}_+(0) = \vec{V}_-(0) = \vec{u}(0) = 0$, the macroscopic momentum equations for the two ionic species and the solvent take the form:

$$m\frac{d\vec{V}_+}{dt} = q(\vec{E} + \vec{V}_+ \times \vec{B}) - m\int_0^t K(t-\tau)[\vec{V}_+(\tau) - \vec{u}(\tau)]d\tau, \tag{3.1}$$

$$m\frac{d\vec{V}_-}{dt} = -q(\vec{E} + \vec{V}_- \times \vec{B}) - m\int_0^t K(t-\tau)[\vec{V}_-(\tau) - \vec{u}(\tau)]d\tau, \tag{3.2}$$

$$\rho_{\text{sol}}\frac{d\vec{u}}{dt} = mn\int_0^t K(t-\tau)[(\vec{V}_+(\tau) + \vec{V}_-(\tau)) - 2\vec{u}(\tau)]d\tau. \tag{3.3}$$

To analytically decouple the intrinsic ionic dynamics from the bulk solvent motion, the system is transformed into relative and center-of-mass coordinates. Defining the relative ionic velocity and ionic center of mass velocity as $\vec{V}_{\text{rel}} = \vec{V}_+ - \vec{V}_-$ and $\vec{V}_{\text{cm}} = \frac{1}{2}(\vec{V}_+ + \vec{V}_-)$, taking the difference and sum of the respective ionic momentum equations yields a transformed system:

$$m\frac{d\vec{V}_{\text{rel}}}{dt} = 2q\vec{E} + 2q(\vec{V}_{\text{cm}} \times \vec{B}) - m\int_0^t K(t-\tau)\vec{V}_{\text{rel}}(\tau)d\tau, \tag{3.4}$$

$$m\frac{d\vec{V}_{\text{cm}}}{dt} = \frac{q}{2}(\vec{V}_{\text{rel}} \times \vec{B}) - m\int_0^t K(t-\tau)[\vec{V}_{\text{cm}}(\tau) - \vec{u}(\tau)]d\tau, \tag{3.5}$$

$$\rho_{\text{sol}}\frac{d\vec{u}}{dt} = 2mn\int_0^t K(t-\tau)[\vec{V}_{\text{cm}}(\tau) - \vec{u}(\tau)]d\tau. \tag{3.6}$$

The Laplace transform is then applied to the integro-differential system to determine the steady-state asymptotic behavior of the fluid velocities, yielding the system:

$$m(s\tilde{\vec{V}}_{\text{rel}}(s) - \vec{V}_{\text{rel}}(0)) = \frac{2q}{s}\vec{E} + 2q(\tilde{\vec{V}}_{\text{cm}}(s) \times \vec{B}) - m\tilde{K}(s)\tilde{\vec{V}}_{\text{rel}}(s) \tag{3.7}$$

$$m(s\tilde{\vec{V}}_{cm} - \vec{V}_{cm}(0)) = \frac{q}{2}(\tilde{\vec{V}}_{\text{rel}} \times \vec{B}) - m\tilde{K}(s)[\tilde{\vec{V}}_{cm} - \tilde{\vec{u}}(s)] \tag{3.8}$$

$$[\rho_{\text{sol}}s + 2mn\tilde{K}(s)]\tilde{\vec{u}}(s) = \rho_{\text{sol}}\vec{u}(0) + 2mn\tilde{K}(s)\tilde{\vec{V}}_{cm}(s) \tag{3.9}$$

In the Laplace domain, the steady state asymptotics are extracted via the Final Value Theorem, which states that asymptotic time behavior of a function is equivalent to near zero behavior of the expression $s\tilde{f}(s)$ [31]:

$$\lim_{t\to\infty} f(t) = \lim_{s\to 0} s\tilde{f}(s). \tag{3.10}$$

Assuming the memory kernel is absolutely integrable, its zero-frequency Laplace transform evaluates to a finite static friction coefficient $\gamma = \int_0^\infty K(t)dt$. Analyzing the transformed Navier-Stokes equation (Eq. 3.6) under this limit reveals the long-time behavior of the solvent:

$$\vec{u}_\infty = \lim_{s\to 0} s\tilde{\vec{u}}(s) = \lim_{s\to 0}\left[\frac{2smn\tilde{K}(s)}{\rho_{\text{sol}}s + 2smn\tilde{K}(s)}\tilde{\vec{V}}_{\text{cm}}(s)\right] = \vec{V}_{\text{cm},\infty}. \tag{3.11}$$

Thus, the macroscopic solvent velocity strictly converges to the ionic center-of-mass velocity in the long-time limit. Applying the identical limiting procedure ($s \to 0$) to the remaining Laplace-domain equations reduces the transient system to a set of coupled, steady-state algebraic force constraints:

$$\vec{V}_{\text{cm},\infty} = \vec{u}_\infty, \tag{3.12}$$

$$\vec{V}_{\text{rel},\infty} \times \vec{B} = 0, \tag{3.13}$$

$$\vec{V}_{\text{rel},\infty} = \frac{2q}{m\gamma}\left(\vec{E} + \vec{V}_{\text{cm},\infty} \times \vec{B}\right). \tag{3.14}$$

Equation 3.13 strictly dictates that any residual relative velocity must be completely parallel to the applied magnetic field. By substituting this condition into the force balance (Eq. 3.14) and performing an orthogonal vector decomposition (the rigorous algebraic decoupling is detailed in Appendix E), the steady-state velocities are uniquely determined. For strictly orthogonal external fields ($\vec{E} \cdot \vec{B} = 0$), the relative velocity evaluates identically to zero ($\vec{V}_{\text{rel},\infty} = 0$), and the system converges to a single, unified steady-state velocity:

$$\vec{V}_{cm,\infty} = \vec{u}_\infty = \frac{\vec{E} \times \vec{B}}{|\vec{B}|^2} \tag{3.15}$$

where the individual ion species velocities are given by:

$$\vec{V}_{\pm,\infty} = \frac{\vec{E} \times \vec{B}}{|\vec{B}|^2} \tag{3.16}$$

Equation 3.15 demonstrates that under a Galilean-invariant, nonequilibrium formulation, an electromagnetized isotropic electrolyte eventually replicates the exact drift kinematics of a fully ionized, collisionless plasma. Figure (3.1) precisely visualizes this phenomenon.

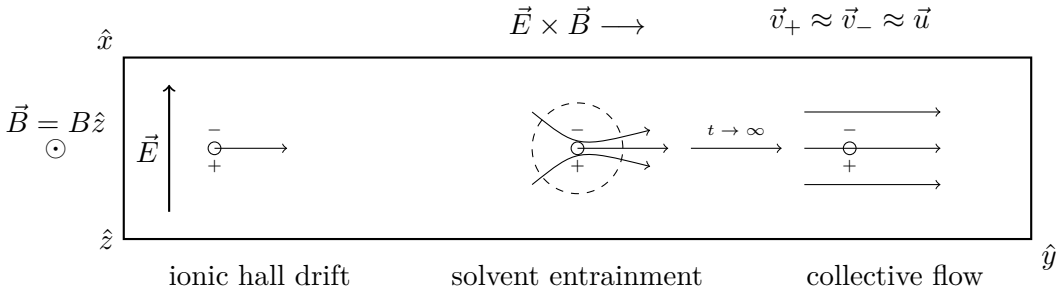


**Figure 3.1:** Diagrammatic Depiction of the Nonlinear Momentum Transfer

Physically, during the transient regime, the externally driven ions transfer momentum to the surrounding solvent via the subdiffusive drag encoded within the memory convolution. Provided the friction kernel is absolutely integrable, the solvent continuously accelerates until it perfectly matches the ionic center-of-mass velocity. At this limit, the relative velocity between the ions and the solvent vanishes, terminating the momentum transfer and establishing a dissipationless steady state. From the perspective of molecular dynamics, this macroscopic phenomenon perfectly aligns with the requisite transport behavior of systems simulated using momentum-conserving local thermostats, such as Dissipative Particle Dynamics (DPD) or the Lowe-Andersen thermostat.

## 3.2 Green-Kubo Formulation and Transient Dynamics of Non-Markovian Ionic Transport

While a true transient solution would involve numerical integration of the coupled Volterra equations, there is a direct, demonstrable connection between the non-Markovian kinetic equation derived in 2.39 and the statistical mechanical formulation of transport coefficients via time-correlation functions of a current operator. Approaching solution through this perspective provides a unified framework in which the conductivity tensor emerges as the time-integrated response of the transient dynamics governed by the generalized kinetic operator. While not precisely the transient dynamics, solving the evolution equation for the correlation tensor yields the dynamics of the velocity autocorrelation function (VACF), which in turn describes transient dynamics via the time-integrated projection of the Non-Markovian operator.

### 3.2.1 Linearization of the Non-Markovian Kinetic Equation and the Conductivity Tensor

Formally, the current macroscopic charge current density is defined in terms of the coarse-grained distribution function $f_\alpha(\vec{v}_\alpha, t)$ as a scaled first velocity moment:

$$\vec{J}(t) = \sum_\alpha q_\alpha \int_{\mathbb{R}^3} \vec{v} f_\alpha(\vec{v}, t) d^3v \tag{3.17}$$

At equilibrium, it was shown that the coarse-grained distribution takes on the form of the Maxwellian, 1.12. Proceeding with the notation for perturbation order adopted in Section 1 ($f_\alpha^{(0)}, f_\alpha^{(1)}, \ldots$), it is clear that upon substitution of the Maxwellian $f_\alpha^{(0)}$ into 3.17, the current density $\vec{J}(t)$ vanishes identically:

$$\langle \vec{J} | f_\alpha = f_\alpha^{(0)} \rangle = 0. \tag{3.18}$$

In similar fashion to before, perturbations due to weak external fields are considered. Linearizing the non-Markovian kinetic equation 2.39, by taking a linear expansion of the distribution to first order,

$$f_\alpha = f_\alpha^{(0)} + \delta f_\alpha^{(1)}, \tag{3.19}$$

the resultant linearized non-Markovian equation takes the form of:

$$\partial_t \delta f_\alpha = \mathcal{L}_\alpha^{NM} \delta f_\alpha + S_\alpha(\vec{v}_\alpha). \tag{3.20}$$

Here, $\mathcal{L}_\alpha^{NM}$ can be thought of as the non-Markovian, non-closed analog of the OU operator, implementing ion-solvent collisions:

$$\mathcal{L}_\alpha^{NM} f_\alpha = -\frac{q_\alpha}{m_\alpha}\left(\vec{v}_\alpha \times \vec{B}\right)\cdot \nabla_{\vec{v}_\alpha} f_\alpha + \nabla_{\vec{v}_\alpha}\cdot \int_0^t K_\alpha(t-\tau)\mathcal{R}_\alpha[f](t,\tau)d\tau \tag{3.21}$$

$$\mathcal{R}_\alpha := F_\alpha^{(2)}(\vec{v},t;\tau) + k_B T[H(t,\tau)\cdot\nabla_{\vec{r}_\alpha} f_\alpha + G(t,\tau)\cdot\nabla_{\vec{v}_\alpha} f_\alpha], \tag{3.22}$$

and $S_\alpha(\vec{v}_\alpha)$ is the source term imposing deterministic perturbations from the external electric field $\vec{E}$, namely:

$$S_\alpha(\vec{v}_\alpha) = -\frac{q_\alpha}{m_\alpha}(\vec{E}\cdot\nabla_{\vec{v}_\alpha}) f_\alpha^{(0)} = \frac{q_\alpha}{k_B T}(\vec{E}\cdot\vec{v}_\alpha) f_\alpha^{(0)} \tag{3.23}$$

At the moment, both collision operators remain exact. However to make analytical progress, closure must be imposed on the correlation functions. First, we impose closure on the two time correlation hierarchy $F_\alpha^{(2)}$ via a molecular chaos-type assumption, e.g.: past velocities decorrelate sufficiently fast such that only instantaneous correlations survive. Such closure reduces the form of $F_\alpha^{(2)} = \langle \vec{v}_\alpha(\tau) N_\alpha(t)\rangle = \vec{v}_\alpha f_\alpha(\vec{v}_\alpha, t)$. Note that such closure does not eliminate memory, but removes explicit two-time phase-space correlations. By isotropy of the surrounding solvent, one can additionally impose diagonality of the velocity response tensor $G_{ij}(t,\tau) = g(t,\tau)\delta_{ij}$ through application of Schur's Lemma [32], and the $SO(3)$ invariance of $\mathbf{G}$. Assuming spatial homogeneity, the spatial gradient term with coefficient $\mathbf{H}(t,\tau)$ vanishes identically, e.g. $\nabla_{\vec{r}_\alpha} f_\alpha = 0$. The non-Markovian collision operator under strict velocity decorrelation closure, spatial homogeneity, and isotropy assumptions reads:

$$\mathcal{L}_\alpha^{NM}\delta f_\alpha = -\frac{q_\alpha}{m_\alpha}(\vec{v}_\alpha\times\vec{B})\cdot\nabla_{\vec{v}_\alpha}\delta f_\alpha + \nabla_{\vec{v}_\alpha}\cdot\int_0^t K_\alpha(t-\tau)\left[\vec{v}_\alpha\delta f_\alpha(\tau) + k_B T g_\alpha(t,\tau)\nabla_{\vec{v}_\alpha}\delta f_\alpha(\tau)\right]d\tau. \tag{3.24}$$

Note that now the linearized kinetic equation is an inhomogeneous evolution equation for the time dependent perturbed function component, e.g:

$$\partial_t \delta f_\alpha^{(1)} - \mathcal{L}^{NM}\delta f_\alpha^{(1)} = S_\alpha(\vec{v}_\alpha), \tag{3.25}$$

and satistfies the respective boundary conditions required to apply Duhamel's principle as detailed in 1.2.1. Applying Duhamel's principle, one writes the evolution operator of the solution—formally a pseudodifferential semigroup—generated by the non-Markovian collision operator $\mathcal{L}_\alpha^{NM}$ as $e^{(t-\tau)\mathcal{L}_\alpha^{NM}}$. The Duhamel formula yields the formal evolution-operator solution to 3.25:

$$\delta f_\alpha^{(1)}(t) = \int_0^t e^{(t-\tau)\mathcal{L}_\alpha^{NM}} S_\alpha(\vec{v}_\alpha)d\tau. \tag{3.26}$$

While the explicit action on the source term $S_\alpha(\vec{v}_\alpha)$ by the evolution operator can be determined, it is not necessary, and one may pertain to abstraction. What is important to note is that the evolution operator introduces time-dependence on velocities, and evolves the physical observables of the fluidic system. Explicitly $e^{(t-\tau)\mathcal{L}_\alpha^{NM}}\vec{v}_\alpha = \vec{v}_\alpha(t-\tau)$. We use this property in the definition of the current correlation tensor, defined componentwise:

$$C_{ij}(t-\tau) := \sum_\alpha q_\alpha^2 \int_{\mathbb{R}^3} v_{\alpha,i} e^{(t-\tau)\mathcal{L}_\alpha^{NM}} v_{\alpha,j} f_\alpha^{(0)} d^3 v_\alpha = \sum_\alpha n_\alpha q_\alpha^2 \langle v_{\alpha,i}(t-\tau) v_{\alpha,j}(0)\rangle_{eq}. \tag{3.27}$$

Note that the evolution operator transforms the integral into the equilibrium VACF, as the velocity is evolved in time under the integral. Substituting 3.26 into the current density 3.17 componentwise, one may begin simplication, recalling that the evolution operator imposes time evolution on the velocities.

$$\begin{aligned} J_i(t) &= \sum_\alpha q_\alpha \int v_{\alpha,i} \delta f_\alpha^{(1)}(t) d^3 v_\alpha \\ &= \int_0^t d\tau \sum_\alpha q_\alpha \int v_{\alpha,i} e^{(t-\tau)\mathcal{L}_\alpha^{NM}} S_\alpha d^3 v_\alpha \\ &= \frac{1}{k_B T} \int_0^t d\tau \sum_\alpha q_\alpha^2 \int_{\mathbb{R}^3} v_{\alpha,i} e^{(t-\tau)\mathcal{L}_\alpha^{NM}} v_{\alpha,j} f_\alpha^{(0)} E_j d^3 v_\alpha \\ &= \frac{1}{k_B T} \int_0^t d\tau \sum_\alpha n_\alpha q_\alpha^2 \langle v_{\alpha,i}(t-\tau) v_{\alpha,j}(0) \rangle_{eq} E_j \\ &= \frac{1}{k_B T} \int_0^t C_{ij}(t-\tau) E_j d\tau \underbrace{\longleftrightarrow}_{s=t-\tau} \frac{1}{k_B T} \int_0^t C_{ij}(s) E_j ds \end{aligned} \tag{3.28}$$

Noting the proportionality between the electric field and the charge current density, in the long time limit one may directly associate the correlation tensor to the first order conductivity $\sigma_{ij}$, deriving the Green-Kubo relation directly from the non-Markovian transport equations [33, 34]:

$$\sigma_{ij} = \frac{1}{k_B T} \int_0^\infty C_{ij}(t) dt. \tag{3.29}$$

The conductivity can be thought of as a direct encoding of the generalized Langevin dynamics of the velocities of the distribution, as the current correlation tensor is precisely composed of the components of the VACF. To determine the conductivity, it is therefore necessary to understand the dynamics of the current correlation tensor and its asymptotic behavior. In Section 2 on the GLE, one understands the stochastic dynamics of the velocties via the stochastic integro-differential equation 2.14. As the evolution of the velocities directly translates to that of the current correlation tensor by linearity of the VACF and corresponding sum, one may write the corresponding stochastic dynamical equation of its components as a corresponding GLE:

$$\frac{d}{dt} C_{ij}(t) = \Omega_{ik}^{(\alpha)} C_{kj}(t) - \int_0^t K_\alpha(t-\tau) g_\alpha(t,\tau) C_{ij}(\tau) d\tau, \quad \Omega_{ik}^{(\alpha)} = \frac{q_\alpha}{m_\alpha} \varepsilon_{ikl} B_l, \tag{3.30}$$

To solve for such dynamics it is useful to perform a tensorial decomposition. The most general form of the current correlation tensor under fludic isotropy can be expressed in terms of its symmetric and antisymmetric components.

$$C_{ij}(t) = C_S(t) \delta_{ij} + C_A(t) \varepsilon_{ijl} \hat{B}_l \tag{3.31}$$

Substituting this decomposition into the general evolution equation 3.30, the Lorentz (frequency matrix) term acts on the symmetric component as:

$$\Omega_{ik}^{(\alpha)} (C_S \delta_{kj}) = C_S \Omega_{ij}^{(\alpha)} = C_S \omega_c \varepsilon_{ijl} \hat{B}_l, \tag{3.32}$$

and the antisymmetric component as:

$$\Omega_{ij}^{(\alpha)} (C_A \varepsilon_{kjm} \hat{B}_m) = C_A \omega_c (\delta_{ij} - \hat{B}_i \hat{B}_j). \tag{3.33}$$

In similar fashion, we reduce the action of the memory term including $K_\alpha$, recalling that the memory term is diagonal in tensor structure acting on the current correlation tensor in both cases. Splitting the evolution equation into a symmetric equation and antisymmetric equation respectively, one achieves a system of dynamical equations in associated matrix form:

$$\frac{d}{dt}\begin{pmatrix} C_S \\ C_A \end{pmatrix} = \begin{pmatrix} 0 & \omega_c \\ -\omega_c & 0 \end{pmatrix} \cdot \begin{pmatrix} C_S \\ C_A \end{pmatrix} - \int_0^t K_\alpha(t-\tau) g_\alpha(t,\tau) \begin{pmatrix} C_S(\tau) \\ C_A(\tau) \end{pmatrix} d\tau. \tag{3.34}$$

Assuming time translation invariance of the velocity response tensor, one may impose stationarity, and let $g_\alpha(t,\tau) = g_\alpha(t-\tau)$. Defining an effective memory kernel $\mathcal{K}(t-\tau) := K(t-\tau)g(t-\tau)$ allows a Laplace transform of the system to diagonalize the convolution term, reducing to multiplication. Taking the Laplace transform of 3.34, one achieves:

$$\tilde{\mathcal{K}}(s) + s\begin{pmatrix} \tilde{C}_S(s) \\ \tilde{C}_A(s) \end{pmatrix} = \begin{pmatrix} 0 & \omega_c \\ -\omega_c & 0 \end{pmatrix} \begin{pmatrix} \tilde{C}_S(s) \\ \tilde{C}_A(s) \end{pmatrix} + \begin{pmatrix} C_S(0) \\ 0 \end{pmatrix}. \tag{3.35}$$

Solving this system algebraically, one determines the explicit form of the Laplace transformed current correlation tensor components to be:

$$\boxed{\tilde{C}_S(s) = \frac{(s+\tilde{\mathcal{K}}(s))}{[(s+\tilde{\mathcal{K}}(s))^2+\omega_c^2]} C_S(0), \quad \tilde{C}_A(s) = -\frac{\omega_c}{(s+\tilde{\mathcal{K}}(s))^2+\omega_c^2} C_S(0).} \tag{3.36}$$

From the derived Kubo relation 3.29 and the Final Value Theorem 3.10, one understands the integral of the current correlation tensor to be equivalent to $\tilde{C}_{ij}(0)$. Substituting the definition of $C_{ij}(t)$, and applying equipartition theorem to the VACF inside, one achieves a final form for the conductivity tensor $\sigma$ in component form:

$$\boxed{\sigma_{ij} = \sum_\alpha \frac{n_\alpha q_\alpha^2}{m_\alpha} \frac{\tilde{\mathcal{K}}_\alpha(0)\delta_{ij} + \omega_{c,\alpha}\varepsilon_{ijl}\hat{B}_l}{\tilde{\mathcal{K}}_\alpha(0)^2 + \omega_{c,\alpha}^2}.} \tag{3.37}$$

From a physical point of view, $\tilde{\mathcal{K}}_\alpha(0)$ serves as an effective friction term including all memory and response propagation of the solvent imposed to the ions in the asymptotic picture. The two terms of the conductivity correspond to the drag-aware ohmic drift and forcing, and the antisymmetric lorentz rotation due to the magnetic field.

### 3.2.2 Markovian Conductivity Tensor

For the memoryless case, where the velocity correlation decays are instantaneous, the memory kernel takes the canonical markovian form $K_\alpha(t-\tau) = \gamma_\alpha\delta(t-\tau) = \frac{\delta(t-\tau)}{\tau_\alpha^*}$, where $\gamma_\alpha$ is to be understood as a Stoke's drag coefficient—equivalent to the reciprocal of the relaxation time $\tau_\alpha^* = \frac{1}{\gamma_\alpha}$. Substituting this specific memory kernel term and assuming response normalization, the conductivity tensor reduces to the familiar drude conductivty, demonstrating the magnetohydrodynamic consistency with the Markovian picture for a two ion species electrolyte.

$$\sigma_{ij} = \sum_\alpha \frac{n_\alpha q_\alpha^2 \tau_\alpha}{m_\alpha} \frac{\delta_{ij} + \omega_{c,\alpha}\tau_\alpha\varepsilon_{ijl}\hat{B}_l}{1+\omega_{c,\alpha}^2\tau_\alpha^2} \tag{3.38}$$

### 3.2.3 Transient Correlation Decay Dynamics from Pole Structure

To determine the transient behavior of the bulk ion species velocities, a complete characterization of the dynamics requires analysis of the VACF. This information is naturally encoded in the Laplace transform of the current correlation function, whose analytic structure governs the transient evolution of the velocities under equilibrium expectation. Formally, the time-dependent correlation function is consequently recovered via the inverse Laplace transform, which reintroduces explicit time dependence. Doing so will provide a natural encoding of the transient velocity behavior. To make analytical progress, the Bromwich formula for the inverse Laplace transform is used, shifting the problem of the inverse transform to the computation of a complex integral [35].

$$C(t) = \mathcal{L}^{-1}\{\tilde{C}\}(t) = \frac{1}{2\pi i}\int_{\gamma-i\infty}^{\gamma+i\infty} e^{st}\tilde{C}(s)ds \tag{3.39}$$

Note that this integral is a contour integral, where the contour lies to the right of all singularities $\{s_1^*, \ldots, s_n^*\}$ of $\tilde{C}(s)$. By deforming the contour into the complex plane, assuming the restriction of $\tilde{C}(s)|_{\mathbb{C}\setminus\{s_1^*,\ldots,s_n^*\}}$ to be holomorphic, and applying the Residue Theorem [36], one obtains:

$$C(t) = \sum_j \operatorname{Res}\left(\tilde{C}(s)e^{st}, s_j^*\right) = \sum_j A_j e^{s_j^* t}, \tag{3.40}$$

where $s_j^*$ are the poles of $\tilde{C}(s)$. Note that this is truly a beautiful result. The exponential component of the inverse Laplace transform is extracted from the residue due to its analyticity, and causes each pole to contribute an exponential mode to the transient dynamics such that the full time evolution admits a unique multi-timescale spectral decomposition in terms of these relaxation modes. From the Laplace-domain solution derived previously, the poles are naturally determined by the condition that the denominators of the correlation tensors in 3.36 are zero:

$$(s + \tilde{\mathcal{K}}_\alpha(s))^2 + \omega_c^2 = 0, \qquad \Longleftrightarrow \qquad s + \tilde{\mathcal{K}}_\alpha(s) = \pm i\omega_c. \tag{3.41}$$

This equation defines a nonlinear dispersion relation for the relaxation modes $s_*$, which must be solved self-consistently. For a pole $s^* = a + ib$ the correlation function is real-valued, and complex conjugate poles combine to yield:

$$C(t) \sim e^{\mathrm{Re}(s^*)t}\cos(\mathrm{Im}(s^*)t), \tag{3.42}$$

so that the real part of the pole determines the decay rate, while the imaginary part determines the oscillation frequency. Note that for the trivial memoryless case where the memory kernel takes the form $\mathcal{K}_\alpha(t) = \gamma_\alpha\delta(t-\tau)$, the kernel reduces to a constant $\gamma$, as the Laplace transform integrates over memory kernel, e.g. $\tilde{\mathcal{K}}_\alpha(s) = \gamma_\alpha$. For the two-species case where $\alpha \in \{+,-\}$, the pole condition for the correlation tensor yields Laplace domain solutions:

$$s_\pm = -\gamma_\pm \pm i\omega_c. \tag{3.43}$$

Substituting 3.43 into the inverse Laplace representation yields the decomposed form:

$$C(t) = A_+ e^{(-\gamma_+ + i\omega_c)t} + A_- e^{(-\gamma_- - i\omega_c)t} \tag{3.44}$$

This expression corresponds to exponentially damped cyclotron motion, arising from the competition between Lorentz rotation and dissipative relaxation of the solvent. Note that the current correlation components decay at infinity, as expected, and that $A_+$ and $A_-$ are tensorial.

In the latter case with a non-Markovian memory kernel, the pole condition takes the implicit form:

$$s^* = -\tilde{\mathcal{K}}(s^*) \pm i\omega_c. \tag{3.45}$$

If $\tilde{\mathcal{K}}(s)$ is analytic near $s = 0$, one may expand:

$$\tilde{\mathcal{K}}(s) \approx \tilde{\mathcal{K}}(0) + s\tilde{\mathcal{K}}'(0), \tag{3.46}$$

which yields, to leading order pole behavior:

$$s^* \approx -\frac{\tilde{\mathcal{K}}(0)}{1 + \tilde{\mathcal{K}}'(0)} \pm i\frac{\omega_c}{1 + \tilde{\mathcal{K}}'(0)}. \tag{3.47}$$

This demonstrates that memory effects renormalize both the decay rate and the effective cyclotron frequency. More generally, if $\tilde{\mathcal{K}}(s)$ possesses some nontrivial analytic structure, the dispersion relation may admit multiple solutions $s_k^*$, leading to:

$$C(t) = \sum_k A_k e^{s_k^* t}, \tag{3.48}$$

corresponding to multi-timescale relaxation. Note that the tensorial coefficients of the exponential modes can again be decomposed into symmetric and antisymmetric components, so that the transient dynamics of the current correlation tensor are fully determined by the pole structure of the Laplace transform of the memory kernel. Performing such a decomposition, one may write the transient current correlation tensor as a sum of symmetric and antisymmetric exponential modes ($A^S$ and $A^A$ respectively), and the B-field enters again explicitly in the antisymmetric component. Componentwise, one writes:

$$\boxed{C_{ij}(t) = \sum_k A_k^S e^{s_k^* t}\delta_{ij} + \sum_k A_k^A e^{s_k^* t}\varepsilon_{ijl}\hat{B}_l.} \tag{3.49}$$

In cases where $\tilde{\mathcal{K}}(s)$ develops branch cuts—such as in the power-law Basset Boussinesq framework—the inverse Laplace transform may yield non-exponential decay laws, however such behavior is dependent on the specific form of the memory kernel and should be treated on a case-by-case basis. To perform this method, it is required that the memory kernel is such that the Laplace transform of the correlation tensor is meromorphic, so that the only singularities are poles. In such cases, the transient dynamics of the current correlation tensor are precisely determined by the pole structure of $\tilde{C}(s)$, which is in turn determined by the structure of $\tilde{\mathcal{K}}(s)$. The poles of $\tilde{C}(s)$ must also have a negative real part, such that the transient modes decay at infinity, and that the coefficients $A_k$ are real-valued, so that the correlation function is real-valued.

Hence, the transient dynamics of the system are determined by the spectrum of the non-Markovian evolution operator. While the conductivity depends only on the zero-frequency value $\tilde{\mathcal{K}}(0)$, the full time-dependent behavior probes the entire functional form of the memory kernel. This establishes a direct correspondence between microscopic memory effects and macroscopic transient transport, providing a unified framework in which relaxation processes can be systematically classified.

### 3.2.4 Analytic Determination of Current Transients and Relaxation Timescales

The current correlation tensor can be thought of as an object which directly encodes the transient dynamics of the velocities through the Green-Kubo convolution equation 3.28. By substituting the known multipole exponential form of the current correlation tensor into such a relation, one may begin the computation of the transient current density, and therefore the transient velocities through a linear transformation. Substituting 3.48 into 3.28, one achieves:

$$\vec{J}(t) = \frac{1}{k_B T}\int_0^t \sum_k \left[A_k^S e^{s_k^* t}\delta_{ij} + \sum_k A_k^A e^{s_k^* t}\varepsilon_{ijl}\hat{B}_l\right]\vec{E}d\tau \tag{3.50}$$

$$= \frac{1}{k_B T}\sum_k \left[A_k^S \int_0^t e^{s_k^* t}d\tau\delta_{ij} + \sum_k A_k^A \int_0^t e^{s_k^* t}d\tau\varepsilon_{ijl}\hat{B}_l\right]\vec{E} \tag{3.51}$$

$$= \frac{1}{k_B T}\sum_k \left[A_k^S \frac{e^{s_k^* t}-1}{s_k^*}\delta_{ij} + \sum_k A_k^A \frac{e^{s_k^* t}-1}{s_k^*}\varepsilon_{ijl}\hat{B}_l\right]\vec{E} \tag{3.52}$$

$$\tag{3.53}$$

Separating the transient current density into time dependent and time-independent components, one may write the current density as a precise decomposition of the asymptotic conductivity signature and transient relaxation modes:

$$\boxed{\begin{aligned} J_i(t) = &\sum_k \underbrace{\left(-\frac{A_k^S}{k_B T s_k^*}\delta_{ij} - \sum_k \frac{A_k^A}{k_B T s_k^*}\varepsilon_{ijl}\hat{B}_l\right)}_{\text{Asymptotic Conductivity } \sigma_{ij}} E_j + \\ &\sum_k \left(\frac{A_k^S}{k_B T s_k^*}e^{s_k^* t}\delta_{ij} + \sum_k \frac{A_k^A}{k_B T s_k^*}e^{s_k^* t}\varepsilon_{ijl}\hat{B}_l\right)E_j \end{aligned}} \tag{3.54}$$

Extracting the coefficient of the electric field from the time independent term of the composition, it can be shown that the asymptotic conductivity tensor $\sigma_{ij}$ is precisely recovered. Recalling the definition of the conductivity tensor $\sigma_{ij}$ from the Green Kubo relation 3.29, one may express the asymptotic conductivity as the Laplace transform of the current correlation tensor evaluated at zero frequency (valid by the Final Value Theorem):

$$\sigma_{ij} = \frac{1}{k_B T}\tilde{C}_{ij}(0) \tag{3.55}$$

Applying the Laplace transform to the transient solution for the current correlation tensor 3.48, one achieves:

$$C(t) = \sum_k A_k e^{s_k^* t} \implies \tilde{C}(s) = \sum_k \frac{A_k}{s - s_k^*} \implies \tilde{C}(0) = \sum_k \frac{A_k}{-s_k^*}. \tag{3.56}$$

$$\implies \tilde{C}_{ij}(0) = \sum_k \left(-\frac{A_k^S}{s_k^*}\delta_{ij} - \sum_k \frac{A_k^A}{s_k^*}\varepsilon_{ijl}\hat{B}_l\right). \tag{3.57}$$

Substituting into 3.55, one recovers the asymptotic conductivity tensor as the exact term present in 3.54:

$$\sigma_{ij} = \frac{1}{k_B T}\tilde{C}_{ij}(0) = \sum_k \left(-\frac{A_k}{k_B T s_k^*}\right)\delta_{ij} + \sum_k \left(-\frac{A_k}{k_B T s_k^*}\right)\varepsilon_{ijl}\hat{B}_l \tag{3.58}$$

This remarkable result demonstrates that for meromorphic Laplace-domain correlation tensors, the transient current density can be precisely decomposed into a sum of the asymptotic conductivity signature and a series of exponentially decaying transient modes, whose decay rates and oscillation frequencies are determined by the pole structure of the Laplace transform of the current correlation tensor. The coefficients $A_k$ encode the relative contribution of each relaxation mode to the transient dynamics, while the poles $s_k^*$ determine the timescales over which these modes decay.

### 3.2.5 Discussion of Markovian Transients and Analytic Summary

Considering the Markovian case yet again, the poles are given by $s_\pm = -\gamma_\pm \pm i\omega_c$, which yields the transient current density as the sum of the asymptotic conductivity of the joint ionic system, and the exponentially damped cyclotron motion of the ions, taking into accound the $\vec{E} \times \vec{B}$ motion in the antisymmetric component:

$$J_i(t) = \underbrace{J_{i,\infty}}_{\sigma_{ij}E_j} + \sum_\pm \left(\frac{A_\pm}{k_B T s_\pm} e^{s_\pm t}\delta_{ij} + \sum_\pm \frac{A_\pm}{k_B T s_\pm} e^{s_\pm t}\varepsilon_{ijl}\hat{B}_l\right) E_j \tag{3.59}$$

This expression corresponds to the well-known exponentially damped cyclotron motion, where the decay rates $\gamma_\pm$ are determined by the effective friction coefficients, and the oscillation frequency is given by the cyclotron frequency $\omega_c$. In the non-Markovian case, the transient dynamics are governed by the more complex pole structure of $\tilde{C}(s)$, which may admit multiple relaxation modes and non-exponential decay behavior depending on the analytic structure of the memory kernel. Under the Markovian picture, typical relaxation times are on the order of the inverse friction coefficients $\tau_\pm = \frac{1}{\gamma_\pm}$, which correspond to the characteristic timescales over which the system relaxes to its steady state.

The analytic framework developed in this section provides a direct connection between the microscopic memory effects encoded in the kernel $\tilde{\mathcal{K}}(s)$ and the nonlinear transient transport behavior of the electrolytic system, as captured by the precise structure of the current correlation tensor and its associated asymptotic conductivity via Green-Kubo. By analyzing such pole structure of the Laplace transform of the correlation tensor, one systematically classifies the relaxation processes and timescales governing the transient dynamics, providing a unified framework for understanding non-Markovian transport phenomena in electrolyte systems. In full generality, the transient velocity behavior of a many species ionic system with a memory kernel imposing a simple pole structure to the correlation tensor is a sum of exponentially decaying cyclotron-oscillatory modes with decay rates $\mathrm{Re}\{s_k^*\}$ and frequencies $\mathrm{Im}\{s_k^*\}$ renormalized by memory effects, and with coefficients determined by the residues of such poles. In its final, most general form, the transient velocity behavior can be written as:

$$\boxed{\begin{aligned} v_i(t) = &\sum_k \left( -\frac{A_k^S}{k_B T s_k^*}\delta_{ij} - \sum_k \frac{A_k^A}{k_B T s_k^*}\varepsilon_{ijl}\hat{B}_l \right) E_j + \\ &\sum_k \left( \frac{A_k^S}{k_B T s_k^*} e^{s_k^* t}\delta_{ij} + \sum_k \frac{A_k^A}{k_B T s_k^*} e^{s_k^* t}\varepsilon_{ijl}\hat{B}_l \right) E_j \end{aligned}} \tag{3.60}$$

At this point, further analytic progress would require the introduction of some perturbative methods applied to the nonlinear dispersion relation $s + \tilde{\mathcal{K}}(s) = \pm i\omega_c$.. One may consider the weaker memory limit, where the memory kernel $K_\alpha(t-\tau)$ is small in some appropriate norm, so that the memory effects can be treated as a perturbation to the Markovian case. In such a limit, one may expand the poles $s_k^*$ in powers of the memory kernel, and compute corrections to the decay rates and oscillation frequencies order by order.

Alternatively, one may consider specific functional forms of the memory kernel that allow for exact solutions of the dispersion relation, such as exponential or power-law kernels, which may yield closed-form expressions for the poles and therefore the transient dynamics. However, for memory kernels which do not yield meromorphic Laplace transformed correlation tensors, such as those contaning branch cuts (Basset-Boussinesq for example), the transient dynamics may not admit a simple exponential decomposition, and may require numerical inversion of the Laplace transform or asymptotic analysis to extract the long-time behavior. While this is theoretically possible, the complexity of the resulting expressions may limit their practical utility.

A more powerful and complementary direction is therefore the incorporation of molecular dynamics simulations, which provide direct access to the velocity autocorrelation function and its transient behavior without requiring correlation closure approximations. In the proceeding chapter, a full treatment of the electromagnetized electrolyte system is given, where the the full DC field configuration is imposed on a $KCl$ system. Through an analysis of the time evolution of the system, and the extraction of relevant observables, the asymptotic velocities are examined and compared to the analytic results derived, particularly those aforementioned in Section 3.1.

# 4 Computational Momentum-Conserving Molecular Dynamics

## 4.1 OpenMM and Momentum Conserving MHD

A common approach to the analysis of emergent phenomena in many-particle, many-interaction systems is molecular dynamics (MHD). It is commonplace for molecular dynamics frameworks to be used to analyze emergent phenomena in specific microscopic systems, such as biological complexes or various molecular structures, all of which sit embedded within a larger equilibrated solvent. In such regular applications, solvents are treated as static baths in some ensemble, external fields are rare and almost always apply constant forces, and the dynamics of the embedded systems—not the solvent—are of interest. This makes the analysis of non-equilibirium solvent dynamics of an electrolytic system a slightly abnormal application, in that one considers momentum-conservation, a highly non-static solvent, and velocity-dependent force fields. Naturally, implementing such an abnormal system requires a molecular dynamics framework which is highly modular and source-code modifiable. These investigation constraints led to the selection of OpenMM for all molecular dynamics investigations, due to its ease of source-code modification.

For momentum-conservation, the dissipative particle dynamics (DPD) thermostat from OpenMM was used. Formally, it is very similar to a traditional Langevin thermostat—which samples particle velocities from the Maxwell-Boltzmann distribution—however thermostats the interparticle pair-wise velocities instead with a half step velocity-verlet form [37]. Collisions and friction are implemented as interactions with virtual particles of the heat bath. The precise pseudocode implementation can be found in Appendix I.

As is the case for most molecular dynamics frameworks, velocity-dependent force fields—such as the Lorentz force from the magnetic field $\vec{B}$—are not natively implemented. To bypass this limitation, the OpenMM DPD thermostat C++ source code was directly modified to step the ion velocities according to a coarse-grained Boris integrator scheme. The precise pseudocode implementation of the Boris integrator can be found in Appendix J. The Boris integrator was used for its stability under long time and large fields. The primary challenge of ensuring a consistent implementation of the Boris integrator was the introduction of the correct physical units. To ensure the magnetic field $\vec{B}$ and lorentz forces were introduced properly, the scaling of the B parameter in the Boris scheme was tweaked to OpenMM units such that the cyclotron frequency $\omega_c = \frac{qB}{m}$ of the ions matched with that predicted by theory. Figure 4.1 visualizes the velocity trajectory data for a $K^+$ and $Cl^-$ ion under a magnetic field strength of 10 T in the $\hat{z}$

direction. Both ions were seeded with an initial velocity of 10 nm/ps in the $\hat{y}$ direction, respectively. Note the cyclotron frequency precisely aligns with predicted values of $\omega_{K^+} \approx 2.4645 \times 10^7$ Hz, $\omega_{Cl^-} \approx 2.7165 \times 10^7$ Hz, which have corresponding cyclotron periods $T_{K^+} \approx 2.546 \times 10^{-7}$ s and $T_{Cl^-} = 2.309 \times 10^{-7}$ s calculated using their theoretical atomic masses and the cyclotron frequency formula, respectively [38].

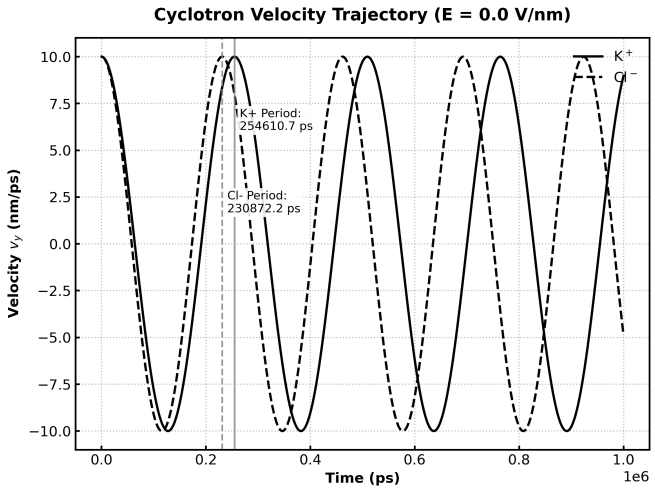


**Figure 4.1:** Transverse Cyclotron Velocity Trajectory Profile for $K^+$ and $Cl^-$ Ions under $\vec{B} = 10$ T$\hat{z}$, $\vec{E} = \vec{0}$ V/m

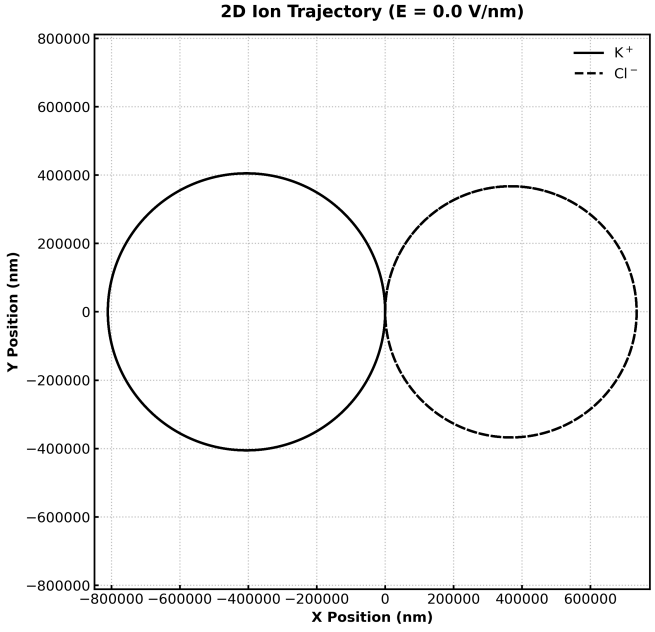


**Figure 4.2:** Cyclotron Ion Trajectory for $K^+$ and $Cl^-$ Ions under $\vec{B} = 10$ T$\hat{z}$, $\vec{E} = \vec{0}$ V/m

Note that the introduction of the electric field in the x-direction would not modify the frequency of the oscillatory behavior, rather immediately relax the ion to cyclotron

frequency about the predicted plasma Hall drift velocity, $\frac{\vec{E}\times\vec{B}}{B^2}$. The trajectory of such a field configuration would be cycloidal, but the velocity would remain oscillatory (see Figures 4.3 and 4.4).

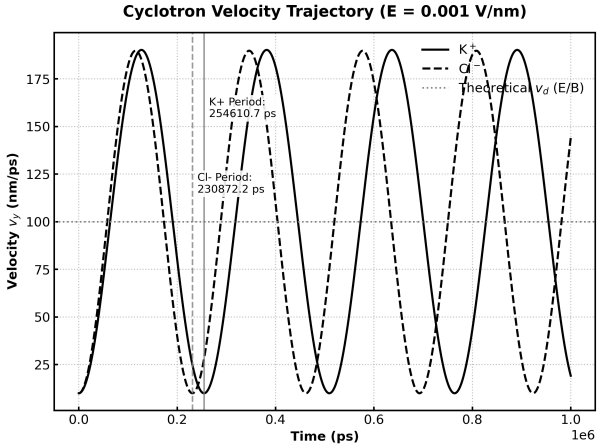


**Figure 4.3:** Transverse Cyclotron Velocity Trajectory Profile for $K^+$ and $Cl^-$ Ions under $\vec{B} = 10\ \mathrm{T}\hat{z}$, $\vec{E} = 0.001\ \mathrm{V/nm}\hat{x}$

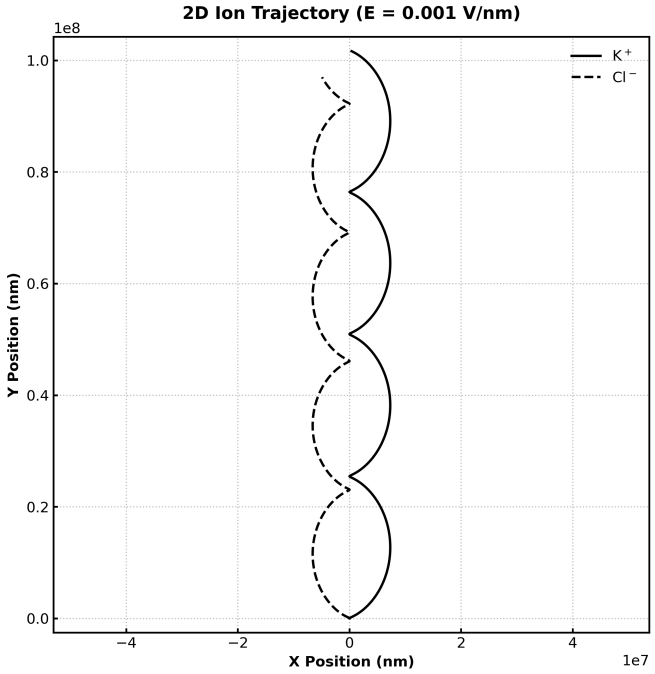


**Figure 4.4:** Cyclotron Ion Trajectory for $K^+$ and $Cl^-$ Ions under $\vec{B} = 10\ \mathrm{T}\hat{z}$, $\vec{E} = 0.001\ \mathrm{V/nm}\hat{x}$

One may note that while the ion motion in Figure 4.4 indeed remains oscillatory due to the absence of dissipative forces from a solvent, and its asymptotic velocity over time oscillates about the expected steady state velocity ($100\,\mathrm{nmps}^{-1}$). It is the prediction of all previous analytic theory that the full ion-solvent electrolytic system will exhibit

such similar dynamical behavior, wherein the y-velocity asymptotically approaches the plasma vacuum velocity under crossed, orthogonal electric and magnetic fields. With a functional, calibrated implementation of a magnetic field integrator into a momentum conserving DPD thermostat, the asymptotic behavior of the electrolytic system can now be examined under electromagnetic fields.

## 4.2 Asymptotic Analysis

### 4.2.1 Timescale Limitations in Magnetohydrodynamic Simulations

The microscopic simulation of electrolyte solutions under orthogonal electric ($\vec{E}$) and magnetic ($\vec{B}$) fields presents a formidable computational challenge. When a uniform electric field is applied, the dissolved ions experience a driving force, accelerating through the solvent and generating a current. The addition of a transverse magnetic field induces a velocity-dependent Lorentz force on these charge carriers:

$$\vec{F}_L = q(\vec{E} + \vec{v} \times \vec{B}) \tag{4.1}$$

Through repeated intermolecular collisions, the moving ions transfer momentum to the neutral solvent. Macroscopically, this hydrodynamic coupling causes the entire bulk fluid to accelerate until the driving Lorentz forces are perfectly counterbalanced by internal fluid friction and the emerging $\vec{v} \times \vec{B}$ deceleration, resulting in a steady-state asymptotic drift velocity, $\vec{v}^*$, as was demonstrated in Section 3.

In an idealized vacuum, the steady-state drift velocity for a crossed-field configuration resolves to $v^* = |\vec{E}|/|\vec{B}|$, and this can be verified with relative ease due to the near-instantaneous relaxation of the plasma ions to the vacuum velocity, as demonstrated when calibrating the OpenMM setup [39]. However, in dense, atomistic fluids experiencing Dissipative Particle Dynamics (DPD) thermostatting, demonstrating transient decay to this exact asymptotic velocity apriori is almost computationally intractable due to the complex, many-body nature of the solvent-solute drag, and much slower system relaxation due to the dissipative forces from the solvent on the ions in the electrolyte. Thus, large timescales would be necessary to permit the sufficient transfer of kinetic energy to the solvent.

In molecular dynamics, typical simulation timescales range on the order of picosecontds, nanoseconds, and rarely microseconds: such transient relaxation proves difficult to visualize for such complex systems [40]. Standard nonequilibrium procedures typically resolve this problem by initializing the system from rest and integrating forward in time until some steady-state bulk velocity is achieved. Unfortunately, the characteristic timescale for a macroscopic fluid volume to overcome its own inertia and reach $v^*$ can span much longer time periods: Note the near-linear relaxation behavior in Figure 4.5 directly characteristic of a longer relaxation time. For atomistic integrators constrained to femtosecond ($\sim 10^{-15}$ s) timesteps, simulating this transient acceleration phase requires a demonstrably unfeasible allocation of computational resources. To combat this, one must approach the problem of asymptotics by ansatzing the existence of a stationary steady state velocity $\vec{v}^*$, and observing the acceleration on the bulk system for much shorter, linear-transient regime trajectories.

**Simulation Parameters:**

For all simulations run during this investigation, a runtime of 50 ps was adopted for a 300 K, 5 nm × 5 nm × 5 nm waterbox containing 1 M molarity $KCl$, a fixed magnetic field $\vec{B} = B\hat{z}$ with $B = 10\,\mathrm{kT}$—to be justified in Section 4.2.2—with varied electric fields $\vec{E} = E\hat{x}$ and initial velocity distributions for purposes of computational analysis.

### 4.2.2 Commentary on Required OpenMM Simulation Parameters

The silver-lining of a linear-transient trajectory approach to long-time asymptotics is the requirement of very large magnetic fields. Should a very large quantitiy of tens-of-picoseconds range simulations be taken, and their accelerations extracted, a sufficient signal to noise ratio between the observed linear gradient and velocity signal noise is required to maintain accuracy. For the purposes of this approach's investigation, magnetic field of 10 kT is used to sit well within the linear response regime, but also be large enough to receive a measurable signal through the stochastic noise introduced by the solvent.

The application of such an exceptionally high magnetic field of 10 kT in this study is a methodological necessity dictated by the fundamental spatiotemporal constraints of numerical-solvent molecular dynamics. Under standard experimental field strengths (1—10 T), the macroscopic Hall drift velocity of an ion is infinitesimally small in comparison to its immense stochastic thermal velocity at ambient temperatures of the solvent. Consequently, isolating a statistically significant transverse drift signal from the thermal noise floor would require microsecond-to-millisecond integration times—a computationally intractable threshold for standard MD. In scaling the magnetic field to the 10 kT regime, one may artificially amplify the transverse Lorentz force without altering the underlying Boris integration mechanics. This parameter scaling acts as a critical signal-to-noise enhancement technique, accelerating the characteristic cyclotron frequency $\omega_c$ and compressing the macroscopic drift development into a computationally accessible picosecond-to-nanosecond simulation window.

While the applied field magnitude is indeed beyond astrophysical, this scaling technique bridges the timescale gap, allowing for the rapid and clear resolution of crossed-field transport behaviors, for the ultimate determination of dynamical fixed points that would otherwise remain completely obscured by thermal fluctuations in these shorter timescale regimes. Such field magnitudes can also be justified mathematically: In an electrolytic system, ion dynamics are understood to be governed by the Langevin equation 1.2. If one applies an effective driving force—as is performed by the electric field present—ionic motion in aqueous solution is strongly overdamped: the momentum relaxation time $\tau = \frac{m}{\gamma} \sim 10^{-14}$ s is many orders of magnitude shorter than the picosecond-to-nanosecond windows accessible to molecular dynamics. Consequently, inertial effects are negligible, and ionic transport is governed by a balance between viscous drag and external forces.

$$q(\vec{E} + \vec{v} \times \vec{B}) = m\gamma\vec{v}. \tag{4.2}$$

Solving for the component of velocity in the transverse direction for short-time steady state conditions, and introducing the auxiliarly mobility parameter $\mu = \frac{q\tau}{m}$—where the solvent is approximately stationary—the transverse velocity $v_y$ for very small time is

given by 4.2 as the relationship:

$$v_y = -\frac{\mu^2 |\vec{B}||\vec{E}|}{1 + |\vec{B}|^2 \mu^2} \tag{4.3}$$

under Markovian solvent assumptions. It is important to note the dependence on $|\vec{B}|\mu$, which naturally defines a dimensionless Hall parameter $\beta = |\vec{B}|\mu$, characterizing the magnitude of transverse drift for linear-response steady state conditions [41]. In standard experimental levels for magnetic fields such as 1 T, the Hall parameter $\beta$ is extremely small. For a Potassium ion in water, the momentum relaxation time is $\tau \approx 3 \cdot 10^{-14}$ s [42]. Using a more physically feasible magnetic field of 1 T, the associated Hall parameter would be $\omega_c \tau \approx 10^{-7}$. Consequently, the transverse drift signal is near non-existent for short time: the macroscopic drift is obscured by microscopic thermal noise. This precise obscuration can be quantified through an analysis of the minimum requirements for a sufficent signal to noise ratio (SNR).

It is well-known from the works of Einstein that the variance of an ion's position over time due to Brownian diffusion scales linearly in time [43]. This quantity serves as the effective noise in the SNR, as it obscures the bulk transverse dynamical behavior of the ion during its dynamical evolution. Formally, one may express the variance $\sigma_x^2$ as:

$$\sigma_x^2 = \langle \Delta x^2 \rangle = 2Dt, \tag{4.4}$$

where $D$ is the diffusion coefficient of the ion in a solvent. For water, the diffusion coefficient of a $K+$ ion is $\approx 2 \times 10^{-9}\,\mathrm{m^2 s^{-1}}$ [44]. For reliably observed Hall drift, the transverse displacement $v_y t$—which can be treated as the signal in the SNR—must exceed the random thermal displacement. Setting the signal to noise ratio (SNR) to some minimal value (for sake of simplicity we pick approximately 1), it is possible to construct a precise inequality which yields a relationship between the required simulation time to achieve a noticeable SNR, and the magnetic field strength:

$$\mathrm{SNR} = \frac{v_y t}{\sqrt{2Dt}} \gtrsim 1 \tag{4.5}$$

$$\implies t \gtrsim \frac{2D}{v_y^2} = \frac{2D(1+\beta^2)^2}{\beta^2 \mu^2 |\vec{E}|^2} \tag{4.6}$$

To achieve a completely minimimal lower bound, one seeks to minimize the right-hand side of the inequality 4.6, optimizing $\beta$ globally, which is a parameter dependent on the magnetic field. From the optimal value for $\beta$, one may determine the optimal magnetic field for the system which minimizes the required simulation time to achieve a noticeable SNR. Differentiating the right hand side with respect to $\beta$ and setting to zero to determine the maximum:

$$\frac{\partial}{\partial \beta}\left[\frac{2D(1+\beta^2)^2}{\beta^2 \mu^2 |\vec{E}|^2}\right] = 0 \tag{4.7}$$

$$\frac{4D\left(\beta^4 - 1\right)}{E^2 \mu^2 \beta^3} = 0 \tag{4.8}$$

One may immediately note that the minimum condition is achieved when the condition for the Hall parameter $\beta^4 = 1$ is fulfilled. Therefore, the optimal Hall parameter $\beta = \omega_c \tau$

for the best SNR ratio is, quite beautifully, 1. Using values associated to the two-species ionic system—$m_{K^+} = 6.48 \cdot 10^{-26}$ kg, $q = e = 1.6 \cdot 10^{-19}$ C, $\tau_{K^+} = 3 \cdot 10^{-14}$ s—and solving for the B-field which yields a Hall parameter $\beta = 1$, one determines the globally optimal B-field that yields the highest SNR.

$$\beta = 1 \implies B = \frac{m_{K^+}}{q\tau_{K^+}} = \frac{6.48 \cdot 10^{-26}}{(1.6 \cdot 10^{-19})(3 \cdot 10^{-14})} = 1.35 \cdot 10^7 T \tag{4.9}$$

Immediately, one observes that the optimal B-field is unfeasibly large, but exists. Should the B-field become too large, then the transverse velocity would decay, as it was shown that $v_y \propto \frac{1}{|\vec{B}|}$, and if it is too little, then the acceleration due to the Lorentz force would be too small to observe a noticeable signal. These two factors contribute to the existence of such an optimal parameter for every possible simulation time. Naturally, this is way too large to avoid numerical errors in the Boris integrator without extremely small timesteps, so it is productive to determine the minimal possible B field for the fixed simulation length used in each MD run which still maintains sufficiently large SNR. For a simulation which runs for $t_0 = 50$ ps we pick the largest electric field $1 \times 10^{11}\,\mathrm{Vm}^{-1}$ analyzed in this investigation in spirit of determining the lower bound of the magnetic field. One may then solve the inequality 4.6 for the minimum B-field for a tighter, simulation relevant bound as:

$$B \gtrsim \frac{\sqrt{2D}}{\mu^2 E\sqrt{t_0}} = \frac{\sqrt{2(2 \cdot 10^{-9})}}{(7.407407 \cdot 10^{-8})^2(10^{11})\sqrt{50 \cdot 10^{-12}}} \approx 5.2 \times 10^3\,\mathrm{T} \tag{4.10}$$

Therefore picking a magnetic field strength of $10^4$ T allows the simulation to sit within this regime of larger SNR, while not reaching magnetic field strengths which would cause numerical error to accumulate drastically in the Boris integrator. As the basis of this investigation involves the extraction of accelerations, it is also relevant that the magnetic field is not chosen so large such that the trajectory deviates from linear response. With $10^4$ T as the chosen magnetic field, the Hall parameter of the system sits well below the global solution $\beta = 1$, namely, $\beta_{sim} = \mu B_{sim} \approx 7 \cdot 10^{-4} \ll 1$, so such linear response approximations for the acceleration computations holds strongly. This is clearly evident in the transverse velocity trajectory visualized for the ionic system in figure 4.5.

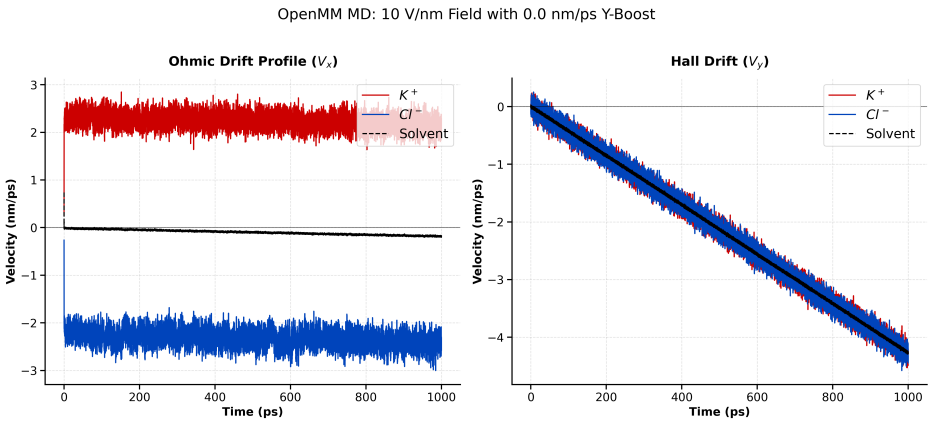


**Figure 4.5:** OpenMM 1ns $1M$ KCl Simulation with $|\vec{E}| = 10^{10}\frac{V}{m}$, and $|\vec{B}| = 10^4 T$ Ohmic Drift Velocity in X (Left), Hall Drift in Y (Right)

One may note that the Ohmic drift in the x-direction is charge antisymmetric, which leads to an abruptly achieved terminal velocity (for periodic boundary conditions) for both species. As Chloride ions have a larger effective ionic radius, one may also notice a slight negative velocity trend as the $Cl^-$ ions drag more of the system in their wake. For the Hall-direction plot, in the y-direction, one may demonstrably observe that the simulation lies well within the linear response regime to the external fields, despite their strength. With a chosen magnetic field strength of $10^4$ T, the SNR ratio is clearly higher, however the large stochastic noise of the solvent is clearly visible by the thick band present on the linear trend, characterizing Brownian variance $\sigma_x^2$.

### 4.2.3 Demonstration of Predicted Drift: 2D Parameter Sweep

To bypass the timescale bottleneck associated with asymptotic analysis, an algorithmic shift is proposed: rather than simulating the full temporal evolution of the fluid, one casts the search for the asymptotic drift velocity as a computational root-finding problem, and treats the issue as the determination of a stable fixed point of a dynamical system in the velocities. For a fixed magnetic and electric field strength, the theory established during the analytic asymptotic examination predicts direct proportionality between the electric field and the asymptotic velocity.

To determine the asymptotic velocity for a specific field configuration, one may procedurally run simulations where the initial velocity of the electrolyte is boosted to some finite value. Analyzing the acceleration on the boosted system, and determining the precise boost which yields net zero acceleration allows one to find the asymptotic velocity without using long timescale simulations. Figure 4.6 which precisely demonstrates the stable fixed point behavior for a magnetic field strength of $\vec{B} = 10\hat{z}$ kT, and an electric field strength of $\vec{E} = -0.9375\hat{x}$ V/nm. Each point in Figure 4.6 is the gradient of the velocity trajectory in the Hall direction of the boosted system extracted through a linear fit. Note that the accelerations are always in an appropriate configuration as to relax the system back towards the steady state velocity.

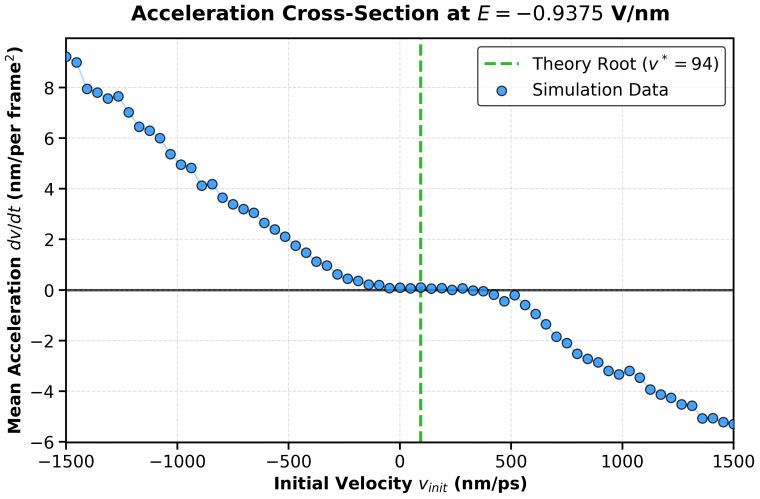


**Figure 4.6:** Measured Accelerations by Linear Fits to an Initial Velocity Parameter Sweep for $|\vec{E}| = -0.9375 \cdot 10^9 \frac{V}{m}$, and $|\vec{B}| = 10^4 T$

The vertical green line in Figure 4.6 is the theoretical $\vec{E} \times \vec{B}$ proportional drift as in 3.15. One may note that theoretical consistency is already observed here, however the precise accuracy of the model is unclear due to the thick band of zeros about the root. At the steady state velocity (94 nm/ps), the electrolyte is said to be in equilibrium. Naturally, if the system is slower than the prediced asymptotic velocity, the ions will begin to relax towards the plasma drift velocity, speeding up, and entraining the solvent as well via a galilean invariant drag coupling, as detailed in Figure 3.1. If the entire system is boosted to a velocity above the predicted asymptotic velocity, then the ions will quickly relax back to their plasma drift velocity, causing the relative velocity between the solvent and the ions to increase, leading to deceleration of the solvent. The combination of these two acceleration regimes leads to a predicted fixed point behavior about the asymptotic plasma drift velocity $v^* = \frac{\vec{E} \times \vec{B}}{|\vec{B}|^2}$ for a nonequilibrium electrolytic system as observed in Figure 4.6.

To perform an overarching examination of this behavior and clearly verify that a linear relationship between electric field and asymptotic drift velocity exists, a coarser two-dimensional sweep over simulation parameter space—electric field and initial velocity boost—was performed. A $65 \times 65$ grid of electric field strengths ranging from $-10$ V/nm to 10 V/nm, and initial velocities ranging from $-1500$ nm/ps, to 1500 nm/ps, was taken. Each simulation was run for 50 ps to ensure computational feasibility in finite time for the large quantity of simulations required, and for reasonable precision of the linear fits to the velocity trajectories which extract the accelerations. Figure 4.7 demonstrates these accelerations for a fixed magnetic field strength of 10 kT, where each cell color represents a corresponding acceleration of the system along the Hall drift direction.

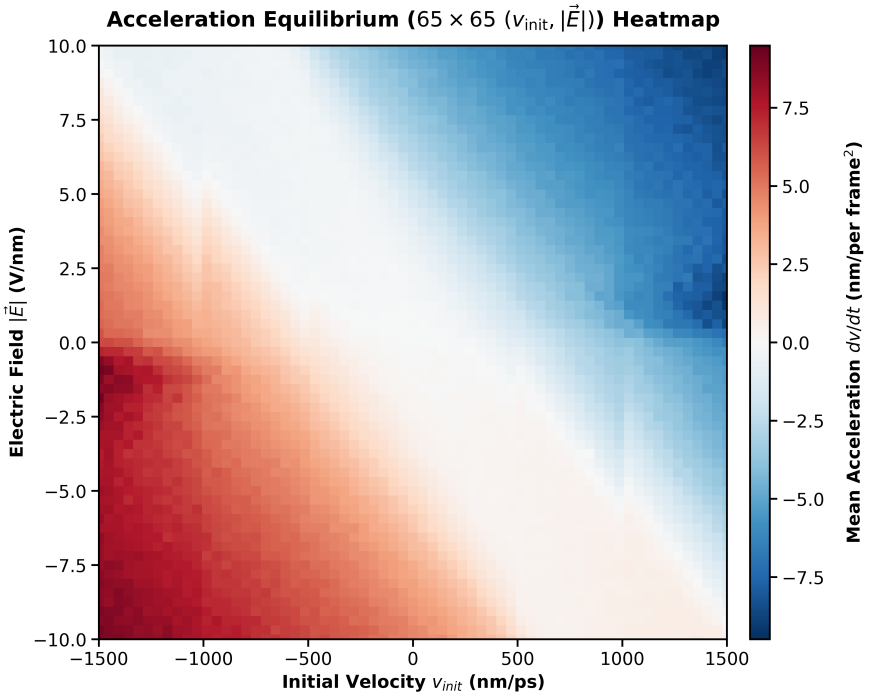


**Figure 4.7:** 2D $65 \times 65$ Heatmap of linear-fit extracted acceleration values over $50ps$ with $|\vec{B}| = 10^4 T$, $|\vec{E}| \in [-10, 10] V/nm$, $v_{init} \in [-1500, 1500] nm/ps$

As one can see, the magnitude of the electric field has a linear effect on the observed steady-state asymptotic velocity $v^*$, where the acceleration is observed to be near zero. As the electric field increases the drift velocity shifts to become negative in the $\hat{y}$ direction, exactly consistent with the $\frac{E\hat{x}\times B\hat{z}}{B^2} = -\frac{E}{B}\hat{y}$ drift. Taking the $(E, v_{init})$ pair with a resultant acceleration closest to zero for each row, and treating these as two-dimensional coordinates, one may perform a linear fit to reconstruct the magnetic field, and verify that the behavior is exactly as expected. Since $v^* = \frac{-E}{B}$, in the specific field configuration detailed in the simulation parameters, the slope of the valley contour in the 2D plot is theoretically of linear form:

$$E(v^*) = -v^* B. \tag{4.11}$$

As each row of the heatmap 4.7—which corresponds to a specific electric field magnitude—exhibits a large 'zero band' as observed in the 1D parameter sweep 4.6, it is assumed that the center of these zero bands is the target asymptotic velocity. To extract these centers, a 5% maximum binary threshold filter was applied to the heatmap image in order to label the zero band centers. These band centers are then treated as points, and fit to linearly. Figure 4.8 details the linear fit to the computed zero band center data overlayed with the theoretical linear trend 4.11.

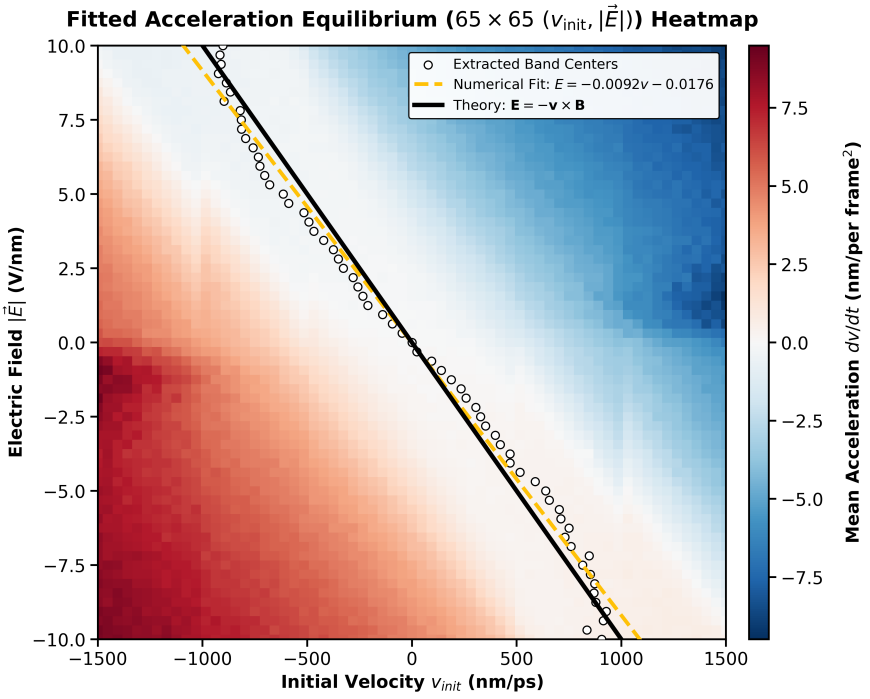


**Figure 4.8:** 2D 65×65 Linear Fit to Heatmap Zero Band Centers of linear-fit extracted acceleration values over $50ps$ with $|\vec{B}| = 10^4 T$, $|\vec{E}| \in [-10, 10] V/nm$, $v_{init} \in [-1500, 1500] nm/ps$

Figure 4.8 is a direct confirmation of the principal asymptotic result of this thesis. The slope of the numerical fit to the thresholded zero band centers is $-9.2 \times 10^{-3}\,\text{Vnm}^{-2}\text{ps}$, which when converted to Tesla via the SI conversion $T \cong Vm^{-2}s$, yields a numerically computed magnetic field of $B_{numerical} = 9.2 \times 10^3\,\text{T}$, which differs from the imposed

magnetic field of $10^4$ T by $\approx 8.7\%$. This commensurable adherence to the theoretical linear field-strength dependence prediction of the asymptotic velocity strongly confirms the tendency of multi-ion-species electrolyte systems to tend to their plasma drift velocity under orthogonal electric and magnetic fields, and the existence of a such stable dynamical fixed points for long-time regimes.

### 4.2.4 Commentary on Asymptotic Computational Results

The demonstrably numerical discrepancy may be attributed to a combination of various systematic and statistical effects which are inhernet in simulation and the associated extraction procedure. Namely, the identification of the zero-acceleration manifold via a fixed percentage threshold introduces an experimental parameter bias. The zero band is not infinitesimally thin, and reflects finite-time fluctuations of the system. Furthermore, the fitting uncertainy in the velocity trajectories due to the strong brownian noise from solvent-ion interactions may have directly contributed to the observed discrepancly. Consequnetly. the extracted band centers systematically deviate from the true fixed point on this basis.

An alternative source of discrepancy is the use of a finite simulation time of 50 ps, which imposes a direct limiation on the accuracy and precision of the linear fits. In the previous section, the SNR was derived as an explicit function of time, and it can be seen that SNR depends on the time on order $\mathcal{O}(t^{\frac{1}{2}})$.

Lastly, the discretization of the parameter space due to constraints on available computational resources imposes a finite resolution, which limits the precision with which the zero-acceleration contour can be localized. In effect, the extracted contour obtained represents the footprint of a discretized approximation of the inherent fixed point curve, and the subsequent linear fit in Figure 4.8 inherits this error.

Looking forward, this framework suggests several natural extensions. One may, for instance, replace the brute-force parameter sweep with more efficient root-finding algorithms (e.g. the Bisection method) applied directly to the measured acceleration, thereby further reducing computational cost in allowing less simulations to be taken for fixed field configurations which in exchange allows for a longer simulation time, and more precise acceleration resolution. Commentary, an associated example plot of a Bisection root finding implementation, and the algorithm's pseudocode implementation on the electrolytic system can be found in Appendices F, G, and H, respectively.

## 4.3 Transient Relaxation Analysis & Electrolyte Memory Kernel Extraction

While the preceding theoretical sections in Chapters 2 and 3 established the formal existence and analytic structure of the generalized memory kernel $K_\alpha(t)$ through the Mori–Zwanzig projection formalism, the explicit functional form of the kernel remains undetermined from first principles and is largely a parameter function. This limitation is direct consequence of the fact that the memory kernel encodes the complex many-body interactions which the previous derivation assumed to be mean field in nature.

The precise temporal, transient structure of the memory kernel is therefore nontrivial, and emergent from the solvent-ion interactions and associated hydrodynamic coupling. To approach this problem computationally, $K_\alpha(t)$ is determined through numerical estimation from nonequilibrium molecular dynamics trajectories.

The principal objective of this section is therefore to establish a computationally tractable inverse methodology for reconstructing the species-wise electrolyte memory kernels directly from microscopic OpenMM simulations. Particular emphasis is placed upon constructing a numerically stable kernel extraction procedure consistent with the non-Markovian Green–Kubo formalism developed previously in Section 3.2, and the multipole transient correlation structure derived in Section 3.2.4. The method derived follows a similar structure to the one proposed by Tepper, Dalton and Netz in their 2024 work on memory kernel reconstruction for protein folding, however is adapted to the much faster trasient decay structure inherent in electrolyte solutions, where the velocity autocorrelation function (VACF) decays on much shorter timescales than that of a protein folding trajectory [45].

Earlier iterations of the kernel reconstruction procedure employed Gaussian process optimization (GPO) for estimation of the memory kernel parameters. Gaussian process methods are highly effective for low-dimensional optimization problems possessing smooth objective landscapes, as they construct a probabilistic surrogate model of the loss functional and iteratively refine parameter estimates through Bayesian acquisition strategies [46].

However, in the present electrolyte memory reconstruction problem, the objective landscape generated by the generalized Langevin fitting procedure was found to violate many of the regularity assumptions underlying Gaussian-process-based optimization. Specifically, the transient VACF reconstruction is highly sensitive to small perturbations of the oscillatory kernel frequencies and decay timescales. Since the generalized Langevin dynamics involve repeated convolution of damped oscillatory modes, small frequency deviations accumulate phase error over time, producing rapidly oscillating loss surfaces populated by numerous local minima. This behavior emerges naturally from the multipole exponential transient structure derived previously in Section 3.2.4. Complex-valued poles of the transformed Volterra-style system induce damped oscillatory relaxation modes, causing the associated objective functional to inherit a strongly non-convex spectral structure. Consequently, nearby parameter vectors may generate VACFs with nearly identical amplitudes but produce sharp local oscillations in the reconstruction error landscape—which is simulated by numerical methods over the GLE.

In such regimes, Gaussian process surrogate models become increasingly unreliable. The probabilistic interpolation inherent to GPO implicitly assumes a comparatively smooth covariance structure of the objective functional over parameter space. The strong phase sensitivity and extremely varied local curvature of the VACF mismatch functional violate these assumptions, causing the acquisition process to repeatedly converge towards suboptimal local minima or become dominated by inaccurate surrogate uncertainty estimates.

### 4.3.1 Proposed Transient Kernel Reconstruction Methodology: Differential Evolution Optimization

To overcome these aforementioned limitations, the optimization procedure was reformulated using Differential Evolution (DE), a population-based stochastic global optimization algorithm specifically designed for rugged, non-convex, and highly multimodal objective landscapes—such as those introduced in an electrolytic fluid [47]. In contrast to the smooth ansatzes of Gaussian process optimization, DE does not attempt to construct a smooth surrogate representation of the objective functional, which was found to be inadequate for the highly non-convex landscape it seeks to replicate, and does not even require gradient computation of the loss functional. Instead, DE performs direct evolutionary exploration of parameter space through stochastic mutation and recombination operations applied across a population of candidate kernel parameter vectors [48].

This global evolutionary strategy proved substantially more robust for the present non-Markovian electrolyte reconstruction problem. In particular, DE demonstrated significantly improved resistance to oscillatory phase-trapping artifacts and was consistently capable of identifying stable kernel parameterizations reproducing the transient molecular dynamics VACF structure over the physically relevant timescale regime. The consequently extracted kernel parameters control the spectral relaxation structure of the generalized Langevin dynamics, and the resulting loss functional inherits the same nonlocal temporal sensitivity characteristic of the underlying non-Markovian transport itself. Thus, the DE optimization procedure provides a natural framework on which functional optimization of the memory kernel, inverted through the Volterra system, can be performed efficiently.

### 4.3.2 Velocity Autocorrelation Formulation

Beginning from the generalized Langevin equation derived previously in Equation 2.20—for purposes of deriving the VACF evolution equation, on which numerical kernel reconstruction is performed—the stochastic dynamics of a tagged ion of species $\alpha \in \{+.-\}$ are governed by:

$$\frac{d\vec{v}_\alpha}{dt} = \frac{q_\alpha}{m_\alpha}\left(\vec{E} + \vec{v}_\alpha \times \vec{B}\right) - \int_0^t K_\alpha(t-\tau)\left[\vec{v}_\alpha(\tau) - \vec{u}(\tau)\right] d\tau + \frac{1}{m_\alpha}\vec{\zeta}_\alpha(t). \tag{4.12}$$

where $K_\alpha(t)$ denotes the non-Markovian memory kernel governing delayed frictional relaxation, while $\vec{\zeta}_\alpha(t)$ represents the fluctuating stochastic force arising from unresolved microscopic solvent and ionic degrees of freedom. For equilibrium transport analysis, the ionic velocity may be decomposed into a macroscopic hydrodynamic contribution and a fluctuating microscopic component,

$$\vec{v}_\alpha(t) = \vec{u}(t) + \delta\vec{v}_\alpha(t). \tag{4.13}$$

As the Green–Kubo formalism concerns equilibrium fluctuations relative to the local fluid rest frame, one may transform into the comoving hydrodynamic frame for which

$$\vec{u}(t) = 0. \tag{4.14}$$

The generalized Langevin equation therefore reduces to

$$\frac{d\vec{v}_\alpha}{dt} = \frac{q_\alpha}{m_\alpha}\left(\vec{E} + \vec{v}_\alpha \times \vec{B}\right) - \int_0^t K_\alpha(t-\tau)\vec{v}_\alpha(\tau)\,d\tau + \frac{1}{m_\alpha}\vec{\zeta}_\alpha(t). \tag{4.15}$$

Recalling the definition of the velocity autocorrelation function (VACF) for species $\alpha$,

$$C_{ij}^{(\alpha)}(t) = \langle v_{\alpha,i}(t)v_{\alpha,j}(0)\rangle\,, \tag{4.16}$$

multiplying by $v_{\alpha,j}(0)$, and taking the equilibrium ensemble average yields

$$\left\langle \frac{dv_{\alpha,i}(t)}{dt}v_{\alpha,j}(0)\right\rangle_{eq} = \frac{q_\alpha}{m_\alpha}E_i\left\langle v_{\alpha,j}(0)\right\rangle_{eq} + \frac{q_\alpha}{m_\alpha}\left\langle (\vec{v}_\alpha \times \vec{B})_i v_{\alpha,j}(0)\right\rangle_{eq} \tag{4.17}$$

$$- \int_0^t K_\alpha(t-\tau)\left\langle v_{\alpha,i}(\tau)v_{\alpha,j}(0)\right\rangle_{eq} d\tau + \frac{1}{m_\alpha}\left\langle \zeta_{\alpha,i}(t)v_{\alpha,j}(0)\right\rangle_{eq}. \tag{4.18}$$

Simplifying, the first term vanishes due to the zero mean velocity in equilibrium, while the last term vanishes by the statistical independence of the stochastic force and the initial velocity. The exact tensorial VACF evolution equation therefore becomes

$$\boxed{\frac{d}{dt}C_{ij}^{(\alpha)}(t) = \frac{q_\alpha}{m_\alpha}\epsilon_{ikl}B_l C_{kj}^{(\alpha)}(t) - \int_0^t K_\alpha(t-\tau)C_{ij}^{(\alpha)}(\tau)\,d\tau} \tag{4.19}$$

which constitutes the full non-Markovian magnetized correlation dynamics for the electrolyte system. Unlike the isotropic zero-field limit, the presence of the external magnetic field induces anisotropic rotational coupling between the tensorial VACF components through the Lorentz force contribution. Consequently, the relaxation dynamics no longer evolve through purely scalar dissipative decay, but instead through coupled oscillatory memory-damped transport modes. For an external magnetic field oriented along the $\hat{z}$-direction, the Lorentz contribution couples the transverse velocity correlation components according to

$$\frac{d}{dt}C_{ij}^{(\alpha)}(t) = \frac{q_\alpha B}{m_\alpha}\epsilon_{ikz}C_{kj}^{(\alpha)}(t) - \int_0^t K_\alpha(t-\tau)C_{ij}^{(\alpha)}(\tau)\,d\tau, \tag{4.20}$$

The magnetic field therefore acts as a conservative rotational operator within the VACF dynamics, continuously transferring correlation amplitude between orthogonal velocity components while the memory kernel simultaneously governs dissipative relaxation. The resulting transient dynamics consist of coupled non-Markovian cyclotron modes whose decay rates and oscillatory structure are jointly determined by the memory kernel and the external magnetic field strength.

Restricting attention to the velocity component parallel to the applied electric field yields the projected correlation equation

$$\boxed{\frac{d}{dt}C_\alpha^{vv}(t) = \omega_{c,\alpha}C_\alpha^{\perp}(t) - \int_0^t K_\alpha(t-\tau)C_\alpha^{vv}(\tau)\,d\tau}$$

where $C_\alpha^{\perp}(t)$ denotes the magnetically coupled transverse VACF component generated by the Lorentz rotation operator. The observable longitudinal correlation dynamics are therefore influenced both by delayed non-Markovian friction and by rotational coupling induced through the external magnetic field.

Consequently, the measured molecular dynamics VACF no longer exhibits purely monotonic relaxation, but instead develops oscillatory transient structure associated with cyclotron rotation, ionic caging, and viscoelastic hydrodynamic backflow. The correlation function therefore encodes both dissipative and conservative transport dynamics simultaneously.

### 4.3.3 Parameterized Memory Kernel Reconstruction

As shown previously in Section 3.2.4, the asymptotic transient structure of the non-Markovian conductivity formalism admits a finite multipole decomposition arising from the pole structure of the Laplace-transformed Volterra system. In the presence of the magnetic field, the Lorentz operator shifts the transient spectrum into complex-valued rotational relaxation modes, generating damped oscillatory VACF dynamics even in the absence of explicitly oscillatory kernels.

Motivated directly by this analytic structure, the species-wise memory kernel is parameterized as

$$\boxed{K_\alpha(t) = \sum_{i=1}^{N_e} A_i e^{-t/\tau_i} + \sum_{j=1}^{N_o} A_{j,\cos}^{(o)} e^{-t/\tau_j^{(o)}} \cos(\omega_j t) + A_{j,\sin}^{(o)} e^{-t/\tau_j^{(o)}} \sin(\omega_j t)} \tag{4.21}$$

where $A_i$ denote relaxation amplitudes—$A_i^{(o)}$ for sine and cosine oscillatory modes respectively—$\tau_i$ denote characteristic timescales, and $\omega_j$ denote oscillatory frequencies associated with transient ionic cage dynamics, delayed hydrodynamic response, and magnetic-field-coupled transport oscillations.

The kernel ansatz therefore inherits the same spectral structure predicted analytically from the transformed Green–Kubo formalism in Section 3.2. Real-valued poles generate exponentially decaying relaxation channels, while complex-valued poles generate damped oscillatory modes whose frequencies are modified jointly by the intrinsic electrolyte memory timescales and the external cyclotron dynamics. Physically, rapidly decaying exponential contributions correspond primarily to local binary solvent collisions and fast stochastic thermalization processes. The oscillatory components instead encode delayed momentum backflow, transient ionic trapping, and magnetically induced rotational transport structure arising from the coupling between the Lorentz force and the non-Markovian electrolyte relaxation dynamics.

### 4.3.4 Numerical Solution of the Coupled Volterra System

Given a trial parameter vector, which was simplified to include two exponential modes and two oscillatory mode for computational tractability,

$$\theta = (A_1, \tau_1, A_2, \tau_2, A^{(o)}_{1,\cos}, A^{(o)}_{1,\sin}, \tau^{(o)}_1, \omega_1, A^{(o)}_{2,\cos}, A^{(o)}_{2,\sin}, \tau^{(o)}_2, \omega_2), \tag{4.22}$$

the corresponding 12 parameter kernel $K_\alpha(t;\theta)$ is substituted directly into the coupled Volterra system governing the VACF evolution. The temporal domain is discretized using a uniform timestep $\Delta t$, taken to be the precise reporter frequency of the OpenMM trajectory data:

$$t_n = n\Delta t, \tag{4.23}$$

and refined to a sub-grid initialization $\delta t = \frac{\Delta t}{N_{sub}}$ to ensure numerical stability against the stiff high frequency components consequent from a large magnetic field. The longitudinal and transverse VACF arrays are initialized at $t = 0$ to match the initial conditions of the molecular dynamics trajectory,

$$C_{\alpha,xx}(0) = C_{\alpha,MD}(0), \quad C_{\alpha,yx}(0) = 0, \tag{4.24}$$

and the coupled Volterra system is solved forward in time to generate the theoretical VACF reconstruction corresponding to the trial kernel parameters in three steps. First, the memory convolution integral is evaluated numerically through trapezoidal quadrature, e.g.

$$I_{xx}(t_i) \approx \sum_{k=0}^{i} w_k K(t_k;\theta) C_{\alpha,xx}(t_i - t_k)\delta t, \tag{4.25}$$

$$I_{yx}(t_i) \approx \sum_{k=0}^{i} w_k K(t_k;\theta) C_{\alpha,yx}(t_i - t_k)\delta t, \tag{4.26}$$

where $w_k$ are the trapezoidal weights (0.5 at boundaries, 1.0 elsewhere). Second the Lorentz coupling term is evaluated at each time step, incorporating the Lorentz rotatinal operator contribution to the transverse VACF component. The discretized GLE step is then computed as

$$\frac{dC_{\alpha,xx}}{dt} = \omega_c C_{\alpha,yx}(t_{i-1}) - \frac{1}{m_\alpha} I_{xx}(t_i), \tag{4.27}$$

$$\frac{dC_{\alpha,yx}}{dt} = -\omega_c C_{\alpha,xx}(t_{i-1}) - \frac{1}{m_\alpha} I_{yx}(t_i). \tag{4.28}$$

Applying a sub-timescale Euler integration step on the refined temporal grid yields the updated VACF values at time $t_i$,

$$C_{\alpha,xx}(t_i) = C_{\alpha,xx}(t_{i-1}) + \frac{dC_{\alpha,xx}}{dt}\delta t, \tag{4.29}$$

$$C_{\alpha,yx}(t_i) = C_{\alpha,yx}(t_{i-1}) + \frac{dC_{\alpha,yx}}{dt}\delta t. \tag{4.30}$$

The Lorentz contribution introduces oscillatory rotational coupling between the transverse and longitudinal VACF components, while the memory convolution simultaneously

governs temporally nonlocal dissipative relaxation. The resulting system therefore constitutes a coupled non-Markovian magnetized transport evolution problem.

Since dense ion-solvent systems frequently exhibit stiff short-timescale dynamics arising from rapid solvent collision processes and high-frequency cyclotron oscillations, the numerical integration is performed on a refined temporal sub-grid in order to maintain stability during the early transient regime.

Unlike direct inversion approaches, which require numerical differentiation of noisy molecular dynamics data and thereby strongly amplify statistical fluctuations, the present methodology repeatedly solves the forward generalized Langevin dynamics for candidate kernels and directly compares the resulting theoretical VACF against the molecular dynamics trajectory data. This forward reconstruction strategy is substantially more numerically stable and naturally regularizes the inverse problem.

### 4.3.5 Global Optimization of the Kernel Parameters

Determination of the optimal kernel parameters constitutes a highly non-convex inverse problem. The simultaneous presence of oscillatory memory relaxation modes and magnetic cyclotron coupling generates strong phase sensitivity within the objective landscape, causing conventional gradient-based optimization methods to become trapped within local minima. Small frequency mismatches accumulate rapidly in time and produce highly oscillatory error hypersurfaces containing numerous nearly degenerate parameter combinations.

To overcome these difficulties, the parameter reconstruction problem was solved using differential evolution, a stochastic population-based global optimization algorithm particularly well suited to rugged high-dimensional objective landscapes.

Defining the loss functional:

$$\boxed{\mathcal{L}(\theta) = \frac{1}{N_t} \sum_{n=1}^{N_t} \left[ C^{vv}_{\alpha,\mathrm{MD}}(t_n) - C^{vv}_{\alpha,\mathrm{GLE}}(t_n;\theta) \right]^2}$$

the differential evolution algorithm evolves a population of candidate parameter vectors through mutation, crossover, and greedy selection operations.

For a candidate parameter vector $\theta_i$, mutant trial vectors are generated according to

$$\boxed{\mathbf{v}_i = \theta_{r_1} + F\left(\theta_{r_2} - \theta_{r_3}\right)}$$

where $F$ denotes the mutation scaling factor and $r_1, r_2, r_3$ are distinct random population indices.

Unlike gradient-based optimization methods, differential evolution does not require evaluation of objective gradients. Instead, the optimization dynamically extracts search directions directly from evolving population differences, making it particularly effective for the present magnetized non-Markovian inverse problem whose oscillatory Volterra

dynamics generate rugged objective surfaces containing numerous local minima and strong parameter degeneracies.

The resulting optimized parameter vector determines the reconstructed species-wise memory kernel $K_\alpha(t)$, whose transient spectral structure may subsequently be analyzed directly in relation to the analytically predicted multipole relaxation decomposition and the underlying magnetized electrolyte transport dynamics.

### 4.3.6 Demonstration of Memory Kernel Reconstruction: Differential Evolution Optimization Computational Results

Applying the reconstruction methodology described above to the an OpenMM trajectory of $10ns$ yields the transient VACF and memory kernel structure visualized in Figure 4.9. Several important qualitative features immediately emerge from the reconstructed correlation dynamics.

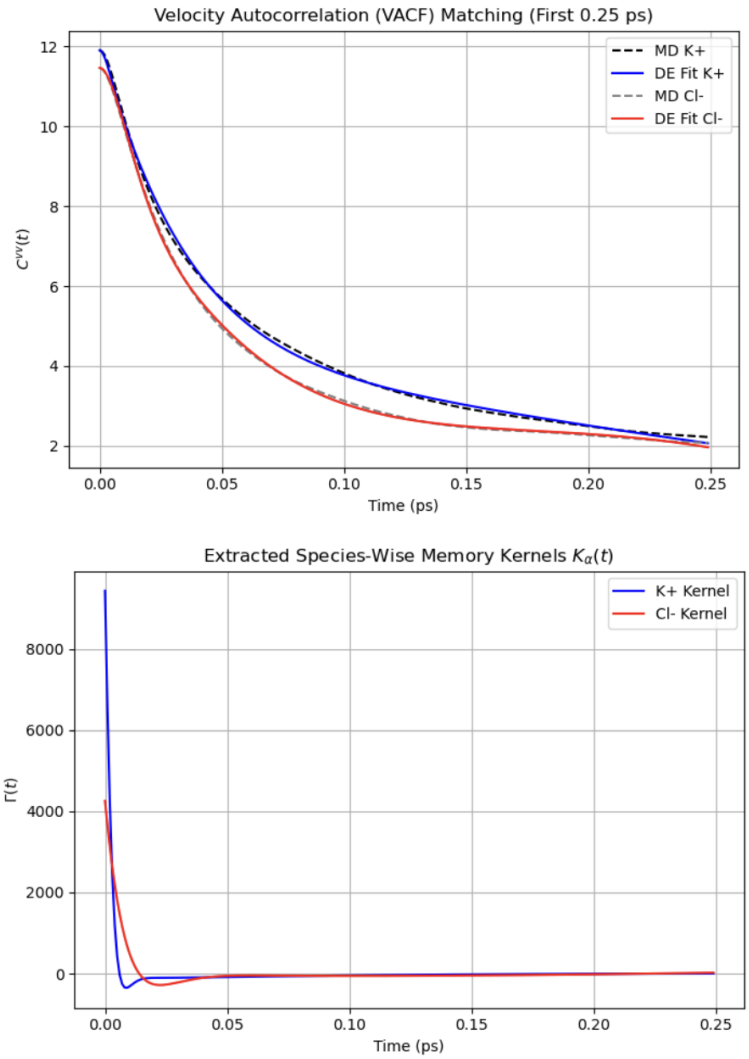


**Figure 4.9:** Differential Evolution fitted Memory Kernel and resultantly integrated VACF under the Volterra System

Rather than relaxing monotonically, the memory kernel briefly crosses through negative values before it returns to exponential decay. This behavior is characteristic of transient ionic caging, commonly referred to as “cage rattling” dynamics in dense fluid systems [45]. Physically, the tagged ion initially accelerates under thermal fluctuations and external forcing, but rapidly encounters some temporary local confinement generated by the surrounding solvation shell, and neighboring ions.

The resulting collective response transiently reverses the ion momentum momentarily, producing the observed negative memory kernel at short times.

It is crucial to acknowledge that such cage rattling behavior is a direct signature of non-Markovian transport in the simulated ion-solvent system. In a purely Markovian electrolyte model, where friction is imposed by an instantaneous memory kernel, the velocity autocorrelation function would necessarily decay monotonically and sharply in the form of a dirac delta, through a single relaxation mode. The observed oscillatory transient structure of the VACF and memory kernel therefore demonstrates the existence of delayed momentum feedback and temporally nonlocal solvent relaxation dynamics within the electrolyte.

Most importantly, the reconstructed transient behavior coincides with the analytic multipole relaxation theory derived in Section 3.2.4. There, the Laplace-space analysis of the generalized Volterra system of integro-differential equations demonstrated that the transient current correlation dynamics decompose into a assumedly finite superposition of damped oscillatory exponential modes determined by the singular pole structure of the Laplace transformed current correlation tensor. The present computational results directly verify this prediction, as visualized quantitatively in Figure 4.9.

The Differential Evolution optimization procedure therefore successfully reconstructes the transient structure of the memory kernel and VACF without requiring direct numerical differentiation of aforementioned noisy molecular dynamics correlation data. It is important to emphasize that the extracted oscillatory relaxation modes are not merely numerical fitting artifacts. The reconstructed kernels therefore provide a physically interpretable spectral representation of the underlying nonequilibrium electrolyte dynamics, and the resulting kernels can be used to better understand the transient dynamics of each ionic species. It was found however, that upon increasing the available parameter range for the amplitudes and frequencies of oscillatory modes, the simulation would tend to extremely large amplitudes, blowing up the memory kernel. To allow for finite-timestep integration, all further Differential Evolution learned memory kernels were run with a reduced parameter range as a form of regularization.

### 4.3.7 Reconstruction of Transient Dynamics from the Differential Evolution Optimized Memory Kernel

The explicit Differential Evolution optimized solutions for the species-wise memory kernels may now be substituted directly back into the coupled generalized Volterra system 2.56, 2.57, in order to reconstruct the full transient electrolyte relaxation dynamics. The resulting reconstructed dynamics therefore constitute a self-consistent forward integration of the generalized Langevin formalism using memory kernels extracted entirely from microscopic molecular dynamics trajectories. For potassium ions, the

optimized memory kernel after parameter regularization was reconstructed as

$$K_K(t) = 158.8862e^{-t/0.1740} + 61.1193e^{-t/4.3428} + e^{-t/0.0094}\left(4262.0415\cos(74.0545t) - 2429.8124\sin(74.0545t)\right) \quad (4.31)$$
$$+ e^{-t/2.4652}\left(-225.8420\cos(5.6596t) - 45.8777\sin(5.6596t)\right) \quad (4.32)$$

Similarly, the optimized chloride memory kernel was reconstructed as

$$K_{Cl}(t) = 158.7262e^{-t/0.2190} + 62.0172e^{-t/4.2938} + e^{-t/0.0089}\left(4312.0415\cos(73.8745t) - 2399.9135\sin(95.0004t)\right) + e^{-t/2.394}\left(-226.9210\cos(5.7106t) - 46.1231\sin(5.1426t)\right) \quad (4.33)$$

Several important physical features emerge immediately upon examining the optimized kernels. Both ionic species exhibit a strongly multiscale relaxation structure consisting of rapidly decaying high-frequency oscillatory modes superimposed upon slower exponential relaxation channels.

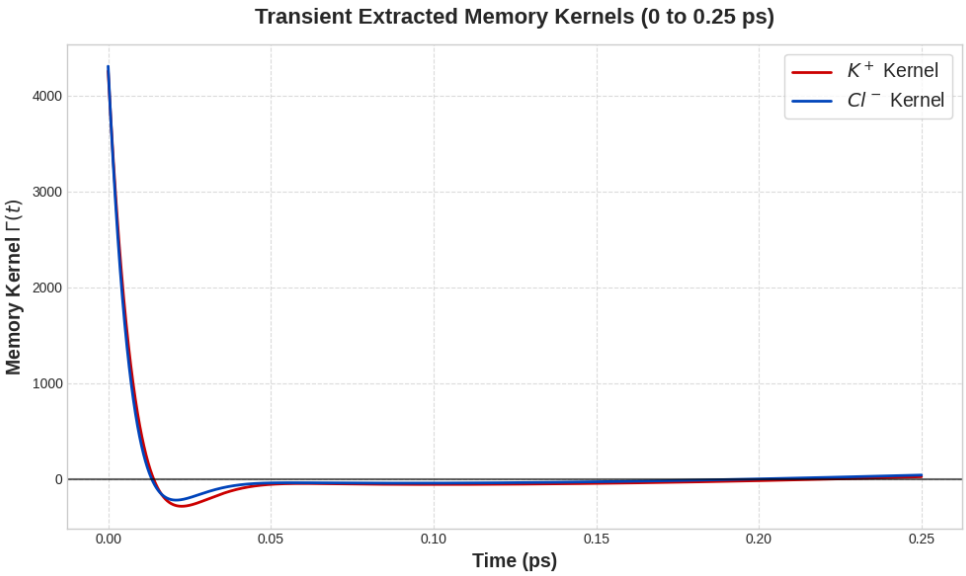


**Figure 4.10:** 0.25ps Plot of Parameter Regularized $K^+$ and $Cl^-$ Memory Kernels 4.32 and 4.33

The shortest-timescale large amplitude oscillatory contributions decay on sub-picosecond timescales and possess extremely large amplitudes and frequencies, indicating intense local transient solvation shell confinement within the surrounding electrolyte environment. These high-frequency contributions correspond directly to the short-time "cage rattling" regime as aforementioned, and previously observed in Figure 4.9, where neighboring ions and solvent molecules collectively generated a temporary restoring force which acted on each ion species.

From a ion-species comparison, the potassium kernel exhibits larger high-frequency oscillatory amplitudes than the chloride kernel. Physically, this is consistent with the smaller ionic radius and larger mobility of potassium ions within aqueous solution,

allowing more rapid transient oscillatory motion prior to solvent-mediated relaxation [49]. The chloride kernel instead exhibits comparatively slower long-timescale relaxation channels, consistent with the larger effective hydrodynamic radius and stronger solvent structuring surrounding the anion.

Substituting these reconstructed kernels directly into the coupled Volterra transport system (equations 2.56, 2.57) and numerically integrating forward in time using an implicit Euler integration scheme and trapezoidal rule on the memory kernel integral yields the transient bulk velocity $V_\alpha(t)$ evolution shown in Figure 4.11. For short timescales, the behavior mimics the linear evolution of the velocity trajectory seen in Figure 3.1. Note the slight deviations in terminal longitudinal drift and transverse acceleration. These deviations are postulated to be caused by training the memory kernel on insufficiently long trajectories, and without presence of an external electric field.

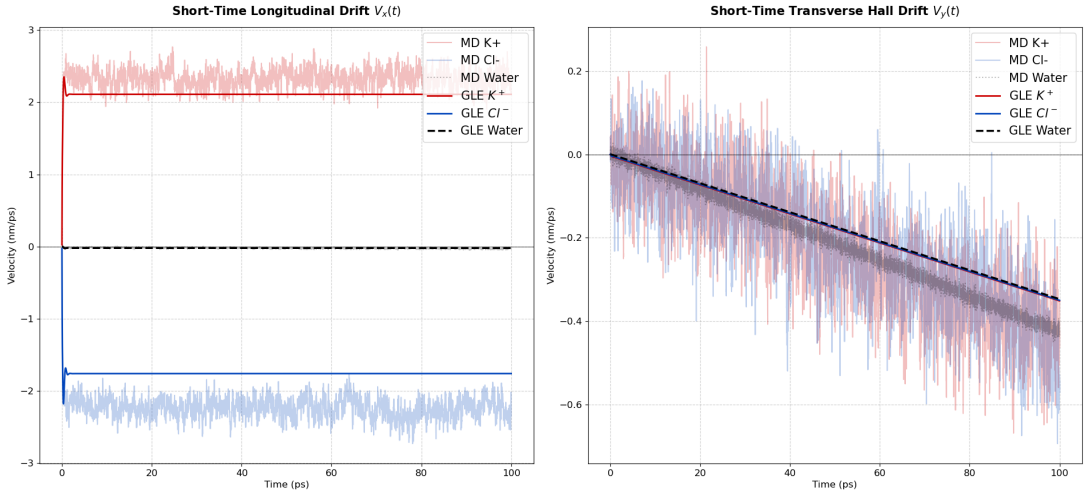


**Figure 4.11:** Reconstruction of short-time transient bulk velocity dynamics obtained via forward integration of the coupled generalized Volterra system using the differential-evolution-optimized electrolyte memory kernel. GLE integrated trajectory is compared against MD under orthogonal $|\vec{B}| = 10$ kT, $|\vec{E}| = 10$ V/nm field configuration.

For larger timescales on the order of a few microseconds, the exponentially damped relaxation structure predicted by the multipole Volterra analysis can be demonstrated, as seen in Figures 4.12 and 4.13. Following the initial linear transient evolution demonstrated during analysis of asymptotic dynamics, the bulk ionic velocity gradually transitions into a slow, exponential relaxation regime governed by the long-timescale memory channels of the reconstructed kernel. Figure 4.12 demonstrates the ion-species behavior when left from rest, tending to the expected asymptotic drift velocity of $-1000$ nm/ps, calculated using the derived theoretical equation for the asymptotic drift velocity 3.15.

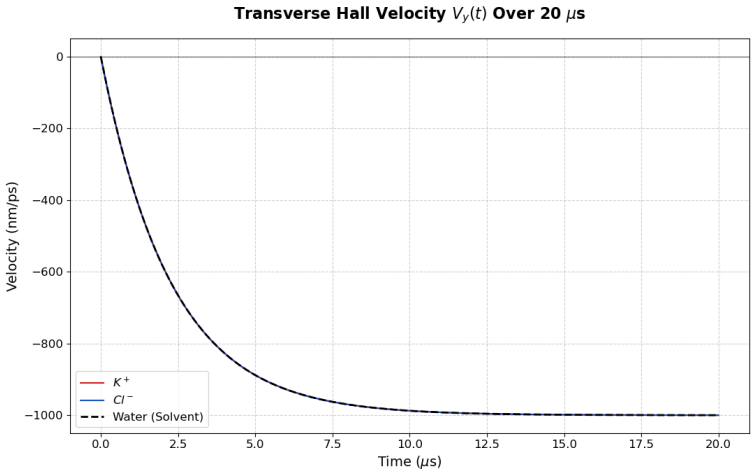


**Figure 4.12:** GLE integrated long time trajectory over $20\mu s$ under an orthogonal $|\vec{B}| = 10$ kT, $|\vec{E}| = 10$ V/nm field configuration from rest.

The GLE integrated dynamics under the machine learned memory kernels subsequently decay exactly towards the asymptotic drift velocity over significantly longer timescales, reflecting the persistence of delayed hydrodynamic relaxation and temporally nonlocal solvent momentum transport within the electrolyte environment. The clear distinction between the early-time near-linear response and the later asymptotic exponential decay further demonstrates the fundamentally multiscale nature of the reconstructed non-Markovian transport dynamics. Upon boosting the system to a velocity larger than the transverse hall velocity, the system still tends exponentially—as predicted by the analytic theory and equation 3.60—to the asymptotic velocity.

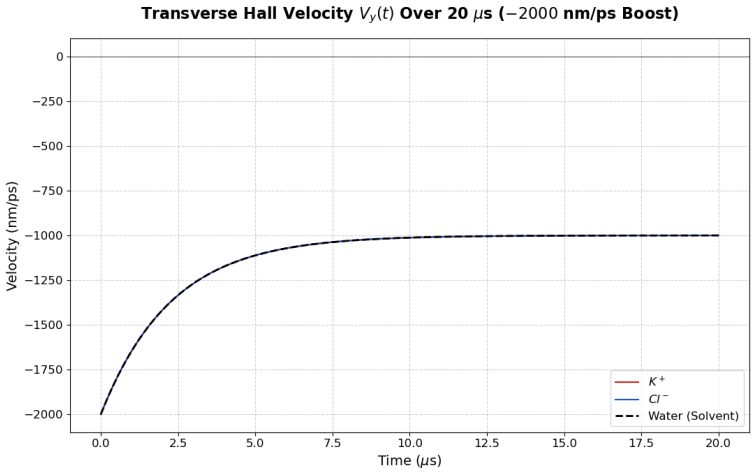


**Figure 4.13:** GLE integrated long time trajectory over $20\mu s$ under an orthogonal $|\vec{B}| = 10$ kT, $|\vec{E}| = 10$ V/nm field configuration from $-2000$ nm/ps.

# 5 Conclusion

## 5.1 Discussion of Computational Results: Asymptotic and Transient

### 5.1.1 Asymptotic Computational Results

By reinterpreting the long-time electrolyte drift velocity as a dynamical fixed-point of the accelerations, rather than the asymptote of a direct long-timescale simulation problem, it was possible to sidestep the prohibitive computational overhead associated with resolving microsecond-scale electrolyte relaxation dynamics. While very computationally demanding, this approach is much less so than simulating the system dynamics using MD for long enough to capture the true asymptotic exponential decays. This computational reformulation proved to be highly successful, allowing a direct numerical verification of the analytically predicted $\vec{E} \times \vec{B}$ ion drift behavior within much more manageable 50 ps simulations.

Most significantly, the 2D parameter sweep analysis—as visualized in 4.7—demonstrated the existence of a stable field-dependent asymptotic transport state toward which the electrolyte relaxes independently of the imposed initial bulk velocity. The cross sections of the observed acceleration map in $(E, v_{init})$ parameter space demonstrated the stable fixed point nature of the asymptotic velocity, e.g: systems initialized below the asymptotic drift accelerated toward the fixed point, while systems initialized above it decelerated back toward the same transport state. The resulting stable fixed-point manifold observed throughout the two-dimensional acceleration phase-space provides strong computational evidence that the electromagnetized electrolyte behaves as an independent dissipative dynamical system possessing a robust asymptotic attractor corresponding to the Hall drift velocity.

A linear fit to such parameter sweep to determine the underlying B-field differed from the imposed field strength by less than 10%. Considering the substantial stochastic fluctuations inherent to nonequilibrium molecular dynamics, such short 50 ps timescales, and the coarse discretization of the parameter space required for computational feasibility, this level of agreement strongly supports both the asymptotic kinetic theory and the associated hydrodynamic coupling assumptions developed earlier in the thesis.

While short 50 ps timescales are sufficient to resolve the emergent sign and approximate magnitude of the acceleration, these timescales remain significantly shorter than the intrinsic long-time relaxation channels predicted by the generalized Volterra analysis and later memory-kernel reconstruction. Extending the simulations to longer timescales or employing aforementioned adaptive root-finding algorithms directly on the acceleration

field would likely improve the quantitative precision of the extracted asymptotic velocities substantially.

Despite these limitations, the asymptotic computational analysis undoubtedly validates the principal theoretical prediction of this thesis: that electromagnetized multi-species electrolytes under orthogonal electric and magnetic fields evolve toward a stable Hall drift state governed by a generalized nonequilibrium transport mechanism.

The close cut agreement between the asymptotic analytical theory, the acceleration fixed-point computational framework, and the nonequilibrium momentum-conseving molecular dynamics results demonstrates that the generalized kinetic-hydrodynamic formalism developed throughout this work captures such large-timescale transport behavior in electromagnetized ionic fluids.

### 5.1.2 Transient Computational Results

Despite the visible qualitative agreement between the reconstructed GLE dynamics and the direct MD velocity trajectories, there exist several important limitations of the present reconstruction methodology which must be definitively acknowledged. First, the optimized $K^+$ and $Cl^-$ memory kernels were extracted from relatively short nonequilibrium trajectories compared to the intrinsic, long relaxation timescales predicted by the Volterra system. Consequently, the slowest exponential relaxation modes are only weakly constrained by the optimization procedure, rendering the asymptotic tails of the reconstructed kernels particularly sensitive to statistical noise and parameter regularization. It was found during the optimization procedure that for decreased solvent molarity, and shorter timescales, the memory kernel learning procedure became increasingly more unstable, as the DE evolution was forced to mutate over more and more sporadic data. Since the late-time transport behavior is governed precisely by these smallest-magnitude poles of the memory kernel, even minor inaccuracies in the reconstructed long-timescale decay structure may produce noticeable deviations in the predicted asymptotic drift trajectories. This should be accounted for and treated with an appropriate level of paramter regularization to achieve a physical model.

Furthermore, the kernel reconstruction was performed under near-equilibrium solvent conditions without explicitly training on strongly driven electric-field exposed nonequilibrium trajectories. The extracted kernels therefore implicitly assume that the delayed solvent response remains approximately linear and stationary under externally imposed Lorentz forcing, without regard to Ohmic drift. In reality, sufficiently strong electromagnetic driving could alter local solvent structure, ion-ion correlations, or hydrodynamic screening behavior, leading to various field-dependent memory effects not captured within the present scalar kernel formulation.

Relatedly, the current reconstruction assumes isotropic diagonal memory kernels and neglects potential tensorial anisotropies induced by the magnetic field itself. While a the implemented OpenMM Boris integrator assumes a coarse-grained electroneutral water model, the anisotropic effect of the B-field on ions could contribute, at sufficiently large magnetic field strengths, cross-correlated transverse memory channels, requiring a fully tensorial non-Markovian closure beyond the present approximation.

Additional limitations arise from the finite system size and accessible simulation timescales of the underlying molecular dynamics calculations. The extremely long microsecond relaxation times predicted by the reconstructed Volterra dynamics substantially exceed the directly simulated MD windows, meaning that the asymptotic regime remains only indirectly inferred through extrapolation of the learned kernels, rather than something to be explicitly computed. Likewise, the fitted kernels remain phenomenological parameterizations rather than uniquely determined microscopic objects; multiple nearby kernel configurations may reproduce similar transient trajectories while differing in their long-time behavior—for varied parameter ranges similarly. The present reconstruction should therefore be interpreted primarily as an effective coarse-grained transport description rather than a unique microscopic characterization of the electrolyte.

Despite these theoretical limitations, the reconstructed dynamics demonstrate several highly significant successes. Most importantly, the optimized non-Markovian kernels successfully reproduced the qualitative multiscale relaxation structure predicted analytically throughout the earlier Volterra and laplace-transformed correlation tensor pole analyses. The emergence of rapid transient response followed by substantially slower exponential relaxation explicitly confirms the presence of temporally nonlocal solvent-mediated transport dynamics absent from conventional Markovian electrolyte theory. The reconstructed trajectories correctly recover both the initial transient acceleration regime, and agree with the subsequent asymptotic relaxation toward the analytically predicted Hall drift velocity.

Equally important is the fact that the reconstructed dynamics remain dynamically stable under exceedingly large Galilean boosts. Independent of the initially seeded hall-drift velocity, the generalized Volterra dynamics consistently relax exponentially toward the same asymptotic transport state predicted by the analytical theory. This behavior strongly supports the physical consistency of the generalized Langevin formulation and demonstrates that the reconstructed memory kernels encode an effective dissipative hydrodynamic relaxation mechanism rather than solely fitting short-time stochastic fluctuations.

As a continuation of this thesis, one may choose to investigate large-timestep methods more suitable for weak field configurations. A principal limitaion of all computational investigation in this thesis were the largely unphysical field magnitudes—necessitated by the need for suffifient SNR despite finite timescale limitations. To ground these theoretical findings more rigorously to real-world magnitudes such as $1 - 10$ T, longer simulations or signal processing techniques should be applied to extract the underlying Hall drift effectively. To conclude this investigation, it is clear that the present framework establishes a concrete bridge between microscopic stochastic dynamics, kinetic memory effects, and macroscopic nonequilibrium electrolyte transport, with results spanning a unified computational and analytical description of ion dynamics in field-exposed electrolytic systems.

# Appendix

## A Time-Reversal Antisymmetry and Entropy Production of the Ornstein-Uhlenbeck Operator

Let $\mathcal{T}$ be the time-reveral operator which acts on the probability density function of each ionic species. Under time reversal, the time and velocity transform antisymmetrically, while position remains invariant:

$$\mathcal{T}t \mapsto -t \quad \mathcal{T}\vec{v}_\alpha \mapsto -\vec{v}_\alpha \quad \mathcal{T}\vec{r}_\alpha \mapsto \vec{r}_\alpha$$

The Ornstein-Uhlenbeck (OU) operator is defined by its action on $f_\alpha$ as:

$$\mathcal{L}_\alpha f = \gamma_\alpha \nabla_{\vec{v}_\alpha} \cdot (\vec{v}_\alpha f + \frac{k_B T}{m_\alpha} \nabla_{\vec{v}_\alpha} f)$$

For an operator $\mathcal{O}$ to be time-reversal invariant, it must be invariant under conjugation with the time-reversal operator, e.g.

$$\mathcal{T}\mathcal{O}\mathcal{T}^{-1} = \mathcal{O}$$

It will now be demonstrated that the OU operator fails to satisfy such property. Let us consider the conjugated operator acting on a test function $f$.

$$\begin{aligned}
\mathcal{T}\mathcal{L}_\alpha\mathcal{T}^{-1} f(\vec{v}_\alpha) &= \mathcal{T}\mathcal{L}_\alpha f(-\vec{v}_\alpha) \\
&= \mathcal{T}\gamma_\alpha \nabla_{\vec{v}_\alpha} \cdot (\vec{v}_\alpha f(-\vec{v}_\alpha) + \frac{k_B T}{m_\alpha} \nabla_{\vec{v}_\alpha} f(-\vec{v}_\alpha)) \\
&= \mathcal{T}\gamma_\alpha \nabla_{\vec{v}_\alpha} \cdot (\vec{v}_\alpha f(-\vec{v}_\alpha) - \frac{k_B T}{m_\alpha} (\nabla f)(-\vec{v}_\alpha)) \\
&= \gamma_\alpha \nabla_{\vec{v}_\alpha} \cdot (-\vec{v}_\alpha f(\vec{v}_\alpha) - \frac{k_B T}{m_\alpha} \nabla_{\vec{v}_\alpha} f(\vec{v}_\alpha)) \\
&= -\gamma_\alpha \nabla_{\vec{v}_\alpha} \cdot (\vec{v}_\alpha f(\vec{v}_\alpha) + \frac{k_B T}{m_\alpha} \nabla_{\vec{v}_\alpha} f(\vec{v}_\alpha)) \\
&= -\mathcal{L}_\alpha f(\vec{v}_\alpha)
\end{aligned}$$

Under conjugation with the time-reversal operator, the OU operator picks up a negative sign, demonstrating the lack of time reversal invariance. To demonstrate entropy production, one may define a Fisher-information-like functional, and apply methods consistent with Boltzmann's H-theorem. One defines the information functional:

$$\mathcal{I}[f_\alpha] := \int f_\alpha(\vec{r}_\alpha, \vec{v}_\alpha, t) \left| \nabla_{\vec{v}_\alpha} \log \frac{f_\alpha}{f_{\alpha,eq}} \right|^2 d\vec{r}_\alpha d\vec{v}_\alpha,$$

where the local normalized (with factor $Z^{-1}$) Maxwellian $f_{\alpha,eq}$ is given by

$$f_{\alpha,eq}(\vec{v}_\alpha) = Z^{-1} \exp\left(-\frac{m_\alpha |\vec{v}_\alpha|^2}{2k_B T}\right).$$

Consider the kinetic equation under which the OU dynamics are imposed:

$$\partial_t f_\alpha + \vec{v}_\alpha \cdot \nabla_{\vec{r}_\alpha} f_\alpha + \frac{q_\alpha}{m_\alpha}(\vec{E} + \vec{v}_\alpha \times \vec{B}) \cdot \nabla_{\vec{v}_\alpha} f_\alpha = \gamma_\alpha \nabla_{\vec{v}_\alpha} \cdot \left(\vec{v}_\alpha f_\alpha + \frac{k_B T}{m_\alpha} \nabla_{\vec{v}_\alpha} f_\alpha\right),$$

and define the relative entropy of the electrolytic system as:

$$H[f_\alpha \,|\, f_{\alpha,eq}] := \int f_\alpha \log \frac{f_\alpha}{f_{\alpha,eq}} \, d\vec{r}_\alpha d\vec{v}_\alpha = -S_\alpha[f] + \text{const.},$$

where $S_\alpha[f]$ is the usual entropy functional. Then, the time derivative of the relative entropy should be non-positive to demonstrate global entropy production. Its time derivative is given by:

$$\frac{d}{dt} H[f_\alpha | f_{\alpha,eq}] = \int (\partial_t f_\alpha) \, \log \frac{f_\alpha}{f_{\alpha,eq}}.$$

Substituting the equation of motions into the time derivative, the transport terms satisfy

$$\int \left(\vec{v}_\alpha \cdot \nabla_{\vec{r}_\alpha} f_\alpha + \frac{q_\alpha}{m_\alpha}(\vec{E} + \vec{v}_\alpha \times \vec{B}) \cdot \nabla_{\vec{v}_\alpha} f_\alpha\right) \log \frac{f_\alpha}{f_{\alpha,eq}} = 0,$$

by integration by parts (as these terms are divergence-free in phase space), only the OU term contributes to the relative entropy:

$$\frac{d}{dt} H[f_\alpha | f_{\alpha,eq}] = \gamma_\alpha \int \nabla_{\vec{v}_\alpha} \cdot \left(\vec{v}_\alpha f_\alpha + \frac{k_B T}{m_\alpha} \nabla_{\vec{v}_\alpha} f_\alpha\right) \log \frac{f_\alpha}{f_{\alpha,eq}}.$$

$$= -\gamma_\alpha \int \left(\vec{v}_\alpha f_\alpha + \frac{k_B T}{m_\alpha} \nabla_{\vec{v}_\alpha} f_\alpha\right) \cdot \nabla_{\vec{v}_\alpha} \log \frac{f_\alpha}{M_\alpha}.$$

Using the identity which exploits the logarithm of the Maxwellian normalized distribution:

$$\vec{v}_\alpha f_\alpha + \frac{k_B T}{m_\alpha} \nabla_{\vec{v}_\alpha} f_\alpha = \frac{k_B T}{m_\alpha} f_\alpha \nabla_{\vec{v}_\alpha} \log \frac{f_\alpha}{M_\alpha},$$

one obtains a final expression for the rate of change of the entropy:

$$\boxed{\frac{d}{dt} H[f_\alpha | M_\alpha] = -\frac{\gamma_\alpha k_B T}{m_\alpha} \int f_\alpha \left| \nabla_{\vec{v}_\alpha} \log \frac{f_\alpha}{M_\alpha} \right|^2 d\vec{r}_\alpha d\vec{v}_\alpha}$$

$$\boxed{\frac{d}{dt} H[f_\alpha | M_\alpha] \leq 0, \implies \frac{d}{dt} S_\alpha[f_\alpha] \geq 0,}$$

with equality if and only if $f_\alpha = M_\alpha$. This demonstrates that under solvent equilibrium conditions, the total entropy of each ionic species subsystem increases monotonically, consistent with thermodynamics, and saturates at the equilibrium distribution.

# B (Action of the OU Semigroup)

Claim: $e^{t\mathcal{L}_\alpha}[(\vec{E}\cdot\vec{v}_\alpha)f_\alpha^{(0)}(\vec{v}_\alpha)] = e^{-\gamma_\alpha t}(\vec{E}\cdot\vec{v}_\alpha)f_\alpha^{(0)}(\vec{v}_\alpha)$

Proof: First consider the action of the usual Ornstein-Uhlenbeck (OU) operator:

$$\mathcal{L}_\alpha f = \gamma_\alpha \nabla_{\vec{v}_\alpha}\cdot(\vec{v}_\alpha f + \frac{k_B T}{m_\alpha}\nabla_{\vec{v}_\alpha} f)$$

It will first be shown that $(\vec{E}\cdot\vec{v})f_\alpha^{(0)}$ is an eigenfunction of the OU operator. First, note that the gradient of the Maxwellian $f_\alpha^{(0)}$ is given by

$$\nabla_{\vec{v}_\alpha} f_\alpha^{(0)} = \frac{-m_\alpha}{k_B T}\vec{v}_\alpha f_\alpha^{(0)},$$

and the divergence of the velocity-scaled Maxwellian $(\vec{E}\cdot\vec{v}_\alpha)f_\alpha^{(0)}$ is

$$\nabla_{\vec{v}_\alpha}(\vec{E}\cdot\vec{v}_\alpha)f_\alpha^{(0)} = \vec{E}f_\alpha^{(0)} - \frac{m_\alpha}{k_B T}(\vec{E}\cdot\vec{v}_\alpha)\vec{v}_\alpha f_\alpha^{(0)}$$

Applying this identity, one may explicitly demonstrate the eigenfunction nature of the scaled Maxwellian, e.g.

$$\begin{aligned}
\mathcal{L}_\alpha[(\vec{E}\cdot\vec{v}_\alpha)f_\alpha^{(0)}(\vec{v}_\alpha)] &= \gamma_\alpha\nabla_{\vec{v}_\alpha}[\vec{v}_\alpha(\vec{E}\cdot\vec{v}_\alpha)f_\alpha^{(0)} + \frac{k_B T}{m_\alpha}\nabla_{\vec{v}_\alpha}(\vec{E}\cdot\vec{v}_\alpha)f_\alpha^{(0)}(\vec{v}_\alpha)] \\
&= \gamma_\alpha\nabla_{\vec{v}_\alpha}[\cancel{\vec{v}_\alpha(\vec{E}\cdot\vec{v}_\alpha)f_\alpha^{(0)}} + \frac{k_B T}{m_\alpha}\vec{E}f_\alpha^{(0)} - \cancel{(\vec{E}\cdot\vec{v}_\alpha)\vec{v}_\alpha f_\alpha^{(0)}}] \\
&= \gamma_\alpha\frac{k_B T}{m_\alpha}\vec{E}\cdot\nabla_{\vec{v}_\alpha}f_\alpha^{(0)} \\
&= -\gamma_\alpha(\vec{E}\cdot\vec{v})f_\alpha^{(0)}
\end{aligned}$$

$$\implies \boxed{\mathcal{L}_\alpha[(\vec{E}\cdot\vec{v}_\alpha)f_\alpha^{(0)}(\vec{v}_\alpha)] = -\gamma_\alpha(\vec{E}\cdot\vec{v})f_\alpha^{(0)}}$$

Extending this rigorously to the semigroup via a taylor expansion,

$$\begin{aligned}
e^{t\mathcal{L}_\alpha}[(\vec{E}\cdot\vec{v}_\alpha)f_\alpha^{(0)}] &= \left(1 + t\mathcal{L}_\alpha + \frac{1}{2}t^2\mathcal{L}_\alpha^2 + \cdots\right)[(\vec{E}\cdot\vec{v}_\alpha)f_\alpha^{(0)}] \\
&= \left(1 - t\gamma_\alpha + \frac{1}{2}t^2\gamma_\alpha^2 + \cdots\right)[(\vec{E}\cdot\vec{v}_\alpha)f_\alpha^{(0)}] \\
&= e^{-\gamma_\alpha t}[(\vec{E}\cdot\vec{v}_\alpha)f_\alpha^{(0)}]
\end{aligned}$$

$$\implies \boxed{e^{t\mathcal{L}_\alpha}[(\vec{E}\cdot\vec{v}_\alpha)f_\alpha^{(0)}] = e^{-\gamma_\alpha t}[(\vec{E}\cdot\vec{v}_\alpha)f_\alpha^{(0)}]} \quad \blacksquare$$

# C Dyson Decomposition

Claim:

$$e^{i\mathcal{L}_0 t} = e^{i\mathcal{Q}_{\vec{p}}\mathcal{L}_0 t} + \int_0^t e^{i\mathcal{L}_0(t-\tau)}\mathcal{P}_{\vec{p}} i\mathcal{L}_0 e^{i\mathcal{Q}_{\vec{p}}\mathcal{L}_0\tau} d\tau$$

Proof:

Defining the helper function $S(\tau) := e^{i\mathcal{L}_0(t-\tau)}e^{i\mathcal{Q}_{\vec{p}}\mathcal{L}_0\tau}$, one obtains the corresponding Dyson decomposition by differentiating and integrating $S(\tau)$:

$$\begin{aligned}
\frac{dS}{d\tau} &= e^{i\mathcal{L}_0(t-\tau)}(-i\mathcal{L}_0 + i\mathcal{Q}_{\vec{p}}\mathcal{L}_0)e^{i\mathcal{Q}_{\vec{p}}\mathcal{L}_0\tau} \\
\frac{dS}{d\tau} &= e^{i\mathcal{L}_0(t-\tau)}(-i\mathcal{P}_{\vec{p}}\mathcal{L}_0)e^{i\mathcal{Q}_{\vec{p}}\mathcal{L}_0\tau} \\
\int_0^t \frac{dS}{d\tau} d\tau &= -\int_0^t e^{i\mathcal{L}_0(t-\tau)}(i\mathcal{P}_{\vec{p}}\mathcal{L}_0)e^{i\mathcal{Q}_{\vec{p}}\mathcal{L}_0\tau} \\
S(t) - S(0) &= -\int_0^t e^{i\mathcal{L}_0(t-\tau)}(i\mathcal{P}_{\vec{p}}\mathcal{L}_0)e^{i\mathcal{Q}_{\vec{p}}\mathcal{L}_0\tau} \\
e^{i\mathcal{Q}_{\vec{p}}\mathcal{L}_0 t} - e^{i\mathcal{L}_0 t} &= -\int_0^t e^{i\mathcal{L}_0(t-\tau)}(i\mathcal{P}_{\vec{p}}\mathcal{L}_0)e^{i\mathcal{Q}_{\vec{p}}\mathcal{L}_0\tau} \\
e^{i\mathcal{L}_0 t} &= e^{i\mathcal{Q}_{\vec{p}}\mathcal{L}_0 t} + \int_0^t e^{i\mathcal{L}_0(t-\tau)}\mathcal{P}_{\vec{p}} i\mathcal{L}_0 e^{i\mathcal{Q}_{\vec{p}}\mathcal{L}_0\tau} d\tau,
\end{aligned}$$

Which is what was to be shown. ■

# D Commentary on the Thermodynamic Consistencies of the Derived Boltzmann Equation

Equation 2.39 formulaically imposes non-markovian solvent dynamics onto the phase space distribution of the cation and anion species, respectively. It could be seen as an important middle step, to verify the consistency of these dynamics with well-known thermodynamic laws. First, we will show that the equilibrium distribution under this PDE is precisely the Maxwell-Boltzmann Distribution. To begin, we posit the standard Maxwell-Boltzmann (MB) distribution for an ionic species $\alpha \in \{+, -\}$ in thermal equilibrium. At equilibrium, there are no external electric fields driving a bulk current ($\vec{E} = 0$), the bulk solvent velocity is zero ($\vec{u} = 0$), and the system is strictly stationary ($\frac{\partial f_\alpha}{\partial t} = 0$) and spatially uniform ($\nabla_{\vec{r}_\alpha} f_\alpha = 0$). The distribution is therefore purely a function of velocity. Ansatzing the Maxwell-Boltzmann (MB) equation,

$$f_{\alpha,eq}(\vec{v}_\alpha) = n_0 \left(\frac{m_\alpha}{2\pi k_B T}\right)^{3/2} \exp\left(-\frac{m_\alpha v_\alpha^2}{2k_B T}\right),$$

one may show that its explicit form directly satistifes the ODE using the equipartition theorem, microscopic time reversibility, and isotropy.

Substituting these equilibrium conditions into Equation 2.39, the entire left-hand side identically vanishes. The streaming and temporal derivative terms are zero by our

stationarity and uniformity assumptions, and the Lorentz force term vanishes because the cross-product is orthogonal to the velocity gradient: $(\vec{v}_\alpha \times \vec{B}) \cdot \nabla_{\vec{v}_\alpha} f_{\alpha,eq} \propto (\vec{v}_\alpha \times \vec{B}) \cdot \vec{v}_\alpha = 0$. Therefore, for the MB distribution to be the true equilibrium solution, the non-Markovian collision integral on the right-hand side must independently evaluate to zero, e.g.

$$\nabla_{\vec{v}_\alpha} \cdot \int_0^t K_\alpha(t-\tau) \left[ \vec{F}_\alpha^{(2)}(\vec{r}_\alpha, \vec{v}_\alpha, t; \tau) + k_B T \mathbf{G}(t,\tau) \cdot \nabla_{\vec{v}_\alpha} f_{\alpha,eq} \right] d\tau \stackrel{!}{=} 0.$$

To prove that the integrand vanishes, we first evaluate the velocity gradient of the MB distribution:

$$\nabla_{\vec{v}_\alpha} f_{\alpha,eq} = -\frac{m_\alpha \vec{v}_\alpha}{k_B T} f_{\alpha,eq}.$$

Substituting this into the second term inside the bracket yields a highly restrictive condition that the two-time correlation term must satisfy:

$$k_B T \mathbf{G}(t,\tau) \cdot \nabla_{\vec{v}_\alpha} f_{\alpha,eq} = -m_\alpha \mathbf{G}(t,\tau) \cdot \vec{v}_\alpha f_{\alpha,eq}.$$

Next, we resolve the two-time correlation function $\vec{F}_\alpha^{(2)}$. By definition, this term represents the correlation between the fine-grained distribution at time $t$ and the stochastic velocity at a past time $\tau$. In an equilibrium ensemble, this equates to the conditional expectation of the past velocity given the present velocity, multiplied by the equilibrium distribution:

$$\vec{F}_\alpha^{(2)}(\vec{r}_\alpha, \vec{v}_\alpha, t; \tau) = \langle \vec{v}_\alpha(\tau) N_\alpha(t) \rangle_{eq} = \mathbb{E}[\vec{v}_\alpha(\tau) \mid \vec{v}_\alpha(t) = \vec{v}_\alpha] f_{\alpha,eq}(\vec{v}_\alpha).$$

For a Gaussian process governed by a linear Generalized Langevin Equation (GLE), the conditional expectation is given exactly by the normalized auto-correlation matrix:

$$\mathbb{E}[\vec{v}_\alpha(\tau) \mid \vec{v}_\alpha(t) = \vec{v}_\alpha] = \langle \vec{v}_\alpha(\tau) \otimes \vec{v}_\alpha(t) \rangle_{eq} \langle \vec{v}_\alpha(t) \otimes \vec{v}_\alpha(t) \rangle_{eq}^{-1} \vec{v}_\alpha.$$

By the equipartition theorem, the equal-time velocity correlation is trivially $\langle \vec{v}_\alpha(t) \otimes \vec{v}_\alpha(t) \rangle_{eq} = \frac{k_B T}{m_\alpha} \mathbf{I}$.To determine the cross-time correlation $\langle \vec{v}_\alpha(\tau) \otimes \vec{v}_\alpha(t) \rangle_{eq}$, we introduce the fundamental relaxation matrix $\mathbf{R}(t,\tau)$ of the unforced GLE, such that the mean velocity decays forward in time as $\mathbf{R}(t,\tau)\vec{v}_\alpha(\tau)$. Consequently, the forward correlation is $\langle \vec{v}_\alpha(t) \otimes \vec{v}_\alpha(\tau) \rangle_{eq} = \frac{k_B T}{m_\alpha} \mathbf{R}(t,\tau)$. Due to microscopic time-reversibility in thermal equilibrium, the backward correlation is simply its transpose:

$$\langle \vec{v}_\alpha(\tau) \otimes \vec{v}_\alpha(t) \rangle_{eq} = \frac{k_B T}{m_\alpha} \mathbf{R}(t,\tau)^T.$$

Applying this to our conditional expectation gives:

$$\mathbb{E}[\vec{v}_\alpha(\tau) \mid \vec{v}_\alpha(t) = \vec{v}_\alpha] = \left( \frac{k_B T}{m_\alpha} \mathbf{R}(t,\tau)^T \right) \left( \frac{m_\alpha}{k_B T} \mathbf{I} \right) \vec{v}_\alpha = \mathbf{R}(t,\tau)^T \vec{v}_\alpha.$$

Finally, we must map the relaxation matrix $\mathbf{R}(t,\tau)$ back to the response tensor $\mathbf{G}(t,\tau)$ used in the Furutsu-Novikov expansion. The response tensor is defined variationally as $\mathbf{G}(t,\tau) = \frac{\delta \vec{v}_\alpha(t)}{\delta \vec{\zeta}(\tau)}$. Because the colored noise $\vec{\zeta}(t)$ enters the single-ion GLE scaled by the inverse mass $(\frac{1}{m_\alpha}\vec{\zeta}(t))$, the velocity response to a noise impulse is proportionally scaled:

$$\mathbf{G}(t,\tau) = \frac{1}{m_\alpha} \mathbf{R}(t,\tau) \implies \mathbf{R}(t,\tau) = m_\alpha \mathbf{G}(t,\tau).$$

Substituting this relation into our conditional expectation, and noting that the macroscopic isotropy of the solvent ensures that $\mathbf{G}(t,\tau)$ is perfectly symmetric ($\mathbf{G}^T = \mathbf{G}$), the two-time correlation function evaluates cleanly to an elegant result (to also be used later on in proof of Boltzmann's H-theorem):

$$\vec{F}_\alpha^{(2)}(\vec{r}_\alpha, \vec{v}_\alpha, t; \tau) = m_\alpha \mathbf{G}(t,\tau) \cdot \vec{v}_\alpha f_{\alpha,eq}(\vec{v}_\alpha).$$

Adding the results inside the integral from our PDE, we arrive at the final equilibrium condition:

$$\vec{F}_\alpha^{(2)} + k_B T \mathbf{G}(t,\tau) \cdot \nabla_{\vec{v}_\alpha} f_{\alpha,eq} = m_\alpha \mathbf{G}(t,\tau) \cdot \vec{v}_\alpha f_{\alpha,eq} - m_\alpha \mathbf{G}(t,\tau) \cdot \vec{v}_\alpha f_{\alpha,eq} = 0.$$

The integrand identically cancels. The non-Markovian collision operator evaluates exactly to zero, robustly proving that the Maxwell-Boltzmann distribution is the precise stationary equilibrium solution to the generalized Vlasov-Fokker-Planck equation, fully satisfying the requirements of classical thermodynamics. With the equilibrium distribution of the ionic-fluid system now analytically verified, one can perform further investigation into the thermodynamic consistency of this probability density theory. Recognizing the formal structure of equation 2.39, one may immediately recognize the equation as a specific manifestation of a Boltzmann equation, where the collision operator is given by the right hand side memory kernel and Furutsu-Nokivov derived response integrals. In strict accordance to Boltzmann's H-theorem, it should explicitly hold that the entropy of the entire system, **solvent and ions**, should increase monotonically. In classical thermodynamics, the Second Law states that for an isolated system, Entropy ($S$) must always increase. But for a system in contact with a heat bath–such as the ions in contact with the solvent–the system's local entropy $S$ is allowed to decrease locally. **Upon my first attempt at demonstrating the monotonicity of the H-function, it was possible to reduce the final form of a derivative down to the sum of a quadratic positive semi-definite form, and a linear term, which could not be verifiably positive. Below is the final form that was reached.**

$$\frac{dH}{dt} = -\int_0^t K(t-\tau) \int_\Gamma k_B T \frac{(\nabla_{\vec{v}_\alpha} f_\alpha)^T G(\tau,t) \nabla_{\vec{v}_\alpha} f_\alpha}{f_\alpha} + \underbrace{(\nabla f_\alpha)^T G(\tau,t)(\vec{v}_\alpha - \vec{u}(\tau))}_{\text{not necessarily} \geq 0} d^3r d^3v d\tau$$

This of course is a problem in proving thermodynamic consistency, as we have not yet set up a precise dynamical coupling to the solvent for each ion species. To circumvent this issue, one may prove instead that the **relative entropy** of this system should monotonically increase, and in turn the **relative H-function** of the ionic system should monotonically decrease. We define the relative H-function as the Kullback-Leibler divergence between the distribution $f_\alpha$ and the equilibrium distribution (MB distribution) that we have just explicitly verified, $KL(f_\alpha || f_{\alpha,eq})$:

$$H_{rel}(t) = \int f_\alpha(\vec{v},t) \ln\left(\frac{f_\alpha(\vec{v},t)}{f_{\alpha,eq}(\vec{v})}\right) d\vec{v}.$$

To understand why the relative H-function is the correct thermodynamic functional for our system, it is instructive to expand the logarithm:

$$H_{rel}(t) = \int f_\alpha(\vec{v},t) \ln f_\alpha(\vec{v},t), d\vec{v} - \int f_\alpha(\vec{v},t) \ln f_{\alpha,eq}(\vec{v}), d\vec{v}.$$

The first term is exactly the standard Boltzmann H-function, $H_\alpha(t)$, which is directly proportional to the negative of the non-equilibrium entropy of the ionic species, such that $S_\alpha(t) = -k_B H_\alpha(t)$.The second term can be evaluated by substituting the explicit form of the Maxwell-Boltzmann distribution, $f_{\alpha,eq}(\vec{v}) = A \exp\left(-\frac{m_\alpha v^2}{2k_B T}\right)$, where $A$ is the normalization constant. The logarithm yields $\ln f_{\alpha,eq}(\vec{v}) = \ln A - \frac{m_\alpha v^2}{2k_B T}$. Inserting this into the integral, we obtain:

$$\int f_\alpha(\vec{v},t)\left(\ln A - \frac{m_\alpha v^2}{2k_B T}\right) d\vec{v} = -\ln A \int f_\alpha(\vec{v},t), d\vec{v} + \frac{1}{k_B T}\int f_\alpha(\vec{v},t)\frac{m_\alpha v^2}{2}, d\vec{v}.$$

Assuming the probability distribution is normalized, the first term simply becomes a constant, $-\ln A$. More importantly, the integral in the second term is the exact definition of the macroscopic, time-dependent kinetic energy of the ionic species, $E_{kin}(t)$. Reassembling the relative H-function gives:

$$H_{rel}(t) = H_\alpha(t) + \frac{E_{kin}(t)}{k_B T} + C.$$

Multiplying the entire expression by $k_B T$ reveals the thermodynamic nature of this quantity:

$$k_B T H_{rel}(t) = E_{kin}(t) - T S_\alpha(t) + C'.$$

Recognizing the form $E - TS$, we see that $k_B T H_{rel}(t)$ is exactly equal to the non-equilibrium Helmholtz Free Energy, $F(t)$, of the ionic system, shifted by some constant. For an isolated system under an NVE ensemble, kinetic energy is strictly conserved ($E_{kin}(t) = \text{const}$), and therefore demonstrating that $H_\alpha(t)$ decreases is entirely sufficient to prove the Second Law of thermodynamics. However, for an NVT ensemble, such as here, where the ions are dynamically coupled to a solvent heat bath, the ions are actively exchanging energy with the background. Consequently, the local kinetic energy $E_{kin}(t)$ is time-dependent. The fundamental principle of classical thermodynamics for a system coupled to a thermal reservoir dictates that the system will evolve such that its Helmholtz Free Energy $E - TS$ is minimized. Therefore, the requirement that the relative H-function monotonically decreases:

$$\frac{dH_{rel}}{dt} \leq 0 \iff \frac{dF}{dt} \leq 0,$$

is completely equivalent to proving the dissipation of free energy. Demonstrating this inequality for the our generalized Vlasov-Fokker-Planck/Botzmann equation robustly verifies that the modeled dynamics are strictly consistent with the Second Law of Thermodynamics, rigorously justifying the bulk-flow equilibrium assumptions without the need to explicitly track the vast microstate geometry of the solvent. With the exploration now motivated, one may explicitly begin the computation of the time dervative of the relative H-functional. Taking the time derivative of the relative H-function defined, we apply Leibniz's rule to bring the derivative inside the integral:

$$\frac{dH_{rel}}{dt} = \int \frac{\partial f_\alpha}{\partial t} \ln\left(\frac{f_\alpha}{f_{\alpha,eq}}\right) d\vec{v}_\alpha + \int f_\alpha \frac{\partial}{\partial t}\left[\ln f_\alpha - \ln f_{\alpha,eq}\right] d\vec{v}_\alpha.$$

Because the equilibrium distribution $f_{\alpha,eq}$ is strictly time-independent, the second integral simplifies to $\int \frac{\partial f_\alpha}{\partial t} d\vec{v}_\alpha$. By the conservation of total probability, the integral of the

time evolution of the density function over all velocity space must vanish ($\frac{d}{dt}\int f_\alpha d\vec{v}_\alpha = 0$). Therefore, the time derivative of the relative H-function is solely determined by the first term:

$$\frac{dH_{rel}}{dt} = \int \frac{\partial f_\alpha}{\partial t} \ln\left(\frac{f_\alpha}{f_{\alpha,eq}}\right) d\vec{v}_\alpha.$$

We now substitute the evolution equation for $\frac{\partial f_\alpha}{\partial t}$. For sake of brevity, the conservative terms of the Vlasov operator—the streaming term and the Lorentz force—describe Hamiltonian phase-space volume preservation and thus contribute exactly zero to the entropy production, this can also be shown directly under phase space density decay assumptions, divergence theorem, and integration by parts, however it is irrelevant to include here due to its length and notational encumberment. To isolate the irreversible thermodynamic behavior, we evaluate Equation 2.39 in the bulk-comoving frame ($\vec{u}(\tau) = 0$) and assume macroscopic spatial homogeneity ($\nabla_{\vec{r}_\alpha} f_\alpha = 0$). Under these conditions, the time evolution is governed entirely by the non-Markovian collision operator:

$$\frac{\partial f_\alpha}{\partial t} = \nabla_{\vec{v}_\alpha} \cdot \int_0^t K_\alpha(t-\tau)\left[\vec{F}_\alpha^{(2)} + k_B T \mathbf{G}(t,\tau)\cdot\nabla_{\vec{v}_\alpha} f_\alpha\right] d\tau.$$

To manipulate this collision operator into a mathematically tractable form, we apply the two-time correlation identity derived during our equilibrium analysis: $\vec{F}_\alpha^{(2)}(\vec{r}_\alpha,\vec{v}_\alpha,t;\tau) = m_\alpha \mathbf{G}(t,\tau)\cdot\vec{v}_\alpha f_\alpha$. Substituting this identity allows us to factor out the integral over the memory kernel and the response tensor. We define the time-dependent macroscopic diffusion tensor $\Xi_\alpha(t)$ as:

$$\Xi_\alpha(t) = \int_0^t K_\alpha(t-\tau)\mathbf{G}(t,\tau)d\tau.$$

This reduces the collision operator to the divergence of a probability current in velocity space, $\vec{J}_{v_\alpha}$:

$$\frac{\partial f_\alpha}{\partial t} = \nabla_{\vec{v}_\alpha}\cdot\left[m_\alpha \Xi_\alpha(t)\cdot\vec{v}_\alpha f_\alpha + k_B T \Xi_\alpha(t)\cdot\nabla\vec{v}_\alpha f_\alpha\right] = -\nabla_{\vec{v}_\alpha}\cdot\vec{J}_{v_\alpha}.$$

We can express the probability current $\vec{J}_{v_\alpha}$ in a highly compact way by just factoring out the thermal energy $k_B T$ and the distribution function $f_\alpha$:

$$\vec{J}_{v_\alpha} = -k_B T \Xi_\alpha(t)\cdot f_\alpha\left[\frac{m_\alpha\vec{v}_\alpha}{k_B T} + \frac{\nabla\vec{v}_\alpha f_\alpha}{f_\alpha}\right].$$

Using the fact that the velocity gradient of the logarithm of the Maxwell-Boltzmann distribution is $\nabla_{\vec{v}_\alpha}\ln f_{\alpha,eq} = -\frac{m_\alpha\vec{v}_\alpha}{k_B T}$, we can substitute this exact relation into the bracketed term to begin simplification:

$$\vec{J}_{v_\alpha} = -k_B T\Xi_\alpha(t)\cdot f_\alpha\left[-\nabla_{\vec{v}_\alpha}\ln f_{\alpha,eq} + \nabla_{\vec{v}_\alpha}\ln f_\alpha\right] = -k_B T\Xi_\alpha(t)\cdot f_\alpha\nabla_{\vec{v}_\alpha}\ln\left(\frac{f_\alpha}{f_{\alpha,eq}}\right).$$

We now return to the time derivative of the relative H-function and substitute our divergence-form collision operator:

$$\frac{dH_{rel}}{dt} = -\int\left[\nabla_{\vec{v}_\alpha}\cdot\vec{J}_{v_\alpha}\right]\ln\left(\frac{f_\alpha}{f_{\alpha,eq}}\right)d\vec{v}_\alpha.$$

Applying integration by parts over the entirety of velocity space, we shift the gradient operator onto the logarithmic term. By imposing standard physical boundary conditions—namely, that the distribution function $f_\alpha$ and its associated currents vanish rapidly as $|\vec{v}_\alpha| \to \infty$—the surface boundary terms evaluate identically to zero, yielding:

$$\frac{dH_{rel}}{dt} = \int \vec{J}_{v_\alpha} \cdot \nabla_{\vec{v}_\alpha} \ln\left(\frac{f_\alpha}{f_{\alpha,eq}}\right) d\vec{v}_\alpha.$$

Finally, substituting the explicit formulation of $\vec{J}_{v_\alpha}$ into the integral yields the precise thermodynamic dissipation rate:

$$\frac{dH_{rel}}{dt} = -k_B T \int f_\alpha \left[\nabla_{\vec{v}_\alpha} \ln\left(\frac{f_\alpha}{f_{\alpha,eq}}\right)\right]^T \Xi_\alpha(t) \left[\nabla \vec{v}_\alpha \ln\left(\frac{f_\alpha}{f_{\alpha,eq}}\right)\right] d\vec{v}_\alpha.$$

The strict sign of this derivative is dictated by the integrand. Because the probability density function is non-negative ($f_\alpha \geq 0$) and the macroscopic temperature is strictly positive ($k_B T > 0$), the entire structural sign depends on the quadratic form involving $\Xi_\alpha(t)$. By the Fluctuation-Dissipation Theorem and the Wiener-Khinchin theorem applied to the background solvent noise, the integrated convolution of the memory kernel and the response tensor, $\Xi_\alpha(t)$, maps directly to the velocity auto-covariance matrix of the solvent. Explicitly, the Wiener-Khinchin theorem states that for any wide-sense stationary random process, its time-delayed auto-correlation function and its frequency-domain power spectral density constitute a Fourier transform pair; this mathematical relationship guarantees that the power spectrum of any physical stationary process is strictly non-negative across all frequencies. In the context of the generalized Langevin dynamics governing the ionic species, the background solvent is assumed to be in macroscopic thermal equilibrium, meaning its microscopic stochastic force fluctuations inherently form a stationary random process. By the Fluctuation-Dissipation Theorem, the integrand of $\Xi_\alpha(t)$—the product of the memory kernel $K_\alpha(t-\tau)$ and the response tensor $\mathbf{G}(t,\tau)$—is precisely proportional to the auto-correlation matrix of this stationary background noise. Consequently, integrating this stationary auto-correlation function over time yields a macroscopic transport tensor (via a Green-Kubo relation) that inherits the non-negative spectral properties of the underlying noise. It is this fundamental spectral constraint, dictated by the Wiener-Khinchin theorem, that mathematically guarantees the diffusion tensor $\Xi_\alpha(t)$ is positive semi-definite, thereby ensuring the quadratic form $\vec{x}^T \Xi_\alpha(t) \vec{x} \geq 0$ and strictly enforcing the monotonic dissipation of the system's relative free energy. As a physical covariance matrix, $\Xi_\alpha(t)$ is inherently positive semi-definite. Therefore, the vector-tensor quadratic form $\vec{x}^T \Xi_\alpha \vec{x}$ is guaranteed to be non-negative for any arbitrary vector $\vec{x}$. Consequently, the integrand is strictly non-negative everywhere in velocity space. Preserving the leading negative sign, we show

$$\frac{dH_{rel}}{dt} \leq 0,$$

and the relative H-function decreases monotonically until $f_\alpha = f_{\alpha,eq}$, at which point the gradient vanishes and entropy production ceases. With this, we have a mathematically rigorous proof that the non-Markovian Furutsu-Novikov operators natively embedded within Equation 2.39 strictly satisfy the Second Law of Thermodynamics.

# E Derivation of the Asymptotic Drift Velocities

This appendix details the algebraic resolution of the steady-state force constraints derived from the limiting procedure of the coupled Volterra integro-differential momentum equations. The governing constraints for the asymptotic relative velocity $\vec{V}_{\mathrm{rel},\infty}$ and the center-of-mass velocity $\vec{V}_{\mathrm{cm},\infty}$ are given by:

$$\vec{V}_{\mathrm{rel},\infty} \times \vec{B} = 0, \tag{.1}$$

$$vecV_{\mathrm{rel},\infty} = \frac{2q}{m\gamma}\left(\vec{E} + \vec{V}_{\mathrm{cm},\infty} \times \vec{B}\right). \tag{.2}$$

Equation .1 explicitly dictates that the relative velocity must be parallel to the magnetic field. Substituting Equation .2 into this constraint and taking the cross product yields:

$$\left(\vec{E} + \vec{V}_{\mathrm{cm},\infty} \times \vec{B}\right) \times \vec{B} = 0. \tag{.3}$$

Expansion of the nested cross product using the standard vector identity $(\vec{A} \times \vec{B}) \times \vec{B} = \vec{B}(\vec{A} \cdot \vec{B}) - \vec{A}B^2$ results in:

$$\vec{E} \times \vec{B} + \vec{B}(\vec{V}_{\mathrm{cm},\infty} \cdot \vec{B}) - \vec{V}_{\mathrm{cm},\infty}B^2 = 0. \tag{.4}$$

To systematically isolate the physically relevant drift, the center-of-mass velocity is decomposed into components parallel and perpendicular to the magnetic field: $\vec{V}_{\mathrm{cm},\infty} = \vec{V}_{\perp} + \vec{V}_{\parallel}$, where $\vec{V}_{\parallel} = (\vec{V}_{\mathrm{cm},\infty} \cdot \hat{\vec{B}})\hat{\vec{B}}$. Recognizing that $\vec{B}(\vec{V}_{\mathrm{cm},\infty} \cdot \vec{B}) = B^2\vec{V}_{\parallel}$, substitution back into Equation .4 produces:

$$B^2(\vec{V}_{\perp} + \vec{V}_{\parallel}) = \vec{E} \times \vec{B} + B^2\vec{V}_{\parallel}. \tag{.5}$$

The parallel terms cancel identically, isolating the perpendicular component of the center-of-mass velocity:

$$\vec{V}_{\perp} = \frac{\vec{E} \times \vec{B}}{B^2}. \tag{.6}$$

The parallel component remains mathematically undetermined by the cross product, as the Lorentz force $q(\vec{v} \times \vec{B})$ inherently vanishes for longitudinal motion. The general steady-state solution thus takes the form $\vec{V}_{\mathrm{cm},\infty} = \frac{\vec{E}\times\vec{B}}{B^2} + \lambda\vec{B}$, where $\lambda$ is an arbitrary scalar. However, in the absence of an external driving field parallel to $\vec{B}$, no longitudinal momentum is continuously injected into the system. The parallel drift must therefore remain zero ($\lambda = 0$), restricting the center-of-mass velocity to:

$$\vec{V}_{\mathrm{cm},\infty} = \frac{\vec{E} \times \vec{B}}{B^2}. \tag{.7}$$

Substituting this strictly perpendicular center-of-mass velocity back into the initial force balance (Equation .2) yields:

$$\vec{V}_{\mathrm{rel},\infty} = \frac{2q}{m\gamma}\left(\vec{E} + \frac{\vec{E} \times \vec{B}}{B^2} \times \vec{B}\right). \tag{.8}$$

Applying the cross-product identity a second time simplifies the relative velocity to:

$$\vec{V}_{\mathrm{rel},\infty} = \frac{2q}{m\gamma}\frac{\vec{B}(\vec{E} \cdot \vec{B})}{B^2}. \tag{.9}$$

Since the specified external fields are strictly orthogonal ($\vec{E} \cdot \vec{B} = 0$), the numerator vanishes identically, proving that the steady-state relative velocity evaluates to zero:

$$\vec{V}_{\mathrm{rel},\infty} = 0. \tag{.10}$$

# F Commentary: Acceleration Root-Finding via the Bisection Method

An alternative method to determining the asymptotic velocity via accelerations ($\frac{dv}{dt}|_{v=v^*} = 0$) in a more computationally efficient way from a naive parameter sweep is the Bisection method for root finding on the acceleration curve. First define an objective function, $a(v_0)$, representing the instantaneous macroscopic acceleration of the bulk fluid when initialized with a uniform starting velocity $v_0$. At the true asymptotic drift velocity $v^*$, the net forces governing the bulk flow sum to zero, meaning the macroscopic acceleration must vanish identically:

$$a(v^*) = \left.\frac{\Delta\langle v_{bulk}\rangle}{\Delta t}\right|_{v_0=v^*} = 0 \tag{.11}$$

Because the acceleration function $a(v_0)$ is assumedly monotonic and continuous with respect to the initial boost velocity (a fluid pushed slower than $v^*$ will accelerate, and one pushed faster will decelerate), the root $v^*$ can be efficiently isolated using a bisection algorithm. The procedure is initialized by defining a velocity bracket $[v_{left}, v_{right}]$ such that the root is strictly bounded:

$$a(v_{left}) \cdot a(v_{right}) < 0 \tag{.12}$$

For each iteration $k$, the midpoint velocity is evaluated:

$$v_{mid}^{(k)} = \frac{v_{left}^{(k)} + v_{right}^{(k)}}{2} \tag{.13}$$

A brief MD simulation ($\sim \mathcal{O}(1)$ ns) is launched with the bulk fluid initial velocity uniformly boosted to $v_{mid}^{(k)}$, and a linear regression is performed on the resultant velocity trajectory to extract the instantaneous acceleration via the gradient, $a(v_{mid})$. The bounds are then strictly updated based on the sign of the measured acceleration:

$$\begin{cases} v_{right}^{(k+1)} = v_{mid}^{(k)} & \text{if } a(v_{left}) \cdot a(v_{mid}) < 0 \\ v_{left}^{(k+1)} = v_{mid}^{(k)} & \text{otherwise} \end{cases} \tag{.14}$$

This iterative bisection strictly halves the search space at each step, ensuring logarithmic convergence, $\mathcal{O}(\log N)$, to the steady-state Hall drift velocity. By extracting the derivative (acceleration) from highly truncated approximately nanosecond-timescale simulations, this algorithm allows for the precise determination of macroscopic transport properties using only a fraction of the computational time required by traditional, continuous time-integration.

Below is a plot which demonstrates the method's application for the field configuration $B = 10^4 T$, $E = 2.5 V/nm$. Note the exponential convergence to the correct drift velocity of $-250 nm/ps$.

# G Plot of Bisection Convergence

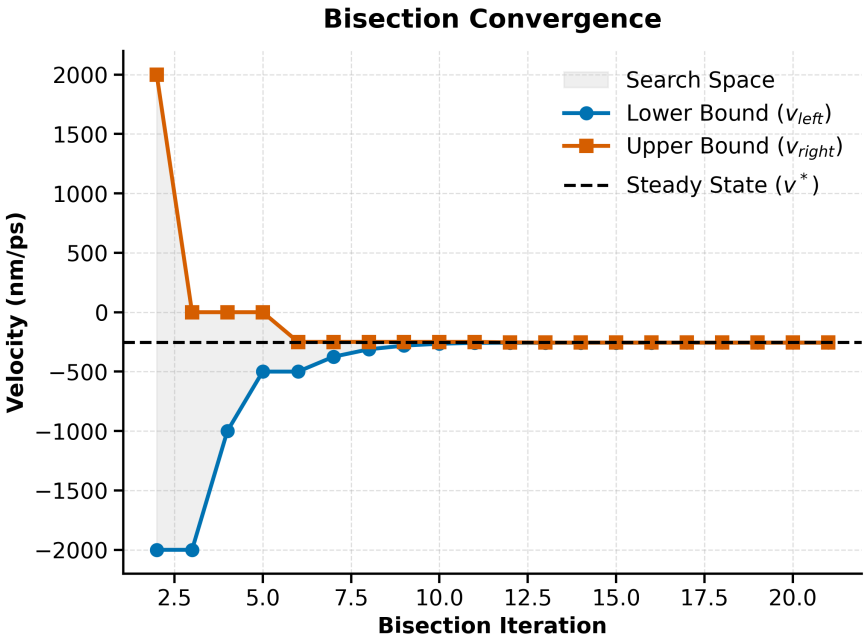


**Figure 1:** Bisection root finding performed for $1ns$ velocity trajectories with $|\vec{B}| = 10^4 T$, $|\vec{E}| = 2.5 V/nm$ Field Configuration

# H Bisection Search Steady-State Velocity Finding Algorithm & Helper Functions Pseudocode

**Algorithm 1** Bisection Search for Asymptotic Fluid Drift Velocity

**Require:** Velocity bracket $[v_{left}, v_{right}]$, Tolerance $\epsilon$, MD duration $\tau$
**Ensure:** Steady-state drift velocity $v^*$

**Phase 1: Initial Bracket Validation**

$a_{left} \leftarrow$ MeasureAcceleration$(v_{left}, \tau)$
$a_{right} \leftarrow$ MeasureAcceleration$(v_{right}, \tau)$
**if** $a_{left} \cdot a_{right} \geq 0$ **then**
    **return** Error: Root is not bounded by $[v_{left}, v_{right}]$
**end if**

**Phase 2: Iterative Bisection**

**while** $(v_{right} - v_{left}) > \epsilon$ **do**
    $v_{mid} \leftarrow \frac{v_{left}+v_{right}}{2}$
    $a_{mid} \leftarrow$ MeasureAcceleration$(v_{mid}, \tau)$
    **if** $a_{left} \cdot a_{mid} \leq 0$ **then**
        $v_{right} \leftarrow v_{mid}$
        $a_{right} \leftarrow a_{mid}$
    **else**
        $v_{left} \leftarrow v_{mid}$
        $a_{left} \leftarrow a_{mid}$
    **end if**
**end while**
$v^* \leftarrow \frac{v_{left}+v_{right}}{2}$
**return** $v^*$

**Algorithm 2** Measure Bulk Acceleration via Truncated MD

**Require:** Initial boost velocity $v_{init}$, MD simulation duration $\tau$
**Ensure:** Instantaneous bulk acceleration slope $a$

Initialize OpenMM context (solvent, ions, **E**, **B**, DPD thermostat)
MinimizeEnergy
Sample Maxwell-Boltzmann velocities at target temperature $T$
Apply uniform macroscopic boost: $\mathbf{v}_i \leftarrow \mathbf{v}_i + \mathbf{v}_{init}$ for all particles $i$
Initialize empty trajectory array $V_{bulk}$
$t \leftarrow 0$
**while** $t < \tau$ **do**
    IntegrateStep(Boris-DPD)
    Record instantaneous bulk velocity $\langle v_y(t) \rangle$ to $V_{bulk}$
    $t \leftarrow t + \Delta t$
**end while**
Extract acceleration slope $a$ via linear regression on $V_{bulk}(t)$
**return** $a$

# I DPD Thermostat Pseudocode

**Algorithm 3** DPD Thermostat (Pairwise Momentum-Conserving, Velocity-Verlet Form)

**Require:** $\{\mathbf{r}_i, \mathbf{v}_i, m_i\}_{i=1}^{N}$, timestep $\Delta t$, cutoff $r_c$, parameters $\gamma, \sigma$
**Require:** Weight $w^R(r)$ with $w^D(r) = (w^R(r))^2$
Compute conservative forces $\{\mathbf{F}_i^C\}$
**for** each particle $i$ **do**
    $\mathbf{v}_i \leftarrow \mathbf{v}_i + \dfrac{\Delta t}{2m_i}\mathbf{F}_i^C$
**end for**
**for** each particle $i$ **do**
    $\mathbf{F}_i^{DPD} \leftarrow \mathbf{0}$
**end for**
**for** each unordered pair $(i, j)$ with $i < j$ **do**
    $\mathbf{r}_{ij} \leftarrow \mathbf{r}_i - \mathbf{r}_j$
    $r_{ij} \leftarrow \|\mathbf{r}_{ij}\|$
    **if** $r_{ij} < r_c$ **then**
        $\hat{\mathbf{r}}_{ij} \leftarrow \mathbf{r}_{ij}/r_{ij}$
        $\mathbf{v}_{ij} \leftarrow \mathbf{v}_i - \mathbf{v}_j$
        $w^R \leftarrow w^R(r_{ij})$
        $w^D \leftarrow (w^R)^2$
        Draw $\theta_{ij} \sim \mathcal{N}(0,1)$ and set $\theta_{ji} = \theta_{ij}$
        $\mathbf{F}_{ij}^D \leftarrow -\gamma\, w^D\, (\mathbf{v}_{ij} \cdot \hat{\mathbf{r}}_{ij})\, \hat{\mathbf{r}}_{ij}$
        $\mathbf{F}_{ij}^R \leftarrow \sigma\, w^R\, \theta_{ij}\, \hat{\mathbf{r}}_{ij}$
        $\mathbf{F}_{ij} \leftarrow \mathbf{F}_{ij}^D + \mathbf{F}_{ij}^R$
        $\mathbf{F}_i^{DPD} \leftarrow \mathbf{F}_i^{DPD} + \mathbf{F}_{ij}$
        $\mathbf{F}_j^{DPD} \leftarrow \mathbf{F}_j^{DPD} - \mathbf{F}_{ij}$
    **end if**
**end for**
**for** each particle $i$ **do**
    $\mathbf{v}_i \leftarrow \mathbf{v}_i + \dfrac{\Delta t}{m_i}\mathbf{F}_i^{DPD}$
**end for**
**for** each particle $i$ **do**
    $\mathbf{r}_i \leftarrow \mathbf{r}_i + \Delta t\, \mathbf{v}_i$
**end for**
Recompute conservative forces $\{\mathbf{F}_i^C\}$
**for** each particle $i$ **do**
    $\mathbf{v}_i \leftarrow \mathbf{v}_i + \dfrac{\Delta t}{2m_i}\mathbf{F}_i^C$
**end for**

# J Boris Integration Step Pseudocode

**Algorithm 4** Boris Velocity Update

**Require:** $\mathbf{v}_i$, charge $q_i$, mass $m_i$, fields $\mathbf{E}_i$, $\mathbf{B}_i$, timestep $\Delta t$
**Ensure:** Updated velocity $\mathbf{v}_i^{n+1/2}$

1: $\mathbf{v}^- \leftarrow \mathbf{v}_i + \dfrac{q_i \Delta t}{2m_i} \mathbf{E}_i$
2: $\mathbf{t} \leftarrow \dfrac{q_i \Delta t}{2m_i} \mathbf{B}_i$
3: $t^2 \leftarrow \mathbf{t} \cdot \mathbf{t}$
4: $\mathbf{s} \leftarrow \dfrac{2\mathbf{t}}{1 + t^2}$
5: $\mathbf{v}' \leftarrow \mathbf{v}^- + \mathbf{v}^- \times \mathbf{t}$
6: $\mathbf{v}^+ \leftarrow \mathbf{v}^- + \mathbf{v}' \times \mathbf{s}$
7: $\mathbf{v}_i^{n+1/2} \leftarrow \mathbf{v}^+ + \dfrac{q_i \Delta t}{2m_i} \mathbf{E}_i$
8: **return** $\mathbf{v}_i^{n+1/2}$

# Bibliography


[1] H. B. G. Casimir. On onsager's principle of microscopic reversibility. *Reviews of Modern Physics*, 17(2–3):343–350, April 1945.

[2] Rongxiang Luo, Giuliano Benenti, Giulio Casati, and Jiao Wang. Onsager reciprocal relations with broken time-reversal symmetry. *Physical Review Research*, 2(2), April 2020.

[3] Hendrik Antoon Lorentz. *Attempt of a theory of electrical and optical phenomena in moving bodies*. E.J. Brill, Leiden, 1895.

[4] Paul Langevin. Sur la théorie du mouvement brownien. *Comptes Rendus Hebdomadaires des Séances de l'Académie des Sciences*, 146:530–533, 1908.

[5] George Gabriel Stokes. On the theories of the internal friction of fluids in motion, and of the equilibrium and motion of elastic solids. *Transactions of the Cambridge Philosophical Society*, 8:287–319, 1845.

[6] Jean-Marie-Constant Duhamel. Sur la méthode générale relative au mouvement de la chaleur dans les corps solides plongés dans des milieux dont la température varie avec le temps. *Journal de l'École polytechnique*, 14(22):20–77, 1833.

[7] Adriaan D. Fokker. Die mittlere energie rotierender elektrischer dipole im strahlungsfeld. *Annalen der Physik*, 348(5):810–820, 1914.

[8] Andrey N. Kolmogorov. Über die analytischen methoden in der wahrscheinlichkeitsrechnung. *Mathematische Annalen*, 104(1):415–458, 1931.

[9] Anatoly A. Vlasov. On vibration properties of electron gas. *Zhurnal Eksperimental'noi i Teoreticheskoi Fiziki (Journal of Experimental and Theoretical Physics)*, 8:291–318, 1938.

[10] G. E. Uhlenbeck and L. S. Ornstein. On the theory of the brownian motion. *Physical Review*, 36(5):823–841, 1930.

[11] James Clerk Maxwell. V. illustrations of the dynamical theory of gases.—part i. on the motions and collisions of perfectly elastic spheres. *Philosophical Magazine Series 1*, 19:19–32.

[12] Paul Drude. Zur Elektronentheorie der Metalle. *Annalen der Physik*, 306(3):566–613, 1900.

[13] Neil W. Ashcroft and N. David Mermin. *Solid State Physics*. Holt, Rinehart and Winston, New York, 1976.

[14] Dominika Lesnicki, Rodolphe Vuilleumier, Antoine Carof, and Benjamin Rotenberg. Molecular hydrodynamics from memory kernels. *Physical Review Letters*, 116(14), April 2016.

[15] Florian N. Brünig, Jan O. Daldrop, and Roland R. Netz. Pair-reaction dynamics in water: Competition of memory, potential shape, and inertial effects. *The Journal of Physical Chemistry B*, 126(49):10295–10304, 2022. PMID: 36473702.

[16] Anand Joseph Michael. *Exploring Brownian Phenomena using Hydrodynamic Memory Kernels*. Licentiate thesis, Chalmers University of Technology, Gothenburg, Sweden, 2025.

[17] Robert Zwanzig. Ensemble method in the theory of irreversibility. *The Journal of Chemical Physics*, 33(5):1338–1341, 1960.

[18] Robert Zwanzig. *Nonequilibrium Statistical Mechanics*. Oxford University Press, New York, 2001.

[19] Hajime Mori. Transport, collective motion, and Brownian motion. *Progress of Theoretical Physics*, 33(3):423–455, 1965.

[20] Robert A. Robinson and Robert H. Stokes. *Electrolyte Solutions*. Dover Publications, Mineola, New York, 2nd edition, 2002.

[21] Ryogo Kubo. Statistical-mechanical theory of irreversible processes. I. General theory and simple applications to magnetic and conduction problems. *Journal of the Physical Society of Japan*, 12(6):570–586, 1957.

[22] Nikolay N. Bogoliubov. Problems of a dynamical theory in statistical physics. In Jan de Boer and George E. Uhlenbeck, editors, *Studies in Statistical Mechanics, Vol. I*, pages 1–118. North-Holland, Amsterdam, 1962. Original Russian edition published in 1946.

[23] M. San Miguel and J. M. Sancho. A colored-noise approach to brownian motion in position space. corrections to the smoluchowski equation. *Journal of Statistical Physics*, 22(5):605–624, May 1980.

[24] Ryogo Kubo. The fluctuation-dissipation theorem. *Reports on Progress in Physics*, 29(1):255–284, 1966.

[25] Michael Bonitz and Anatoly Zagorodny. Yuri l'vovich klimontovich, his theory of fluctuations and its impact on the kinetic theory. *Contributions to Plasma Physics*, 64(5):e202400014, 2024.

[26] Yu. L. Klimontovich. On the fluctuations in a plasma. *Journal of Experimental and Theoretical Physics (JETP)*, 33:982–991, 1957. Russian original: Zh. Eksp. Teor. Fiz. 33, 1282-1293 (1957).

[27] Kyoji Nishikawa. Statistical mechanics of turbulent plasmas. i: Diagram formulation for the klimontovich equation. *Progress of Theoretical Physics*, 36(2):193–223, August 1966.

[28] Koichi Furutsu. On the statistical theory of wave propagation in a random medium. *Journal of the Radio Research Laboratories*, 10(50):285–304, 1963.

[29] Evgenii Aleksandrovich Novikov. Functionals and the random-force method in turbulence theory. *Soviet Physics JETP*, 20(5):1290–1294, 1965.

[30] Claude-Louis Navier. Mémoire sur les lois du mouvement des fluides. *Mémoires de l'Académie Royale des Sciences de l'Institut de France*, 6:389–440, 1823.

[31] Murray F Gardner and John L Barnes. *Transients in Linear Systems*. John Wiley & Sons, 1942.

[32] Brian C. Hall. *Lie Groups, Lie Algebras, and Representations: An Elementary Introduction*, volume 222 of *Graduate Texts in Mathematics*. Springer, Cham, Switzerland, 2nd edition, 2015.

[33] Melville S. Green. Markoff random processes and the statistical mechanics of time-dependent phenomena. ii. irreversible processes in fluids. *The Journal of Chemical Physics*, 22(3):398–413, 1954.

[34] Ryogo Kubo. Statistical-mechanical theory of irreversible processes. i. general theory and simple applications to magnetic and conduction problems. *Journal of the Physical Society of Japan*, 12(6):570–586, 1957.

[35] Thomas John I'Anson Bromwich. On the relations between conjugate functions and the integral theorem of fourier. *Proceedings of the London Mathematical Society*, 2(1):106–125, 1916.

[36] Augustin-Louis Cauchy. Mémoire sur les intégrales définies, prises entre des limites imaginaires. *De l'Imprimerie Royale*, 1825.

[37] P. J. Hoogerbrugge and J. M. V. A. Koelman. Simulating microscopic hydrodynamic phenomena with dissipative particle dynamics. *Europhysics Letters*, 19(3):155, jun 1992.

[38] Ernest O. Lawrence and Niels E. Edlefsen. The production of high speed canal rays without the use of high voltages. *Science*, 72(1867):376–377, Oct 1930.

[39] Igor D. Kaganovich, Andrei Smolyakov, Yevgeny Raitses, Eduardo Ahedo, Ioannis G. Mikellides, Benjamin Jorns, Francesco Taccogna, Renaud Gueroult, Sedina Tsikata, Anne Bourdon, Jean-Pierre Boeuf, Michael Keidar, Andrew Tasman Powis, Mario Merino, Mark Cappelli, Kentaro Hara, Johan A. Carlsson, Nathaniel J. Fisch, Pascal Chabert, Irina Schweigert, Trevor Lafleur, Konstantin Matyash, Alexander V. Khrabrov, Rod W. Boswell, and Amnon Fruchtman. Physics of exb discharges relevant to plasma propulsion and similar technologies. *Physics of Plasmas*, 27(12), December 2020.

[40] Various Authors. Long-timescale simulations: Challenges, pitfalls, best practices, for development and applications. In *Molecular Modeling and Simulation*. Springer, 2020.

[41] Edwin H. Hall. On a new action of the magnet on electric current. *American Journal of Mathematics*, 2(3):287–292, 1879.

[42] Matthew J. Ryan, Lujia Gao, Francis I. Valiyaveetil, Alexei A. Kananenka, and Martin T. Zanni. Water inside the selectivity filter of a k+ ion channel: Structural heterogeneity, picosecond dynamics, and hydrogen bonding. *Journal of the American Chemical Society*, 146(2):1543–1553, 2024. PMID: 38181505.

[43] Albert Einstein. Über die von der molekularkinetischen theorie der wärme geforderte bewegung von in ruhenden flüssigkeiten suspendierten teilchen. *Annalen der Physik*, 322(8):549–560, 1905.

[44] Herbert S Harned and Benton B Owen. *The Physical Chemistry of Electrolytic Solutions*. Reinhold Publishing Corporation, New York, 1958.

[45] Lucas Tepper, Benjamin Dalton, and Roland R. Netz. Accurate memory kernel extraction from discretized time-series data. *Journal of Chemical Theory and Computation*, 20(8):3061–3068, 2024. PMID: 38603471.

[46] Eric Schulz, Maarten Speekenbrink, and Andreas Krause. A tutorial on gaussian process regression: Modelling, exploring, and exploiting functions. *Journal of Mathematical Psychology*, 85:1–16, 2018.

[47] Rainer Storn and Kenneth Price. Differential evolution – a simple and efficient heuristic for global optimization over continuous spaces. *Journal of Global Optimization*, 11(4):341–359, 1997.

[48] Swagatam Das and Ponnuthurai N. Suganthan. Differential evolution: A survey of the state-of-the-art. *IEEE Transactions on Evolutionary Computation*, 15(1):4–31, 2011.

[49] Robert D Shannon. Revised effective ionic radii and systematic studies of interatomic distances in halides and chalcogenides. *Acta Crystallographica Section A: Crystal Physics, Diffraction, Theoretical and General Crystallography*, 32(5):751–767, 1976.